University of Arkansas, Fayetteville
ScholarWorks@UARK

Theses and Dissertations

12-2011

# Development of a Structured Concrete Thermocline Thermal Energy Storage System

Bradley M. Brown
*University of Arkansas, Fayetteville*

Follow this and additional works at: http://scholarworks.uark.edu/etd

 Part of the Civil Engineering Commons, Energy Systems Commons, and the Other Engineering Science and Materials Commons

Recommended Citation
Brown, Bradley M., "Development of a Structured Concrete Thermocline Thermal Energy Storage System" (2011). *Theses and Dissertations*. 208.
http://scholarworks.uark.edu/etd/208

This Thesis is brought to you for free and open access by ScholarWorks@UARK. It has been accepted for inclusion in Theses and Dissertations by an authorized administrator of ScholarWorks@UARK. For more information, please contact scholar@uark.edu, ccmiddle@uark.edu.

# DEVELOPMENT OF A STRUCTURED CONCRETE THERMOCLINE THERMAL ENERGY STORAGE SYSTEM

# DEVELOPMENT OF A STRUCTURED CONCRETE THERMOCLINE THERMAL ENERGY STORAGE SYSTEM

A thesis submitted in partial fulfillment
of the requirements for the degree of
Master of Science in Civil Engineering

By

Bradley M. Brown
University of Arkansas
Bachelor of Science in Civil Engineering, 2010

December 2011
University of Arkansas

**ABSTRACT**

The past couple of decades have shown a concern when considering the way the world obtains its power. The focus has been switching from fossil fuels that have been used for hundreds of years to renewable energy sources, such as the sun. Solar energy is readily and infinitely available for harnessing. One problem with solar energy, though, is its inability to be used during the night time and during cloud covered weather. A solution to this problem is the use of energy storage mechanisms. For solar plants that use solar thermal energy (concentrating solar power plants), thermal energy storage (TES) has been the focus. Single tank thermocline TES systems have been used on a limited basis with packed beds as the filler material to lower costs compared to traditional two tank storage options. In this type of system, a thermal gradient is maintained inside of the tank in order to keep the hot and the cold fluid within the same tank without thermal mixing. The problem with packed beds is that settling of the filler material during thermal cycling causes thermal ratcheting on the tank from increased wall hoop stresses. This could ultimately cause a catastrophic failure of the tank wall. This research focuses on concrete being used in a thermocline type TES system with nitrate solar salt as the heat transfer fluid. The goal of this research is to use modeling based on finite difference method to design a structured concrete thermocline TES system. A structure concrete thermocline replaces the packed bed filler material with concrete structures, eliminating the issue of thermal ratcheting. Also this research covers testing of proprietary concrete mixtures designed at the University of Arkansas to determine their compatibility with nitrate solar salt heat transfer fluid at an operating temperature of 585° C. Discharge efficiencies were found for structured concrete filler material geometries that reached a maximum of 65.59%. Proprietary mixes created by the University of Arkansas were found to be adequate for long term use in the solar salt environment.

This thesis is approved for recommendation to the Graduate Council

Thesis Director:

_____

Dr. R. Paneer Selvam

Thesis Committee:

_____

Dr. Micah Hale

_____

Dr. Ernest Heymsfield

**THESIS DUPLICATE RELEASE**

I hereby authorize the University of Arkansas Libraries to duplicate this thesis when needed for research and/or scholarship.

Agreed _____
Bradley M. Brown

Refused _____
Bradley M. Brown

**ACKNOWLEDGEMENTS**

First I would like to thank Dr. R. Paneer Selvam for his guidance through the year and a half spent doing my Master's program at the University of Arkansas. I would like to thank him also for his advice and opinion on multiple other areas of life and learning.

I would also like to acknowledge Dr. Micah Hale and Dr. Ernie Heymsfield for their willingness to join my Master's committee. Not only were they great members to be able to share what I have discovered in my research, but great people to be able to sit and chat with and that cared how my life and school were progressing.

Next I would like to thank the United States Department of Energy (DOE) for believing in the University and me and funding our research for this project.

And finally, I would like to express a very special thanks to everyone that has worked with me along the way on this project for the DOE. These men have become more than colleagues; they have become friends: Joel Skinner, Emerson John, and Matt Strasser.

**DEDICATION**

This thesis is dedicated to my grandfather Charles "P-Pop" Brown for his encouragement when I was a kid to learn about how things work, how to build things, and how to have fun while doing it. This mentality put me into the field I am in today and has given me the perseverance through the past five and a half years of being in college.

I would also like to dedicate this thesis to my parents, Marty and Stephanie Brown, who have supported me and grown me in to the man I am today. I thank them for their love, support, and the family they have raised for me to be a part of. Along with my parents, I dedicate this to my brothers, Andrew and Jon, and my sister, Chelsea. Thank you all for encouraging me to do my best and expecting better than my best from me.

**TABLE OF CONTENTS**

**LIST OF FIGURES**

**LIST OF TABLES**

# CHAPTER 1: INTRODUCTION AND THESIS OBJECTIVES

## 1.1 INTRODUCTION

The industrialized nations of the world are forever increasing the amount of energy that is being consumed. The current standards for energy usage are fossil fuels (EIA 2011). The problems with using fossil fuels are the increasing prices and the high environmental concerns. Solar energy is a renewable energy that has many positive attributes. The supply of solar energy is infinite and is a clean way to produce energy in large scales.

Energy from the sun can be harnessed in two ways. This can be done using photovoltaic (PV) panels or by concentrating solar power (CSP). PV panels make electrical power by converting sunlight using semiconductors (Skinner 2011). CSP systems, on the other hand, take the heat from the sun's rays and use it to superheat steam that turns a turbine to create electrical power with a generator.

A problem for both PV and CSP systems is that they cannot produce energy during times when the sun's rays are not available. This includes times when the sky is cloud covered or when it is night time. Storage systems are being developed for CSP systems in order to store the thermal energy for use during the plant's down time. These systems are known as thermal energy storage (TES) systems. There are three methods to store energy for TES concepts: sensible heat, latent heat, and chemical storage. Sensible heat has been recommended as the most practical way to store thermal energy thus far (Herrmann and Kearny 2002).

To lower the cost and raise the effectiveness of TES systems, concrete, which has an approximate media cost of $1 per kilowatt-hour thermal (Herrmann and Kearny 2002), has been researched as a storage medium for sensible heat systems using synthetic oil as a heat transfer

fluid (Laing et al. 2009). Using concrete with a combination of molten solar salt has shown promise for an effective TES system. The molten solar salt used in CSP plants can run at operating temperatures in excess of 500°C if needed (Coastal Chemical Company 2011).

The University of Arkansas has developed concrete mixtures that have been proven in oven testing to withstand temperatures up to 600ºC (John et al. 2010). Using the combination of molten salt and concrete, TES systems have been researched and tested through the University of Arkansas. Preliminary testing using concrete with an embedded stainless steel tube heat exchanger allowed for temperatures in the storage media to reach 450ºC (Skinner 2011). It was concluded that the cost of the stainless steel tubing and the concrete mix designs needed for this type of system were not competitive when trying to achieve the DOE's goal for solar thermal energy storage by 2020, which is a cost of 6 cents per kilowatt-hour with 12 to17 hours of storage (DOE 2011).

In this research, a thermocline-type TES system is proposed and developed for the combination of molten salt and concrete. A thermocline system is a single tank thermal energy storage unit that has a low cost filler material to displace high cost heat transfer fluids. The heat transfer fluid has a thermal stratification caused by the natural buoyancy forces of the fluid and enhanced by the filler material so that both the hot fluid and cold fluid can be held in the same tank without thermal mixing (Mawire et al. 2009). In this system, the hot molten salt would be circulated around a structured concrete filler material in a storage tank. The structured concrete will eliminate the issue of thermal ratcheting of the tank walls which is seen in traditional packed bed thermocline systems. It is proven in this work that the structured concrete thermocline has similar roundtrip discharge efficiencies when compared to previously modeled systems of up to 65.59%.

Thermal computer modeling using the finite difference method was completed in this work to design a viable structured concrete thermocline system. The two geometries modeled are concrete blocks with holes running vertically through them and concrete plates standing vertical within the thermocline tank. The two geometries will be detailed in Chapter 3 of this thesis. The optimized design could be used for testing a large scale structured concrete thermocline TES system.

## 1.2 THESIS OBJECTIVES

*Task 1:* To conduct a literature review of thermal energy storage technologies with an emphasis on the current industry standards for sensible heat, thermocline TES systems.

*Task 2:* To use an axisymmetric, finite difference method (FDM) computer model to optimize a design for a structured concrete thermocline-type TES system designed as concrete blocks with holes running vertically through them for molten salt to flow through. Optimization will be done on the hole spacing, hole size, velocity of the fluid, and charging and discharging times.

*Task 3:* To use a 2-dimensional (2-D) plate, FDM computer model to optimize a design for a structured concrete thermocline-type TES system designed as concrete plates standing vertically inside of a thermocline tank, separated by a space for the molten salt to flow through. Optimization will be done on the thickness of the plate, the thickness of the molten salt flow path, the velocity of the molten salt, and the charging and discharging times.

*Task 4:* To determine the best geometric configuration from Task 2 and Task 3 that will lead to the most efficient thermocline system. Round trip discharge efficiencies for the

system will be the basis of this decision, as well as energy retrieval per unit area of thermocline filler material.

*Task 5:* To test Arkansas limestone and sandstone in a molten salt isothermal bath for 500 hours at a temperature of 585ºC so they can be evaluated for their compatibility with the molten salt environment and viability for use in concrete mix designs for the structured concrete thermocline-type TES system. They will be determined to be viable if there is no visual degradation or weight loss.

*Task 6:* To test two inch cubes made of concrete that has been designed for this project in a molten salt isothermal bath for 500 hours at a temperature of 585ºC so that they can be evaluated for their viability as a useful mix design in the structured concrete thermocline-type TES system. They will be determined to be viable if there is no visual degradation of the cubes, if they don't have weight loss, and if they don't lose a majority of their original compressive strengths.

*Task 7:* Determine a large, laboratory scale thermocline system to be implemented by further research team members at the University of Arkansas. This will include the geometry configuration determined from Task 4 as well as a suggestion of a mix design from Task 6.

# CHAPTER 2: LITERATURE REVIEW

## 2.1 INTRODUCTION

Concentrating solar power (CSP) technologies have been in use for many years. They allow for a clean and renewable energy that is also cost competitive. The three main technologies are parabolic troughs, solar power towers, and dish/engines (Brosseau et al. 2005). For more information on CSP technologies, refer to Skinner (2011).

Thermal Energy Storage (TES) has been put in place to increase the efficiency of these CSP technologies so that they can be run not only during the daylight hours, but also during peak hours when the sun is not visible or when the skies do not permit effective solar energy exchange. This is done by charging TES systems with fluids that are heated by the sun's rays during off-peak hours and discharging during peak hours, some of which occur after dark. This storage helps to meet peak demands without the use of fossil fuel backup systems. A power plant with these capabilities has potential to generate much more revenue than one that doesn't, therefore increasing economic viability for this type of energy (Pacheco et al. 2002). There are multiple different types of TES systems. They include two-tank direct thermal storage, two-tank indirect thermal storage, and single tank thermocline thermal storage (www.nrel.gov).

## 2.2 THERMAL ENERGY STORAGE

When it comes to CSP plants, it is often easiest and most effective to leave the energy in its thermal state instead of turning it into a chemical state, such as in batteries. CSP plants function by heating a fluid in a collector field and using that heated fluid to power turbines either out of the collection field or, in the case of dish/engine plants, on the engine that is attached to the reflector. Thermal energy storage has been developed using multiple different methods. The

three main methods for thermal storage are sensible heat storage, latent heat storage, and chemical storage. For more in depth details on CSP plants and thermal energy storage types, refer to Skinner (2011) and Castro (2010).

### *2.2.1 Sensible Heat Storage*

Sensible heat storage is based on the temperature change of a substance. This is the change in internal energy due to the addition of heat, causing the material to heat up (Herrmann and Kearny 2002). The total energy stored is based on the mass of the material, the specific heat of the material, and the temperature change experienced by the material. The basic equation for this type of thermal energy storage is represented by equation 2-1 (Çengel and Ghajar 2011).

$$Q = m_m c_{p_m} \Delta T_m \tag{2-1}$$

$Q_m$ = energy stored

$m_m$ = mass of the material

$c_{p\,m}$ = specific heat of the material

$\Delta T_m$ = Temperature change of the material

For sensible heat storage, the storage material's properties are very important. Other important properties include the operating temperatures of the collector fields, the thermal conductivities and diffusivities of the materials, compatibility of the different materials, vapor pressure, heat loss coefficients, and cost (Herrmann and Kearny 2002). All of these factors affect the productivity and efficiency of the CSP plant and its storage mechanism. Since sensible heat storage is the technique considered in this thesis, it will be described further in later sections.

### *2.2.2 Latent Heat Storage*

Latent heat storage, or phase change, is based on the change of state of a material. The thermal energy is stored when the material changes state as the heat of fusion, heat of vaporization, or heat of crystalline phase transformation (Skinner 2011). The heated fluids from the collector fields change the state of the phase change material (PCM) so that the heat is stored. The thermal energy is then extracted from the PCM in the reverse change of state. These types of storage systems can take up less space due to the high amount of storage density, but they are more difficult to perfect. These systems call for more complex heat transfer designs with very specific selection of PCMs. Also, it has been noted that the PCMs that are available tend to degrade as the number of freeze-thaw cycles increase (Herrmann and Kearny 2002).

### *2.2.3 Chemical Storage*

Chemical storage is the third mechanism for thermal energy storage. This type of storage requires the use of a chemical reaction that must be completely reversible so that very little energy is lost in the process (Gil et al. 2010). The heated fluid in the collector field is used to fuel an endothermic chemical reaction. This means that the heat is absorbed during the reaction. In the reverse reaction, the heat is extracted due to the reaction being exothermic. Often the reverse reaction calls for a catalyst to start the reaction. The catalyst allows for the reaction to be controlled. This type of storage would allow for very high storage densities but it is in very early stages of development and there are many concerns to be handled before it can be used in a full scale CSP plant; toxicity and flammability name a few of the concerns (Herrmann and Kearny 2002).

## 2.3 SENSIBLE HEAT STORAGE SYSTEMS

Sensible heat storage has been the most widely developed and studied form of thermal energy storage for CSP plants. There are multiple different designs and concepts used to effectively store heat for later use. Each design has been implemented in different types of CSP plants for their different operating temperatures. There are direct and indirect systems, dual and single media systems, and two-tank systems and single tank thermocline systems.

### *2.3.1 Direct and Indirect TES Systems*

Direct and indirect systems relate to the way the storage media is heated. In a direct sensible heat TES system, the heat transfer fluid (HTF) used in the collector field is the fluid that is used to heat the storage media. That fluid can also be used as the storage material and store the thermal energy in a tank for later use. Direct systems are proven to be cheaper than indirect systems because they eliminate the need for heat exchangers that are used in the indirect systems. An example of a direct sensible heat storage system is presented in figure 2.1. Notice that the fluid from the collector goes directly to the storage tank or the power block.

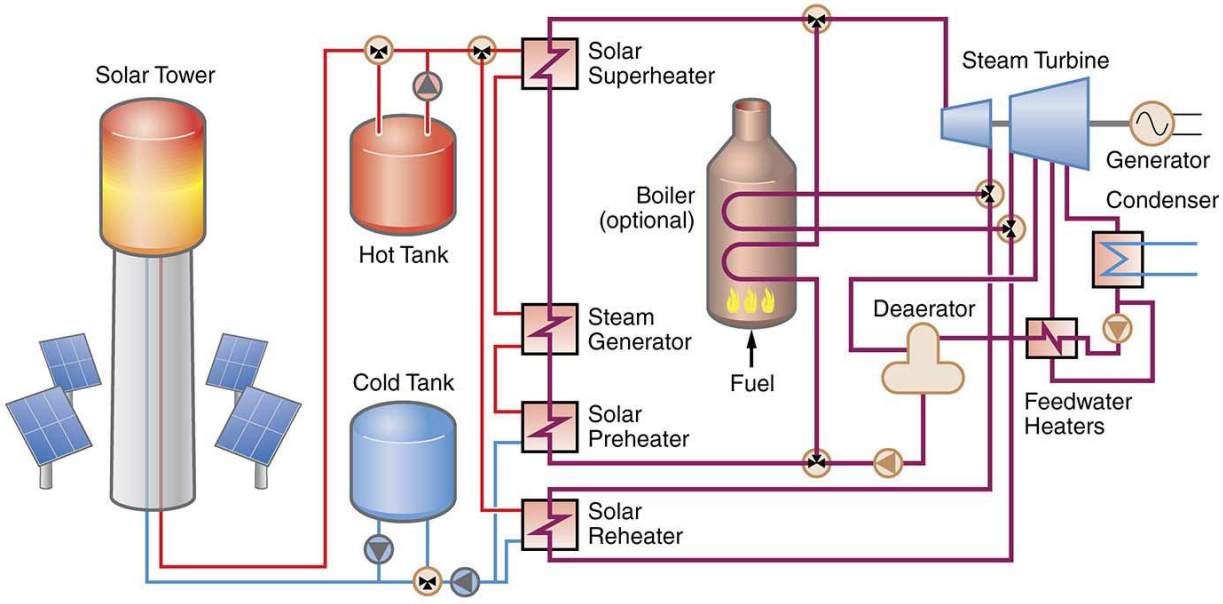


**Figure 2.1: Two-tank direct thermal storage system (EPRI 2010)**

Indirect sensible heat TES systems use two different fluids to achieve thermal storage. One fluid is used in the collector field to receive the energy from the sun. That fluid is then passed through a heat exchanger to transfer the heat to another fluid. The fluid from the collector field then returns back to the collector field to be heated again. The second fluid is then used to either store the thermal energy or is used to transfer the heat to a storage media. An example of an indirect sensible heat storage system is presented in figure 2.2. Notice that the collector fluid goes through a heat exchanger and never goes to the actual storage system.

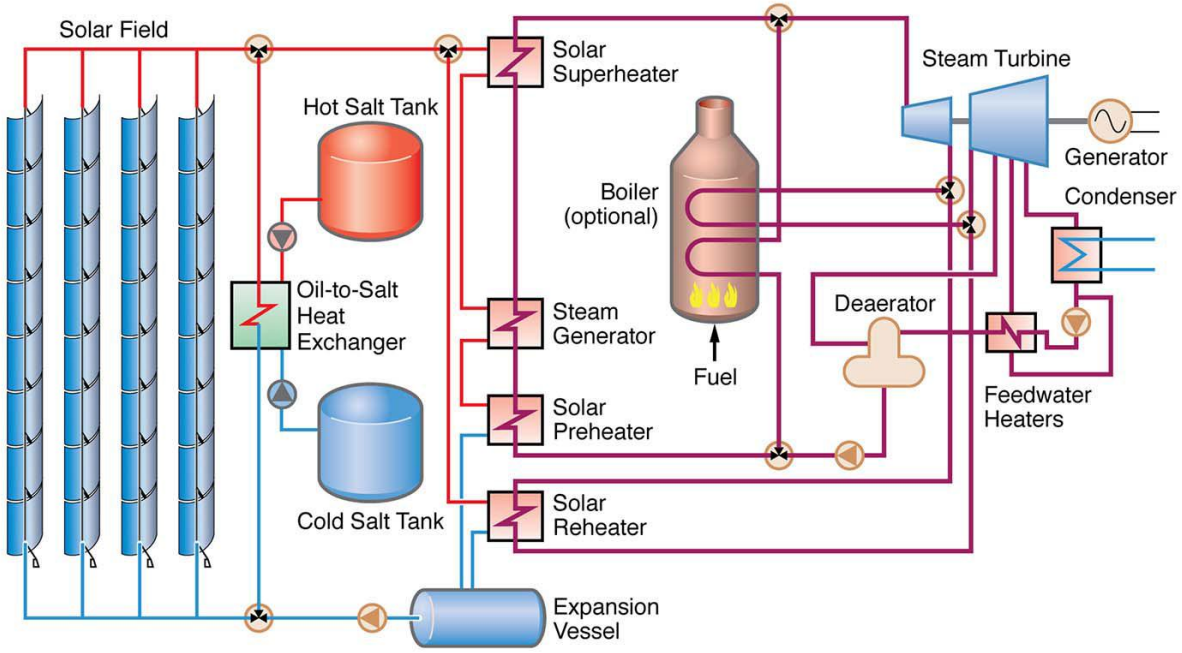


**Figure 2.2: Two-tank indirect thermal storage system (EPRI 2010)**

### *2.3.2 Dual and Single Media Systems*

Dual and single media systems describe the way the thermal energy is stored. In a single media system, there is only one material that stores the thermal energy. This is done in one of two ways. First, the liquid media could be the HTF from the collector field or the heat exchanger. This makes it to where the fluid is actually the storage material and will be held in a tank to extract the heat at a later time. This type of systems calls for a fluid that has a decent heat

capacity (Gil et al. 2010). Secondly, there can be a solid material that is heated by a fluid that has very little heat capacity. This means that the fluid does not store the thermal energy but the solid material does. The fluid will transfer all of its heat energy to the solid material for storage (Gil et al. 2010).

A dual media system uses two types of materials to store the thermal energy. This is usually done with a solid material and a liquid material that has a higher heat capacity. The fluid is held in a tank with a solid material so that both materials will store energy. The fluid may be pulled from the collector field during charging or it may be heated in a heat exchanger. The solid material will most likely be in the form of a packed bed in order to maximize thermal storage (Gil et al. 2010).

### *2.3.3 Two-Tank Systems*

Two-tank sensible heat TES systems consist of a hot tank and a cold tank. The hot tank is where the heated fluid from the collector field in a direct system, or the heat exchanger in an indirect system, is stored for use during cloudy periods or night time hours. When ready to be used, the fluid is taken from the hot tank and is used to heat steam for power generation.

The cooled liquid that has released its stored thermal energy is then moved to the cool tank. The cool tank holds the liquid until it is needed again to charge the TES system. At this point, the liquid is pulled from the cool tank, heated by the collector field or heat exchanger, and is then deposited into the hot tank for storage. An example of a two-tank design is shown in figure 2.3.

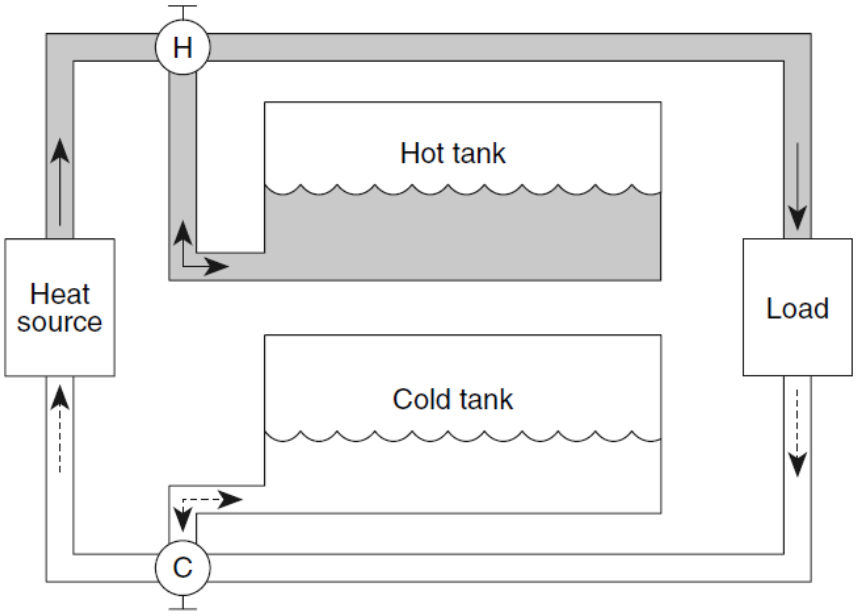


**Figure 2.3: Two-tank storage system (Hammerschlag et al. 2006)**

Two-tank systems have a few advantages and disadvantages. The first advantage is that the hot and cold liquids are always separate. This keeps the liquids from mixing and causing energy loss. Another advantage in a direct two-tank system is that there can be a large difference in the temperatures of the hot and cold tank which will increase the Rankine cycle efficiency. A disadvantage of these systems is the high cost of the system in general. The tank cost and the fluid cost make this option a considerably expensive one. Also, there is a high chance of solidification of the fluids for high temperature storage due to their high freezing temperatures (Gil et al. 2010).

## 2.4 THERMOCLINE TES SYSTEM

The thermocline TES system uses a single tank to store both the hot and cold fluid, along with a low cost filler material. A thermal stratification is present in the tank due to the natural buoyancy forces of fluids and is enhanced by the filler material. Colder fluids are denser than hot fluids so they rest lower in the tank. The filler material enhances the thermal stratification by

heating up to the surrounding fluid temperature. All of this combined helps to control the mixing of the hot and cold fluid within the tank, making it competitive against two-tank systems.

One single cycle for the thermocline system consists of two half-cycles. Both charging and discharging are done during the entire cycle. This breaks down the daily cycle into a charging half-cycle and a discharging half-cycle. Both the charging and discharging are treated differently in regards to length of time it takes to complete the half-cycle and the velocity of flow during the half-cycle (EPRI 2010)

The system is charged by pulling cold heat transfer fluid from the bottom of the tank, heating it up either in the collector field or via heat exchanger, and pumping it into the top of the tank. This moves the thermal stratification lower in the tank until it reaches the bottom. Discharging is done by pulling the hot heat transfer fluid in the tank out of the top and sending it through a heat exchanger that transfers heat for steam generation. The cooled fluid is then pumped back into the bottom of the tank. This moves the thermal stratification higher in the tank until it reaches the top (Pacheco et al. 2002). An example of this type of system is shown in figure 2.4.

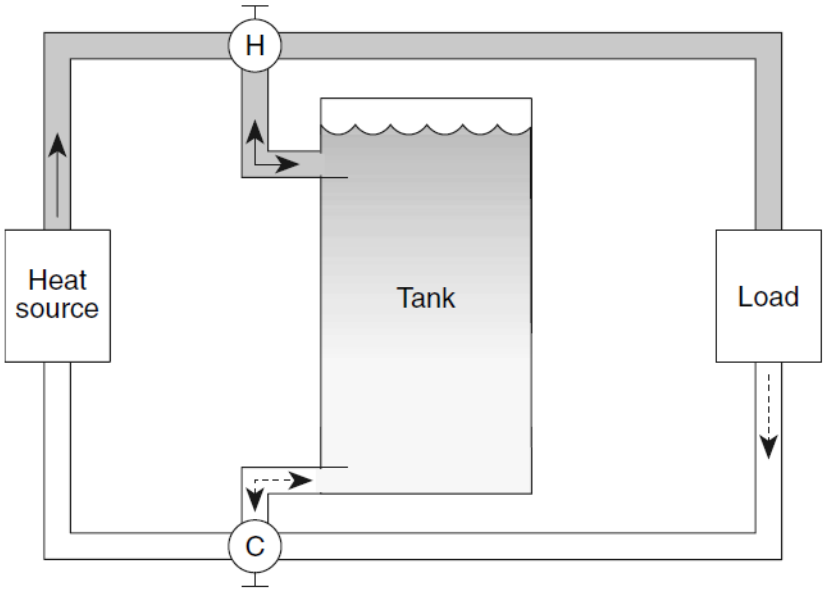


**Figure 2.4: Single tank thermocline system (Hammerschlag et al. 2006)**

This type of system is promising as a cheaper and more efficient TES solution for solar power plants compared to two tank systems. The relative cost is estimated to be about 35% cheaper than a two tank design (Brosseau et al. 2005). This paper will describe more about these systems and where they stand in current research and implementation.

Thermocline systems are made up of two essential components: the heat transfer fluid and the filler material. The key to a thermocline system is that they reduce the cost of a two-tank design. This is done by downsizing to one tank that is slightly larger than one of the tanks from a two-tank design and by replacing the expensive heat transfer fluid with a filler material that acts as part of the storage medium. An example of the thermocline tank with a filler material is given in figure 2.5.

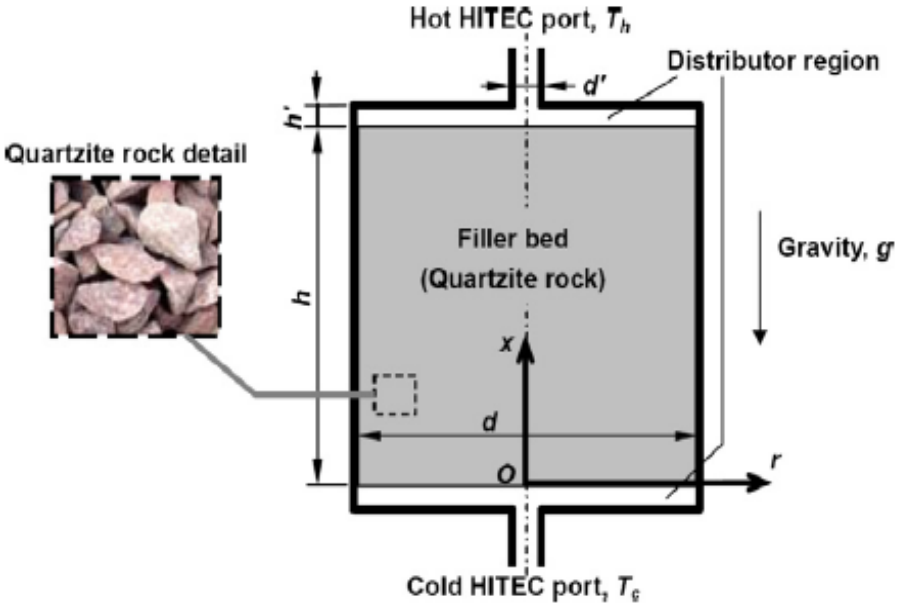


**Figure 2.5: Elevation of a packed bed thermocline tank (Yang and Garimella 2010a)**

The way the thermocline works is a natural stratification of differing liquid temperatures. The lower density, hot fluid is at the top of the tank and the higher density, cool fluid is at the bottom of the tank. The density difference in the fluid allows for the natural stratification. The filler material helps to enhance this affect. An example of the stratification inside of the tank is given in figure 2.6. Since both the fluid and the filler material are used to store the thermal energy, the most effective thermocline systems are dual media sensible heat systems. It is important to understand the heat capacities of the two different media, as well as their ability to remain stable within each other's presence when designing a thermocline system (Brosseau et al. 2005).

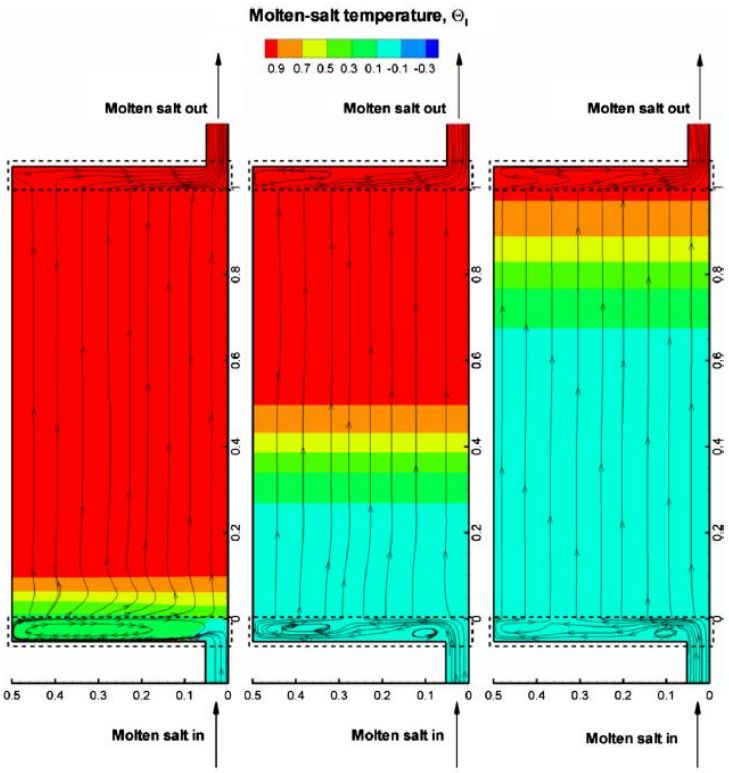


**Figure 2.6: Thermal stratification in a thermocline tank during a discharge half-cycle (Yang and Garimella 2010a)**

### *2.4.1 Heat Transfer Fluid*

In a thermocline, a heat transfer fluid (HTF) has to be used to store the heat in the filler material inside of the tank. The heat transfer fluid must also have a high heat capacity because it will also be storing the thermal energy. Of the HTFs that have been tried in all of the different types of TES systems, synthetic oils such as Caloria® and Therminol, water, and air likely all need to be ruled out for CSP TES systems (Mawire et al. 2009). All three types of fluid have low operating temperatures. The lower the operating temperature, the lower the temperature difference in the tank and this causes a lower efficiency for the system. Also, the higher temperatures that these fluids can operate at cause a need for expensive pressure vessel tanks (Yang and Garimella 2010b). Another problem with the synthetic oils is the relatively high cost.

Molten salts have been tested for use not only in thermocline systems, but two tank systems as well. The advantage to a molten salt is that they operate at a higher temperature range than synthetic oils with a negligible rise in pressure. Molten salts, such as HITEC (binary) and HITECXL (ternary) have operating temperatures in the range of 450-500° C with very low vapor pressure (Coastal Chemical Company 2011). This allows for steam generation at high temperatures of roughly 450° C which can increase the Rankine cycle efficiency to 40% compared to 21% by synthetic oils with a maximum operating temperature of 315° C or 37.6% by high temperature synthetic oils with a maximum operating temperature of 400° C (Yang and Garimella 2010b). CSP plants known as power tower plants have been able to increase the operating temperatures on HITEC Solar Salts to an even higher degree to further increase the Rankine cycle efficiency. With the newer formulation of HITEC Solar Salt, the maximum temperature output is raised to over 600°C (Turchi 2011).

A disadvantage to molten salts is that they have high freezing points. This means that special care has to be taken in order to keep the salt from freezing within the system, which would cause considerable damage. The high temperatures pose a threat as well. The receivers in the parabolic trough fields could have durability issues and the piping and other materials would become more expensive to withstand the heat (Brosseau et al. 2005).

An advantage illustrated by Brosseau et al. (2005) was that the molten salt could be used not only as the HTF in the thermocline tank, but also as the HTF that would flow through the solar field, allowing the field to have higher temperature outputs. This would also take out the expensive oil-to-salt heat exchangers that would usually have to be used due to synthetic oil running through the field and salt running through the tank. This is known as a direct sensible heat system and allows for higher storage temperatures to increase efficiency

### *2.4.2 Filler Materials*

Tests have been done on different types of minerals and their compatibility with molten nitrate salts (Pacheco et al. 2002; Burolla and Bartel 1979). Burolla and Bartel showed that taconite (iron ore) maintained integrity while Granite eroded significantly.

Pacheco et al. (2002) went through tests with 17 different minerals to narrow down to a few that would be compatible with molten nitrate salts. Tests were done with HITEC XL. The tests were done with regard to mass loss and contaminate analysis of the minerals with the first test being an isothermal bath in the salt from 10-1000 hours. Then the acceptable samples were subjected to thermal cycling to get conclusive evidence for acceptable filler material. Also included in the tests was cost in order to narrow down the choices to a cheap material that was readily available, which is necessary to lower the cost of energy storage in a thermocline TES system. After the initial test, only certain materials were allowed to continue due to the high price of some of the minerals. After thermal cycling, a combination of quartzite rock and silica sand were chosen to be the best material for a thermocline filler material at the temperatures that are needed for a high efficiency thermocline system. Quartzite has been the focus of many papers (Brosseau et al. 2005; Flueckiger et al. 2011; Kolb 2006; Pacheco et al. 2002; Yang and Garimella 2010a; Yang and Garimella 2010b) but other materials should be researched that could take the place of these mineral pebbles.

The filler material used in previous works was a packed bed or pebble bed. Packed beds used different size aggregates to achieve a low porosity. Pebble beds used one type of aggregate which caused a higher porosity. The packed bed system consisted of quartzite rock and silica sand. The porosity of these systems was recorded as 0.22 to 0.25 (Brosseau et al 2005; Flueckiger et al 2011; Pacheco et al. 2002; Yang and Garimella 2010b). The low porosity of the

filler material minimizes the amount of molten salt needed. For a pebble bed, Mawire et al. (2009) used fused silica, alumina, or stainless steel. The porosity for this type of system was recorded as 0.42.

### *2.4.3 Existing Systems*

The Solar One central receiver pilot plant used a thermocline TES system with Caloria® oil as a heat transfer fluid (Pacheco et al. 2002). This system had a low operating temperature of 218° C to 302° C because the use of Caloria®, which becomes pressurized when the temperature is increased above the upper operating temperature. The capacity of the tank was designed to be 182 $MWh_t$. The tank dimensions were 13.3 m tall and 18.2 m in diameter. The system only reported 21% efficiency on Rankine cycle conversion efficiency due to the low temperature range of the oil (Mawire et al. 2009). This proves the Caloria® oil to be ineffective in systems such as this. The plant began operation in 1982 and shut down in 1988 when the thermocline tank ruptured due to a steam explosion (EPRI 2010).

In the 1980's, Plataforma Solar de Almeria in Europe successfully ran a thermocline TES system. The system was at their test facility. It was a 5 $MWh_t$ storage capacity, dual media system. The direct system ran Therminol 55 as the HTF with a metal filler material inside of the tank. The test ran successfully but no further commercial development was done at this facility (EPRI 2010).

National Solar Thermal Test Facility at Sandia National Laboratories tested a molten salt thermocline system in 2000-2001 (EPRI 2010). This system was a 2.3 $MWh_t$ laboratory-scale test. The filler material used in this test was quartzite rock with silica sand and was decided on using the test results of Pacheco et al. (2002) on optimal filler material for thermocline TES systems. It was cycled 553 times from 290° C to 400° C. The test proved the feasibility of this

system with the proposed filler material. The filler showed no decomposition (Brosseau et al. 2004; Brosseau et al. 2005)

There is a proposed thermocline TES system to be implemented at the Saguaro plant in Arizona. This is the location of the first parabolic trough to come into use after a 15 year stagnant period. It is a 1 MW plant that has an organic Rankine power cycle with a maximum operating temperature of 300° C. It is using Solargenix parabolic trough collectors. The proposed thermocline would be a scaled-down version of the thermocline at Solar One. It would be able to store 30 $MWh_t$ which would allow for the Rankine cycle to operate for 6 hours after sundown on a full load (Kolb 2006). This system was only tested as a modeling problem. The modeling of this system and testing done by Sandia National Laboratories suggested that the thermocline system at this plant is viable (EPRI 2010).

### *2.4.4 Thermocline Modeling*

Modeling of thermocline systems is done to design a system that can be tested accurately. It keeps from having to do expensive trial and error attempts, especially on larger scale testing. Multiple different researchers have modeled many aspects of thermocline systems in order to solve problems and predict outcomes for different variables of the system.

The works of Kolb (2006), Mawire et al. (2006), Pacheco et al. (2002), Van Lew et al. (2009), and Yang and Garimella (2010a) all have modeling equations that simulate the temperature gradient in a thermocline tank, as shown graphically in figure 2.7. This is important in knowing if the filler material and HTF will produce a viable thermocline thermal stratification. It is also important in understanding the efficiency of the system in concern to thermal energy that is retained.

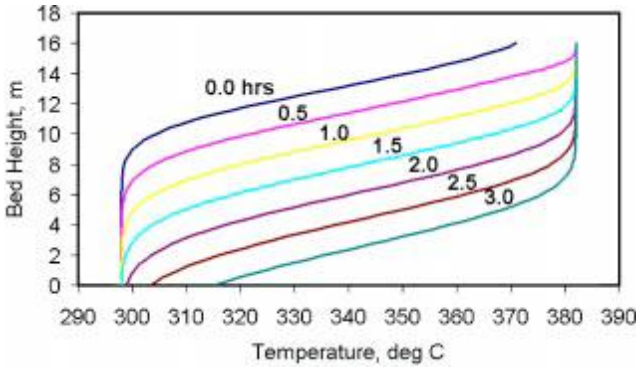


**Figure 2.7: Temperature gradient in a thermocline tank during charging (Pacheco et al. 2002)**

The key modeling equation used by many of the researchers is the Schumann's equation. It is presented in the works of Mawire et al. (2009) and Pacheco et al. (2002). The assumptions developed for this equation make this equation a simplified model for simulating the temperature distribution in a packed bed thermocline (Mawire et al. 2009). This equation is broken into a fluid phase, shown in equation 2-2, and solid phase, shown in equation 2-3 since the two materials don't share similar properties (Pacheco et al. 2002). The equations are shown with "f" being the subscript for the fluid and "b" being the subscript for the packed bed.

$$\left(\rho C_p\right)_f \varepsilon \frac{\partial T_f}{\partial \tau} = -\frac{\left(mC_p\right)_f}{A}\frac{\partial T_f}{\partial y} + h_v\left(T_b - T_f\right) \tag{2-2}$$

$$\left(\rho C_p\right)_b (1-\varepsilon)\frac{\partial T_b}{\partial \tau} = h_v\left(T_f - T_b\right) \tag{2-3}$$

Also presented in the works of other researchers was the effect that the thermocline tank walls had on the temperature distribution inside of the tank during charging, discharging, and stand-by phases. Hess and Miller (1982) first presented this approach. A problem that was noted was natural convection in the tank induced by heat transfer to the wall of the tank. Yang and Garimella (2010a) further researched this with a comparison of an adiabatic tank wall to a

non-adiabatic tank wall. The disturbed flow of a non-adiabatic thermocline tank during a discharge phase of the thermocline TES is presented in figure 2.8.

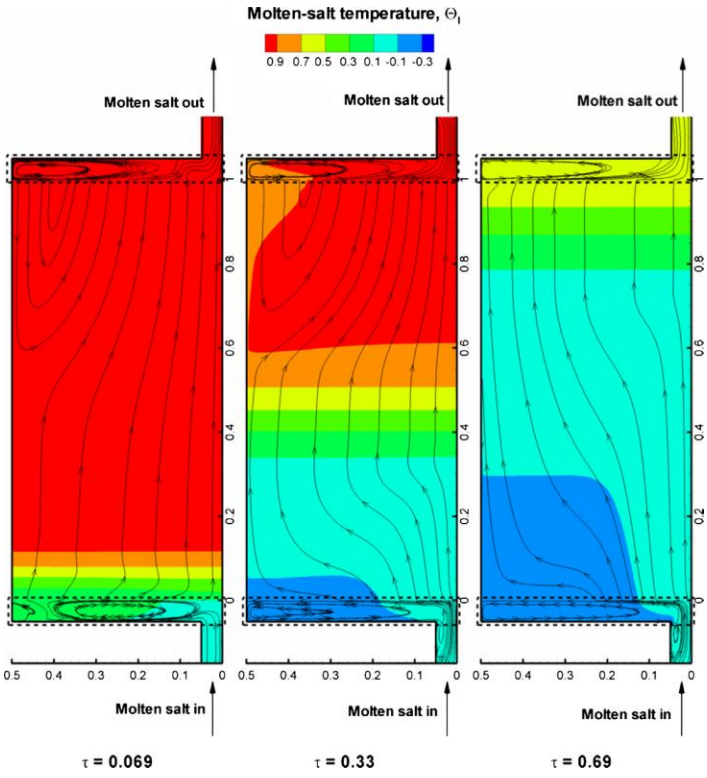


**Figure 2.8: Effect of the tank wall on thermal stratification (Yang and Garimella 2010a)**

Flueckiger et al. (2011) presented a study on thermal ratcheting in a thermocline tank. They modeled the flow inside of the tank as well as the heat transfer. They then went into modeling the heat conduction in the walls in order to model the mechanical stress in the walls which was calculated using the mechanical strain. Multiple cases were run to simulate the thermal ratcheting problem, as presented in figure 2.9.

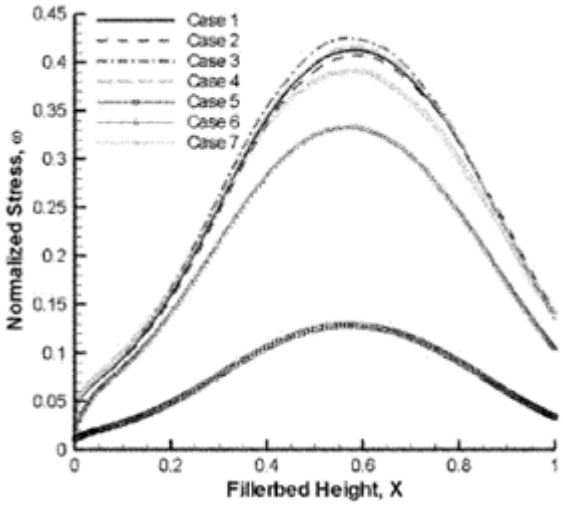


**Figure 2.9: Thermal ratcheting stress assessment (Flueckiger et al. 2011)**

### *2.4.5 Thermocline Design*

Thermocline design procedures have been outlined slightly by researchers. Yang and Garimella (2010b) laid out a design procedure for thermocline tanks. It was set up for HITEC molten salt and quartzite rock filler but could be used for similar materials. It was assumed that discharge power and useful thermal energy were predetermined by the application and that the porosity of the filler region was 0.22. Refer to their work for the 9 step design procedure.

EPRI (2010) reported a more in-depth design procedure. They included process design, tank sizing, material selection, tank design, heat and material balancing, insulation, impoundment wall design, thermocline distributor design, surge tanks and molten salt pump design, and heat exchangers. Refer to their work for an in-depth design procedure.

### *2.4.6 Current Problems and Motivation for the Thesis*

As of the current time, there are a few issues that must be addressed in order to make the thermocline system a solid competitor as a TES system to the two tank systems that are in use today. First is the selection of molten salt. Brosseau et al (2005) noted that their choice of HITEC XL ternary nitrate salt and the formulation of the Ca:Na:K had a few negative side

effects. When heated above 450° C to 500° C, the salt began to emit $CaCO_3$ as a byproduct inside of tank. This was evident on the tank walls and within the filler material. A specialized ratio needs to be developed in order to minimize this occurrence. This could be solved by nitrogen or oxygen blanketing or another type of chemical treatment that could be discovered in future studies. Also, valve design and construction needs to be analyzed better in order for the systems to withstand the higher temperatures and molten salts.

Another issue that is hard to control in thermocline systems is the operation of the unit and how it effects the stratification of the thermocline inside of the tank. The densities of the HTF at different temperatures along with the filler material's presence help to maintain the buoyant forces inside of the tank (Haller et al. 2010). If the two different temperatures of the fluid begin to mix, the stratification breaks down and causes generation of entropy and loss of exergy. Cooler HTF cannot be pulled from the tank and taken to a steam turbine and be expected to have a high Rankine cycle efficiency. The stratification has to stay intact with a large thermal gradient over a relatively short area compared to the height of the tank.

Thermal ratcheting is the final and main issue that affects the further research and development of the thermocline system. Occurrence of thermal ratcheting happens during the discharge period and the cold holding period. This is a problem for the packed bed systems that are in effect. During the charging half-cycle, the stainless steel tank that houses the filler material expands due to there being no structure to resist the expansion. At the full charge temperatures, the thermal strain on the stainless steel is at its maximum point. This means that there is extra space that is created in the bottom of the tank. The filler medium begins to settle because in a packed bed, there are fine particles of silica sand and small quartzite rock that can fill the now available space. As the discharging half-cycle begins, the tank begins to contract

back to its normal size. However, there is now a larger volume in the bottom of the tank that resists contraction. This puts a mechanical strain on the tank walls as it cools to the discharging low temperature. Thermal ratcheting occurs upon plastic deformation of the tank walls (Flueckiger et al. 2011).

Since thermal ratcheting is a significant problem in existing thermocline systems, a new filler material must be designed. To solve this problem, concrete blocks could be used to replace the packed bed filler material. This structured concrete filler material would eliminate thermal ratcheting while also maintaining the natural buoyancy forces within the tank. This thesis will be based on the design of a structured concrete filler material for a thermocline TES system that will eliminate thermal ratcheting and still be a competitive solution to the existing systems.

# CHAPTER 3: FDM MODELING FOR THERMOCLINE TES SYSTEM

In reality, a thermocline TES system is very expensive to build and test. Without proper knowledge of the problem at hand, there would most likely be multiple trials that would have to be tested in order to get the most efficient thermocline system. For this reason, modeling was done in order to determine the most logical setup of a structured concrete thermocline system. This modeling is the most economic way to eliminate poor and inefficient designs for a thermocline system. Modeling programs created by Selvam (2011) were used in the design of the structured concrete thermocline TES system.

## 3.1 STRUCTURED THERMOCLINE BASIS

The basic thermocline TES system is composed of a cylindrical stainless steel tank filled with a filler material and a HTF that has a thermal stratification. In the case of the structured concrete thermocline TES system, the previously tested packed bed filler material of quartzite rock and silica sand is being replaced with two different types of structure concrete cells. The first type of geometry that was considered for the system was a network of concrete rectangular prisms that have a full length cylindrical hole running vertically throughout the concrete. A tank cross-section looking down into the tank from the top is shown in figure 3.1. This cross section is on a normal x-y grid. The z-direction for this tank runs into the page and is the axis for the height of the thermocline tank.

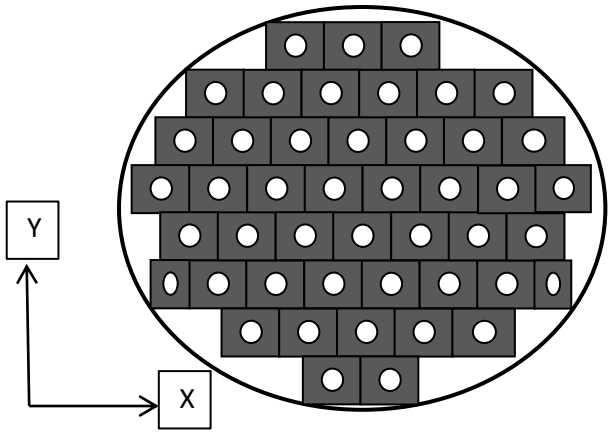


**Figure 3.1: Cross-section of a thermocline tank filled with rectangular concrete prisms with holes running vertically through the concrete blocks.**

The second type of geometry that was considered for the system was a number of concrete plates that would stand vertical within the thermocline tank. These plates would be as wide as the tank at each point and would have a small space between them for the HTF to flow through. A tank cross-section looking down into the tank from the top for this type of configuration is shown in figure 3.2. The same coordinate system is used as in figure 3.1.

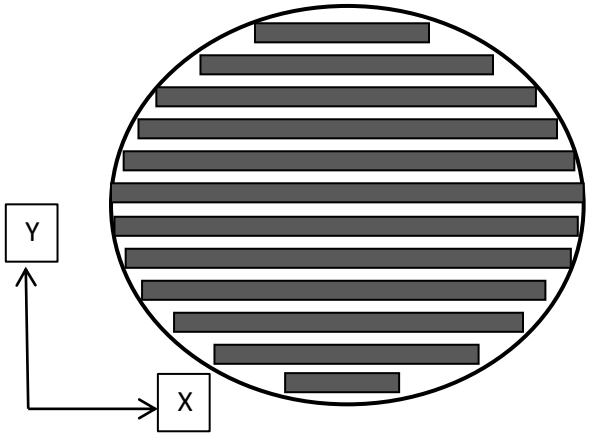


**Figure 3.2: Cross-section of a thermocline tank filled with concrete plates standing vertical within the tank.**

### 3.2 MODELING BASIS

In order to model the structured concrete thermocline, the geometries of the filler material must be broken down into easily represented modeling designs. The first geometry was the rectangular prisms of concrete with holes running vertically throughout the tank. Rectangular prisms prove very difficult to model because the symmetry of the block falls on a finite number of planes. In order to simplify the model, the concrete rectangular prisms were represented by concrete cylinders with cylindrical holes running vertically throughout the height. By doing this, the filler material cells become axisymmetric: symmetrical around a common axis. The common axis is the center of each cylindrical hole, on the z-axis. The deletion of the corners of the rectangular prisms is considered negligible in regards to energy storage. The cross-section for the tank which shows the actual representation of the thermocline system considered by the model is shown in figure 3.3.

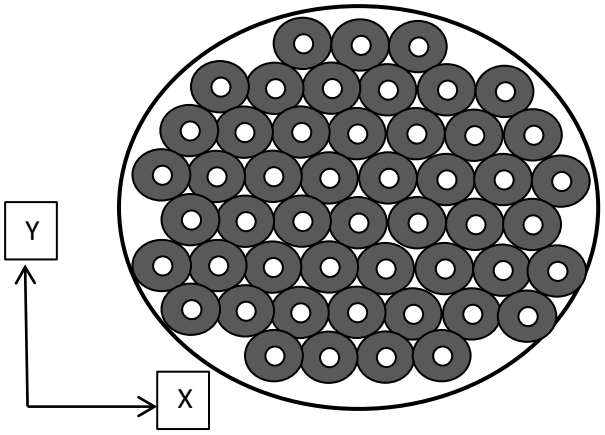


**Figure 3.3: Modeling representation of a cross-section of a thermocline tank with axisymmetric concrete cylinders with cylindrical holes running vertically throughout the tank.**

The second geometry was concrete plates standing vertically within the thermocline tank. This type of geometry proves to be very simple to model. Because of this, the plates can be

modeled as the basic geometry shown in figure 3.2. No further adjustment to the geometry is needed. To set up the model, the plate is broken into sections that are one meter wide. So, the tank and filler material will be represented by figure 3.4. Each space between the red lines is representative of a one meter width of the concrete plate filler material. From this one meter width of the plate, the energy stored and energy retrieved will be calculated.

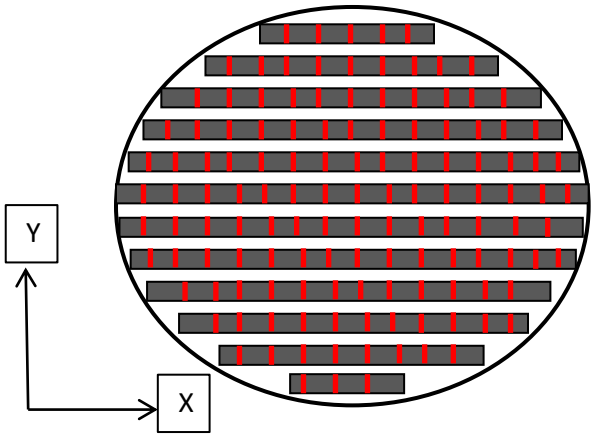


**Figure 3.4: Modeling representation of a cross-section of a thermocline tank with concrete plates standing vertical within the tank.**

### 3.3 AXISYMMETRIC MODEL

The first geometry of cylindrical concrete cells with cylindrical holes running vertically throughout the height of the tank is modeled as an axisymmetric model. The HTF being used in this research is molten solar salt that runs through the holes in the concrete cells. In a thermocline system, heat is transferred from the HTF to the filler material. The axisymmetric model makes the heat transfer from the fluid to the storage material uniform throughout each concrete cell at each specific distance into the tank. As the HTF continues to flow through the tank, the concrete cells heat up further into the tank causing more of the volume of the concrete cell to be fully charged with thermal energy.

In this model, it is assumed that each concrete cell will behave the same. This means that each cell will be charged or discharged with heat equally at each specific height in the tank. Because of this, the thermocline tank, as shown in figure 3.3 will be originally modeled as one single cell. The energy that is stored and released from that single cell can be multiplied by the number of cells in the tank to determine the total amount of energy stored and released from the system. Figure 3.5 represents how the model will produce each cell. Notice that the model represents each cell as if it was lying horizontal. This is not to be confused with how each cell will actually be within the tank, which is standing vertical. Horizontal orientation was only done for ease of modeling. The effect of gravity on the outcome of the model is considered negligible because of the slow operating velocities, so there is no concern when orienting the model in a horizontal direction. The axis orientation is the same as that presented in figure 3.1.

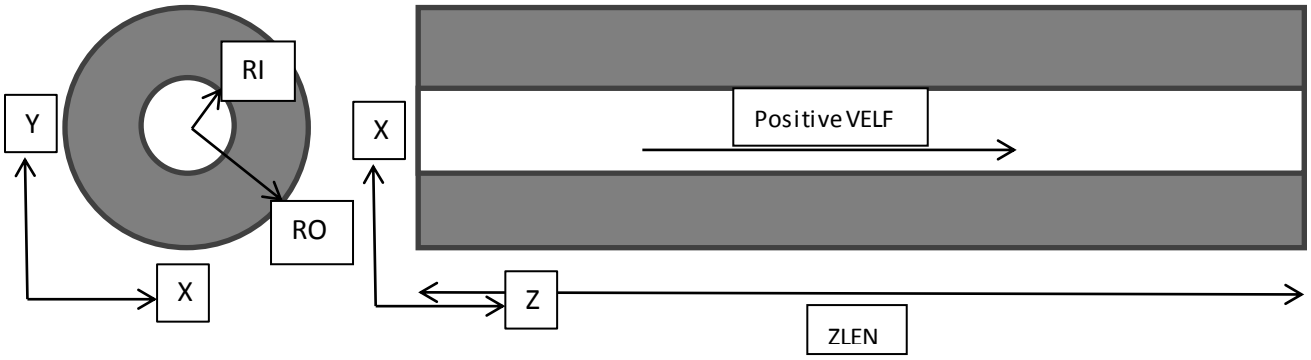


**Figure 3.5: Axisymmetric model layout**

RI = radius of the flow channel for the molten salt

RO = total radius of each cell, including the flow channel and thickness of the concrete storage material

Positive VELF = velocity of the HTF as it travels through the structured concrete thermocline system (positive = charging the system, negative = discharging the system)

ZLEN = height of the structured concrete filler material within the tank (0 = top, zlen = bottom)

### 3.4 2-DIMENSIONAL PLATE MODEL

The second geometry used was concrete plates standing vertically within the thermocline tank. This type of filler was modeled using a 2-dimensional plate model. Like the axisymmetric model, the heat transfer from the HTF to the concrete storage material is considered uniform at each specific height in the tank. As the HTF continues to flow through the tank, the concrete plates heat up further into the tank causing more volume of the concrete plates to be fully charged with thermal energy.

In this model, it is assumed that each concrete plate will behave the same. This means that the heat transfer will be uniform for each plate at each specific height in the tank. Because of this, the thermocline tank shown in figure 3.4 will be modeled as one half of a plate and one half of a flow channel for the HTF. This is done because only half of each plate will be charged or discharged from each flow channel while the next flow channel over will charge or discharge the other half of the plate. Also, only half of the energy presented in each flow channel will be stored in each plate while the other half is stored in the plate on the opposing side of the channel. The modeling representation of this is shown in figure 3.6. Again, notice that the model represents each cell as if it was lying horizontal. This is not to be confused with how each cell will actually be within the tank, which is standing vertical. Horizontal orientation was only done for ease of modeling. The effect of gravity on the outcome of the model is considered negligible because of the slow operating velocities, so there is no concern when orienting the model in a horizontal direction. The same axis orientation is used in this figure as in figure 3.1.

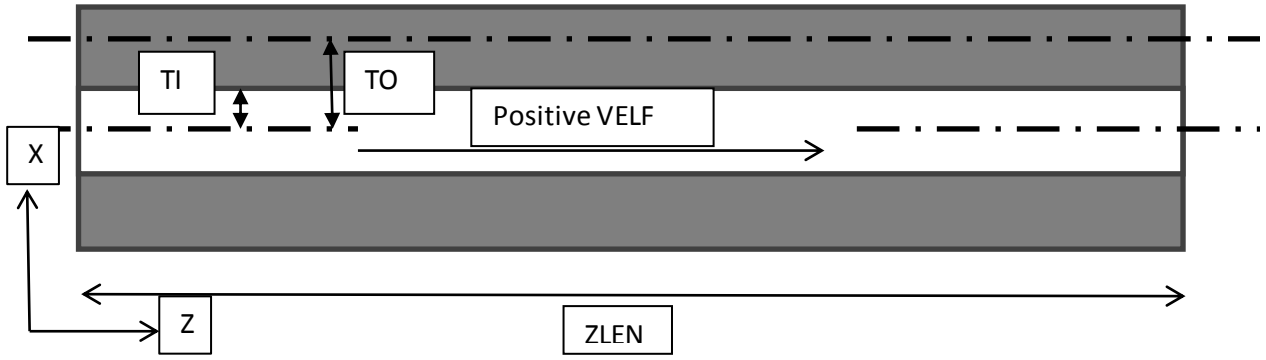


**Figure 3.6: 2-D plate model layout**

TI = half of the thickness of each flow channel in the tank

TO = total thickness of the modeling area, which is half of the thickness of the flow channel plus half of the thickness of a plate

Positive VELF = velocity of the HTF as it travels through the structured concrete thermocline system (positive = charging the system, negative = discharging the system)

ZLEN = height of the structured concrete filler material within the tank (0 = top, zlen = bottom)

The amount of energy stored and retrieved is represented by a meter width of the plate. To determine the total amount of energy stored and released from the system, the energy stored per meter width would need to be multiplied by two to get the full thickness of the plate and then by the total width of all of the concrete plates within the tank.

**3.5 MODELING EQUATIONS**

The basis of the modeling programs is finite difference method (FDM). Both of the types of models are based off of similar equations with only minor differences. The models are based off of internal flow with internal forced convection. There are two resisting forces when transferring heat in a thermal storage unit. First is at the surface of the storage material, at the interface of the liquid and solid. Second is within the storage material as the heat transfers from the interface of the solid and the liquid to the interior (Schmidt and Willmott 1981). Since the

heat transfer is not negligible inside of the storage material, both the material and the HTF must be taken into account via modeling equations.

### *3.5.1 Fluid and Material Equations*

The concrete proposed will have a thermal gradient throughout the volume of the material. Due to this, a heat diffusion equation must be used so that the amount of energy taken into the material is accurately portrayed. The heat diffusion equation for the energy in the storage material is represented by equation 3-1 (Selvam 2011).

$$\frac{1}{\alpha_m}\frac{\partial T_m}{\partial t} = \frac{1}{r}\frac{\partial}{\partial r}\left(r\frac{\partial T_m}{\partial r}\right) + \frac{\partial^2 T_m}{\partial z^2} \tag{3-1}$$

$\alpha_m$ = thermal diffusivity of the material

$T_m$ = temperature of the material

t = time

r = radius

z = distance along the length of the system

The difference between the axisymmetric model and the 2-D plate model is that the 2-D plate model uses a value of one (1) for the radius. This is due to the program taking a unit width of the plate for each specific height in the tank and not a cylindrical concrete cell.

Equally, since the fluid is losing thermal energy to the storage material, an equation had to be derived in order to accurately portray the heat transfer of the fluid to the storage material. To be able to add the equation to the program, a rearranged and simplified internal forced convection equation was derived. The effect of the liquid at the interface of the solid and the energy loss of the fluid as it runs through the concrete is shown by equation 3-2 (Selvam 2011).

$$\frac{\partial T_f}{\partial t} + v\frac{\partial T_f}{\partial z} + \frac{hP}{S_f \rho_f c_f}\left(T_f - T_m\right) = 0 \tag{3-2}$$

$T_f$ = temperature of the fluid

h = convective heat transfer coefficient

P = perimeter of the fluid flow

$S_f$ = cross sectional area of the fluid flow

$\rho_f$ = density of the fluid

$c_f$ = specific heat of the fluid

$T_f$ = temperature of the fluid

### *3.5.2 Boundary Conditions*

To run the models, certain boundary conditions were put in place. These boundary conditions are used to make the model simpler for ease of use of the programs. An illustration of these boundary conditions for both the axisymmetric model and the 2-D plate model can be seen in figure 3.7 at the end of this section.

The boundary condition to make the outer surface adiabatic is shown in equation 3-3.

$$\frac{\partial T_m}{\partial n} = 0 \tag{3-3}$$

n = normal to the outer surface

The boundary condition to have a constant heat flux at the interface of the fluid and the material is represented by equation 3-4.

$$k_m \frac{\partial T_m}{\partial r} = h\left(T_m - T_f\right) \tag{3-4}$$

$k_m$ = thermal conductivity of the material

The boundary condition for the change in the fluid temperature at the ends of the length used in the model is represented by equation 3-5.

$$\frac{\partial T_f}{\partial z} = 0 \tag{3-5}$$

The charging half-cycle of a thermocline is when hot fluid enters the top of the tank and cold fluid leaves the bottom. For this aspect of the thermocline, a boundary condition is put in place for the fluid starting at the entrance of the length of the model which is represented by equation 3-6. This boundary condition is only applied to the modeling program that represents the charging half-cycle.

$$@\ z = 0, T_f = T_{hot} \tag{3-6}$$

$T_{hot}$ = hot operating temperature of the fluid

Likewise, the discharge half-cycle must have a similar boundary condition. This is when the cold fluid flows into the bottom of the tank and the hot fluid leaves the top of the tank. This is represented by the boundary condition in equation 3-7.

$$@z = L, T_f = T_{cold} \tag{3-7}$$

$T_{cold}$= cold operating temperature of the fluid

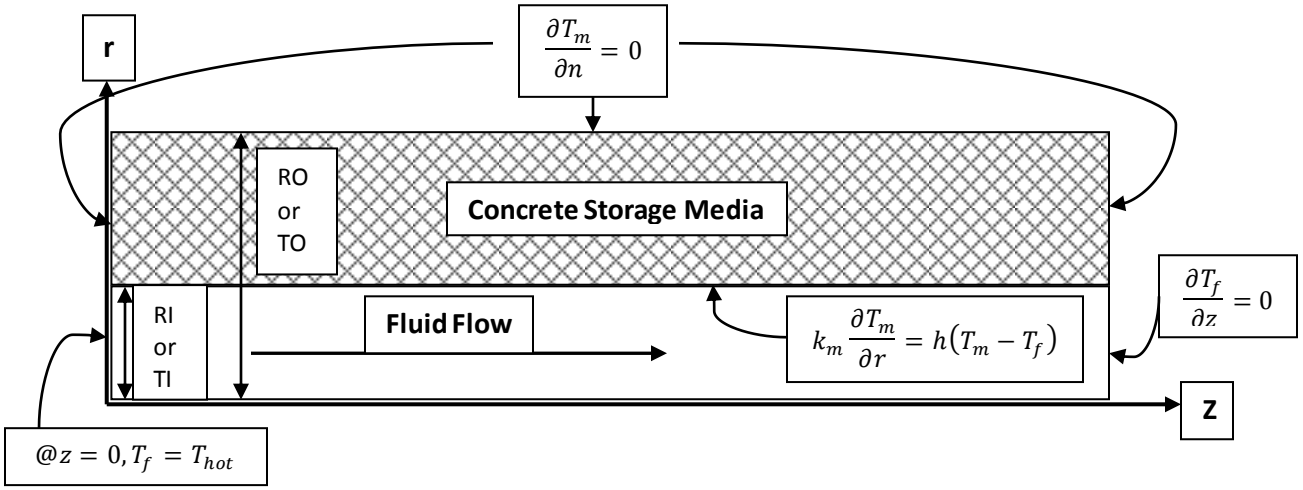


**Figure 3.7: Boundary conditions represented on the model**

### 3.6 MODELING ASSUMPTIONS

The works of other researchers, who are referenced in this section, help lay down a basis for the beginning of the modeling phase of this thesis. From these basic thermocline assumptions, the modeling can be done:

1. There must be a thermal stratification inside of the tank at all times. This means that there will always be hot liquid and cold liquid in the tank.
    a. The thermocline region (this is the area of thermal stratification) will either be resting on the bottom of the tank or at the top of the tank. When it isn't resting, it is either moving towards the bottom during charging or towards the top during discharging.
    b. This is important because it eliminates the chances of mixing within the tank. If the HTF mixes inside of the tank, the outlet temperatures cannot be controlled. This leads to lowering the efficiency of the system because the discharge phase would have different temperature liquids coming out of the tank which causes problems in the conversion to superheated steam for electric generation (Yang and Garimella 2010a; Hess and Miller 1982).
2. The thermocline region must be as narrow as possible.
    a. The narrower the thermocline region, the more volume within the tank that can be heated to its full potential.
    b. This is important because the more volume that is heated to the full potential of the storage medium, the more energy that is stored. The more energy that is stored means more energy that can be extracted later on, even after losses, which increases the efficiency of the region.

3. The velocity of the fluid within the tank will be extremely slow.
    a. According to Hess and Miller (1981), the velocities within a thermocline tank are in the range of 0.2-0.3 cm/s (0.002-0.003 m/s)
    b. Similar numbers were derived from Faas et al (1986) at Solar One in California.
    c. This is important because the low velocity lets the salt transfer its heat energy to the storage medium completely so that energy is not wasted. It is also important because it helps to prevent mixing within the tank, which ruins the thermocline region.
4. The inner radius/inner thickness in the model has to be as small as possible. This is the area within the model that coincides to the space that salt would flow through.
    a. One of the key factors for a thermocline system is that the cost is reduced when compared to a two tank design. The key part to doing this is reducing the amount of the high cost HTF. This means that as little salt needs to be used as possible within the system. If there is less space for the salt to pass through and fill, then less salt needs to be used. A large inner radius/inner thickness would mean that more salt is being used than economically viable.
5. Along with the inner radius/inner thickness being as small as possible, the outer radius/outer thickness has to be as large as possible. This is the area within the model that coincides to the space that is occupied by the concrete.
    a. This is important because the more concrete that is present, the more storage medium there is that can be charged and discharged for energy.

b. This is also important because it reduces the amount of salt that has to be added to the system.

### 3.7 CHARGING HALF-CYCLE INPUT DATA

The charging half-cycle is the first part of the TES daily cycle. The input data for this cycle is different than the input data for the discharging half-cycle, which is the second part of the TES daily cycle. Both models, along with the basic assumptions, have similar input data for the charging half-cycle. The input file looks similar to the version shown in figure 3.8.

**tc-i.txt**

```
101, 51, 16, 0.025, 0.05, 1
1804, 1520, 0.53, 0.003, 46.22
2243, 750, 2, 300, 585, 300, 14400
    READ (1,*) IM, JM, ZLEN, RI, RO, NTUBE
    READ (1,*) DENF, CPF, TKF, VELF, HTRFS
    READ (1,*) DENM, CPM, TKM, TEMFI, TEMFM, TEMSI, TTIME
C    IM = 101          Number of points along the tube
C    JM =51            Number of points along the radial direction
C    ZLEN = 16         Length of the tube - meters
C    RI = 0.025        Inner radius - meters
C    RO = 0.05         Outer radius - meters
C    NTUBE = 1         Number of tubes to calculate total energy
C    DENF = 1804       Density of fluid - kg/m3-solar salt
C    CPF = 1520        Specific heat of fluid at constant pressure - J/kg.K - solar salt
C    TKF = 0.53        Thermal conductivity of fluid - W/m.k - solar salt
C    VELF = 0.003      Velocity of fluid - m/s
C    HTRFS = 46.22     Convection heat transfer coefficient - W/m2.K
C    DENM = 2243       Density of material - kg/m3 - concrete
C    CPM = 750         Specific heat of solid at constant pressure - J/kg.K - concrete
C    TKM = 2           Thermal conductivity of solid - W/m.k - concrete
C    TEMFI = 300       Initial temperature of the fluid - C
C    TEMFM = 585       Maximum temperature of the fluid - C
C    TEMSI = 300       Initial temperature of the solid - C
C    TTIME = 4*3600    Total time to run the model – seconds
```

**Figure 3.8: Input file example for modeling programs**

The values provided in the input file in figure 3.8 are actual values used in the models that are run. Most of the values are set so that there is a baseline for all of the models to compare. Densities, thermal conductivities, specific heat, and operating temperatures (initial and

maximum temperature of the fluid) are actual values for the materials used (Coastal Chemical 2011). John (2011) evaluated the thermal conductivity of the specially designed concrete mixtures and the value shown is an average for the mixes.

The convection heat transfer coefficient is a calculated value for a constant surface heat flux boundary condition shown in equation 3-4. The value is calculated from the basic equation for circular tubes with laminar flow (Çengel and Ghajar 2011). It is presented in equation 3-8.

$$Nu = \frac{hD}{k} = 4.36 \tag{3-8}$$

Nu = Nusselt number for laminar flow

h = convective heat transfer coefficient

D = diameter of flow path

k = thermal conductivity of the fluid

The number 4.36 is used as the Nusselt number because the thermocline is considered laminar flow. Laminar flow is used because the Reynolds number, represented by equation 3-9, is determined to be less than 2300. Also the Prandtl number, represented by equation 3-10 is determined to be greater than 0.6 (Çengel and Ghajar 2011).

$$Re = \frac{VD}{\nu} \tag{3-9}$$

Re = Reynolds number

V = velocity of the flow

ν = kinematic viscosity of the fluid

$$Pr = \frac{\nu}{\alpha} \tag{3-10}$$

Pr = Prandtl number

α = diffusivity of heat

The length used in the model is set at sixteen (16) m. This coincides with Pacheco et al. (2002) and their modeling parameters. This allows for a comparison of the model in order to check the initial thermocline zone shapes as well as the viability of the system.

To optimize the model, four (4) variables are changed: inner radius, outer radius, velocity of the fluid, and time. All four of these input values can drastically change the models. These variables were optimized so that the most efficient thermocline set-up could be accomplished. It is important to get a model that is similar to those that are found in literature so that the programs created can be validated.

## 3.8 CHARGING HALF-CYCLE OUPUT FILES

### *3.8.1 Axisymmetric Output Files*

The program writes four (4) files as it is run. One of the files is not used for evaluation of the charging program. This program file is written and combines all of the data from the charging program. It remains unused until the discharging program is run. This file, along with the input file used for the discharging program, coordinates the collaboration of the two programs. From this, discharge data are produced.

Three (3) useful output files were produced when running the charging model program. The first output file showed the amount of energy stored in the system for the specific charging time being modeled, as well as the power being used by the system. This is calculated using the NTUBE variable. The total energy stored is proportional to the number of tubes in the system and therefore is proportional to the amount of storage material that is present in the system. This variable was held constant at one (1) tube so that the models could be compared. Also shown on this plot is the amount of power being used by the modeled system. This is important because

the model needs to use the maximum amount of power for the longest period of time. An example of the visualization of this type of output file is shown in figure 3.9.

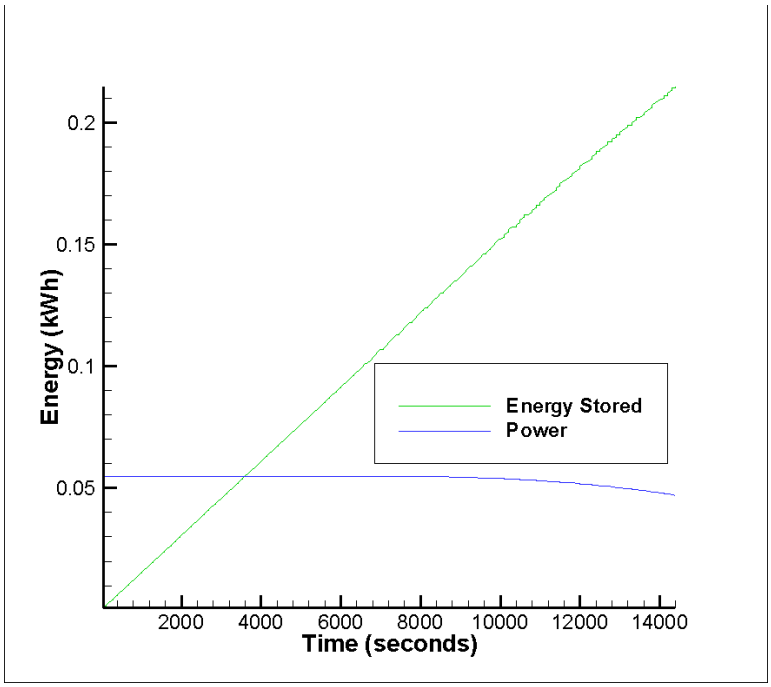


**Figure 3.9: Example of axisymmetric output file for energy stored and power used**

The second file was a temperature gradient plot. This showed the position of the thermocline zone along the length of the thermocline during five (5) equal time steps during the charging period with the last step being at the end of the charging time. This is comparable to figure 2.7 in section 2.4.4. The key to the thermocline zone is that it takes up as little space as possible so that a maximum amount of the solid material can be completely charged with thermal energy. An example of the visualization of the output file is shown in figure 3.10. The term "bed height" on the horizontal axis represents the depth in the thermocline tank. The height is set at 16 m. Reading on the output graph from any number on the horizontal axis represents that specific depth into the thermocline tank. The zero (0) position represents the top of the tank; the 16 position represents the bottom of the tank.

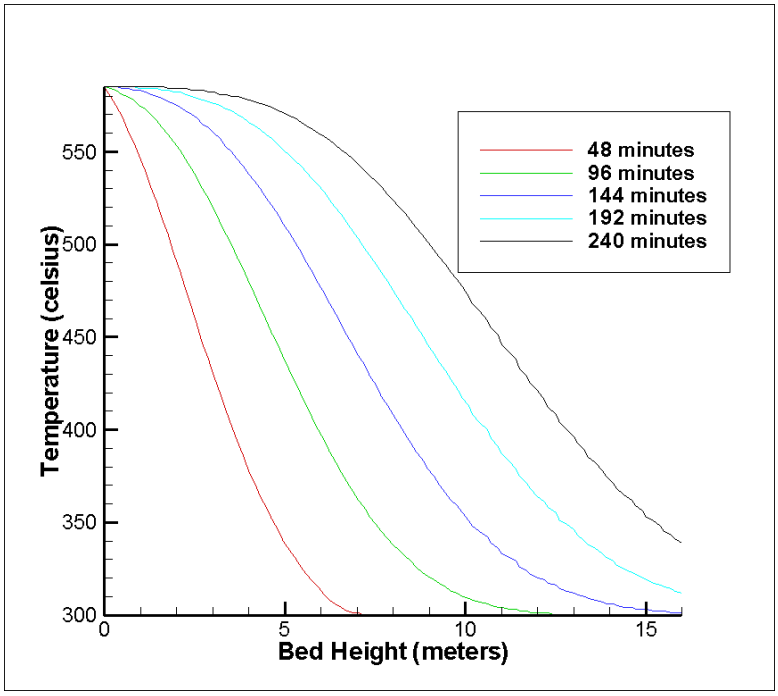


**Figure 3.10: Example of axisymmetric output file for thermocline zone movement**

The third output file illustrated how the concrete storage material reacted to the thermal stratification moving throughout the thermocline tank. This file was similar to the second file showing the thermocline zone movement in the fluid. The difference between the two files is that this file shows the temperature of the concrete storage material at the RO distance from the center of the flow channel for the molten salt at five (5) equal time steps during the charging period with the last step being at the end of the period. An example of the visualization of this output file is shown in figure 3.11. Again, the "bed height" horizontal axis represents the depth into the 16 m thermocline tank.

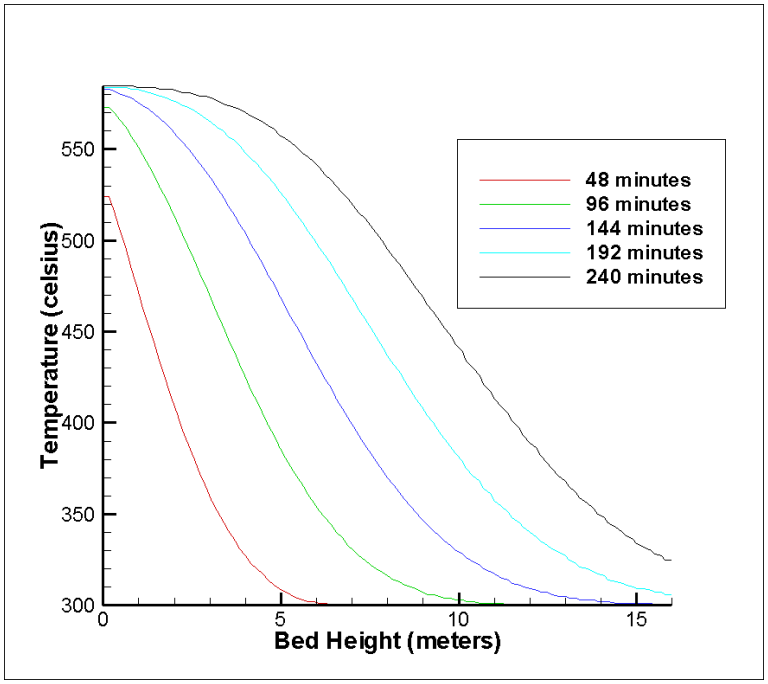


**Figure 3.11: Example of axisymmetric output file for the concrete temperature at the furthest point from the flow channel for each thermal cell**

### *3.8.2 2-Dimensional Plate Output Files*

Like the axisymmetric model, a file is written combining all of the data from the charging program. This file is not used until the discharging program is run. It coordinates the collaboration of the charging and discharging program.

The output files for the 2-D plate model are very similar to the ones found in the axisymmetric model. There are three output files that are produced. All three files read the same as the ones found for the axisymmetric model. The first output file shows the amount of energy stored by the system, as well as the power being used by the system, for the amount of time that the system is charged. For this model, the NTUBE variable is held constant at one (1). This is done due to the fact that the radius in the model is recorded as one (1). To find the total amount of energy stored by the system, the data from this output file would be multiplied by two (2) to get the thickness of a full plate, and then by the total amount of storage material.

The second output file showed the temperature gradient in the fluid throughout the tank. This was done at five (5) equal time steps through the charging period with the last step being the temperature distribution at the end of the charging period. Also added for this program was an initial temperature line to show what happens to the fluid directly at the beginning of the charging half-cycle. An example of the visualization of this output file is shown in figure 3.12. Like the axisymmetric model, the "bed height" horizontal axis is representative of the depth in the thermocline tank.

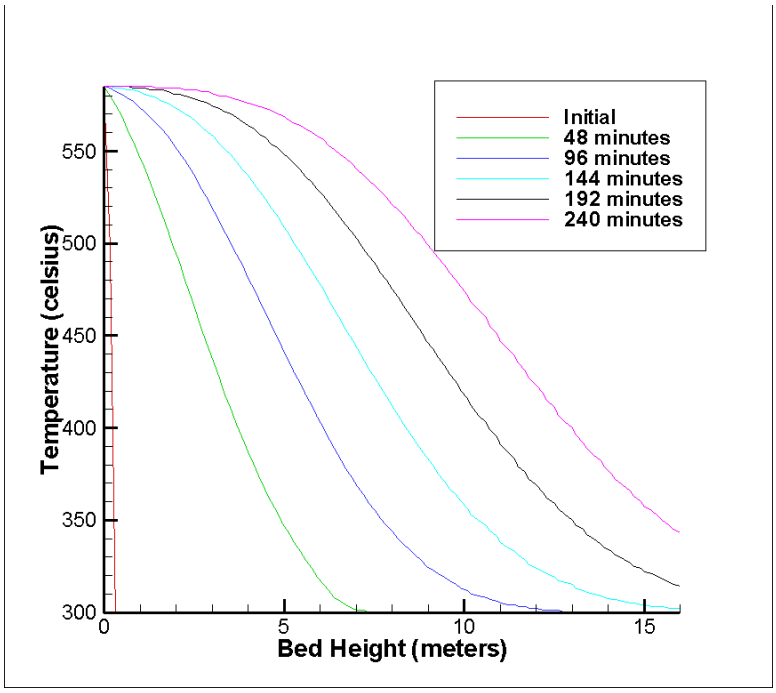


**Figure 3.12: Example of 2-D plate output file for thermocline zone movement**

The third output file for the 2-D plate program was the temperature distribution at the center of each concrete plate, also known as the TO distance. This is the outer thickness for the modeling program which is half the thickness of the plate. This allowed for determining the amount of useful storage space as it was a reflection of the effect of the fluids thermocline zone on the storage material. This output file was also broken into five (5) equal time steps over the

charging period and an initial step showing what happens to the concrete at the beginning of the charging period. An example of the visualization for this output file is shown in figure 3.13.

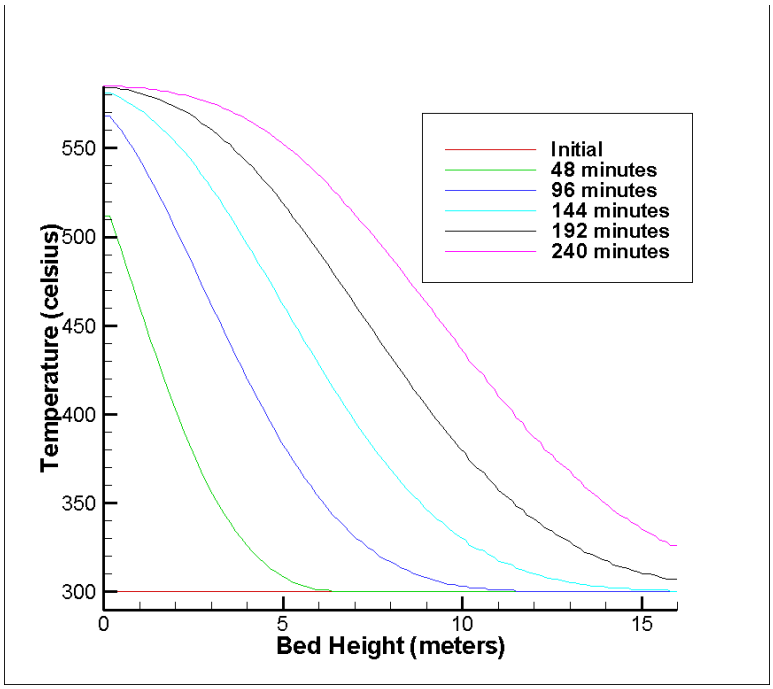


**Figure 3.13: Example of 2-D plate output file for the concrete temperature at the furthest point from the flow channel for each concrete plate**

## 3.9 DISCHARGING HALF-CYCLE DATA

### *3.9.1 Input File Data*

The input data for the discharging half-cycle is similar for both programs to the input data for the charging half-cycle shown in figure 3.8 presented in section 3.7. The difference between the input file for the charging program and the input file for the discharging program is the velocity of flow. The velocity term is entered as a negative number. Referring to figures 3.5 and 3.6, notice that the positive velocity goes from the position z equal to zero (0) to position z equal to ZLEN. Since discharging is done from the bottom of the tank, the velocity of flow must flow in the direction from position z equal to ZLEN to position z equal to zero (0). Because of this, the velocity term is negative.

Another factor that is different is that the program does not use the TEMSI variable that is recorded in the file. The value for this variable comes from the recorded data that the charging program produces.

Only two variables are allowed to change in the discharge program. Since the discharge program relies on data from the charging program, all of the variables stay the same for material properties, plus the addition of the RI, TI, RO, and TO variables. This makes the amount of concrete storage material the same for the charging and discharging program. The only variables that are allowed to vary are the time variable, TTIME, and the velocity variable, VELF. Both of these variables can realistically be adjusted in practice to extract the most amount of energy from the system.

### *3.9.2 Output File Data*

The output files that come from the discharging modeling program are similar to those that come from the charging modeling program. Three files come from the modeling program. One is the energy retrieved and power output file, one is the thermocline zone movement, and one is the temperature distribution at the outer thickness or radius distance for the concrete filler material.

An example of the first output file visualization with the energy retrieved and power being used by the system over the discharging time is shown in figure 3.14. An example of the thermocline zone movement visualization is shown in figure 3.15. An example of the concrete temperature distribution at the outermost concrete thickness or radius is shown in figure 3.16.

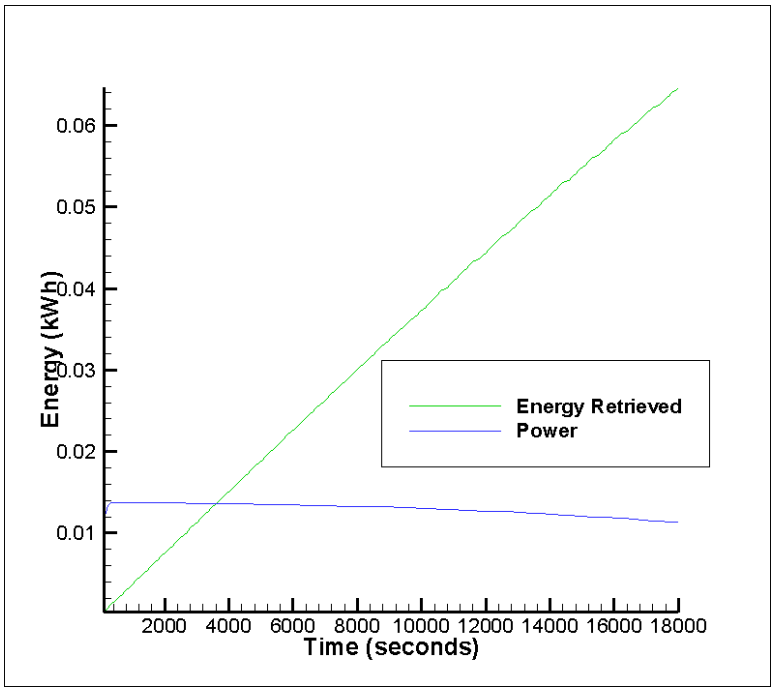


**Figure 3.14: Example of output file for discharging energy retrieved and power**

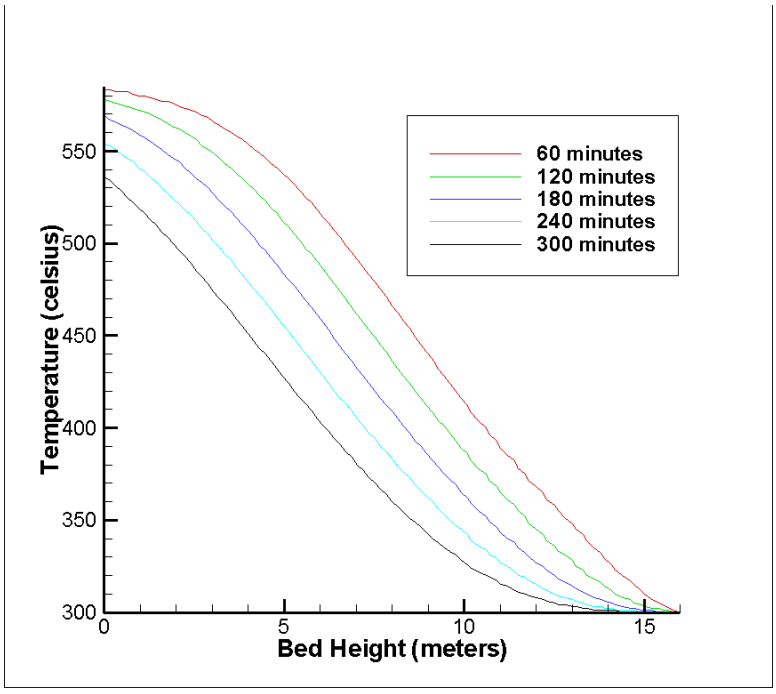


**Figure 3.15: Example of discharge output file for thermocline zone movement**

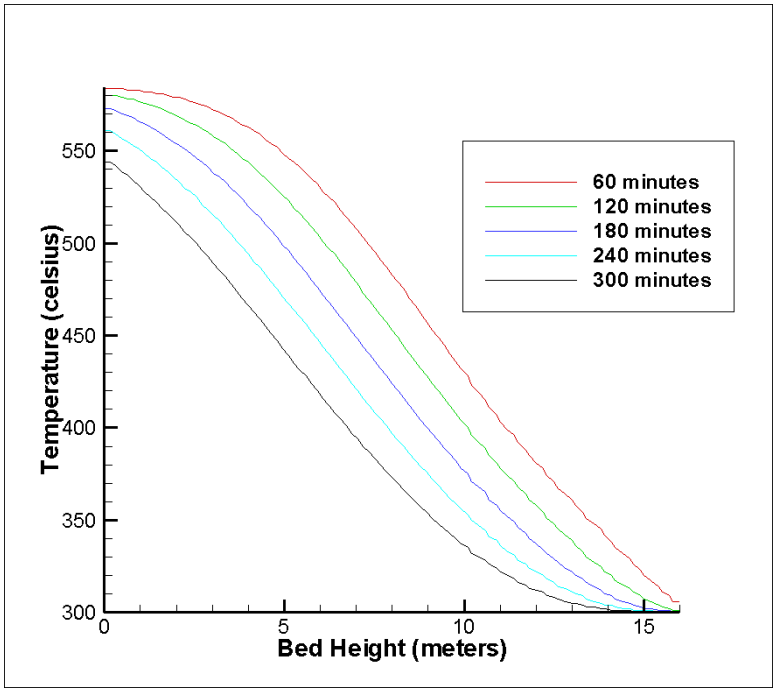


**Figure 3.16: Example of discharge output file for concrete temperature distribution**

# CHAPTER 4: MODELING NUMERICAL ANALYSIS AND VARIABLE TRIALS

## 4.1 CONVERGENCE TESTING

To be sure that the model being used was accurate and precise in the data produced, convergence testing was done. The number of grid points that the storage material consisted of needed to be the optimum number so that a median could be reached between accuracy and program processing speed. Two options for convergence were allowed: in the radial direction out from the flow channel and the z-direction in the length of the flow channel.

### *4.1.1 Radial Convergence*

For the radial direction, it is important to come to a convergence of grid points because it is necessary in accurately predicting the concrete's temperature at the furthest point from the flow channel. The more points added into the grid in this direction allow for more precise predictions due to the energy and heat being transferred between more points. At each point, a specific amount of energy is held in the previous grid square and a specific amount is transferred. Since concrete has a low thermal conductivity, this is important because it allows for the natural thermal gradient within the concrete. Each grid square will have a different temperature, allowing for a more accurate portrayal of the thermal gradient within the storage material. Convergence was done using data from output files produced by the axisymmetric model. Figure 4.1 is a plot of convergence for the radial direction.

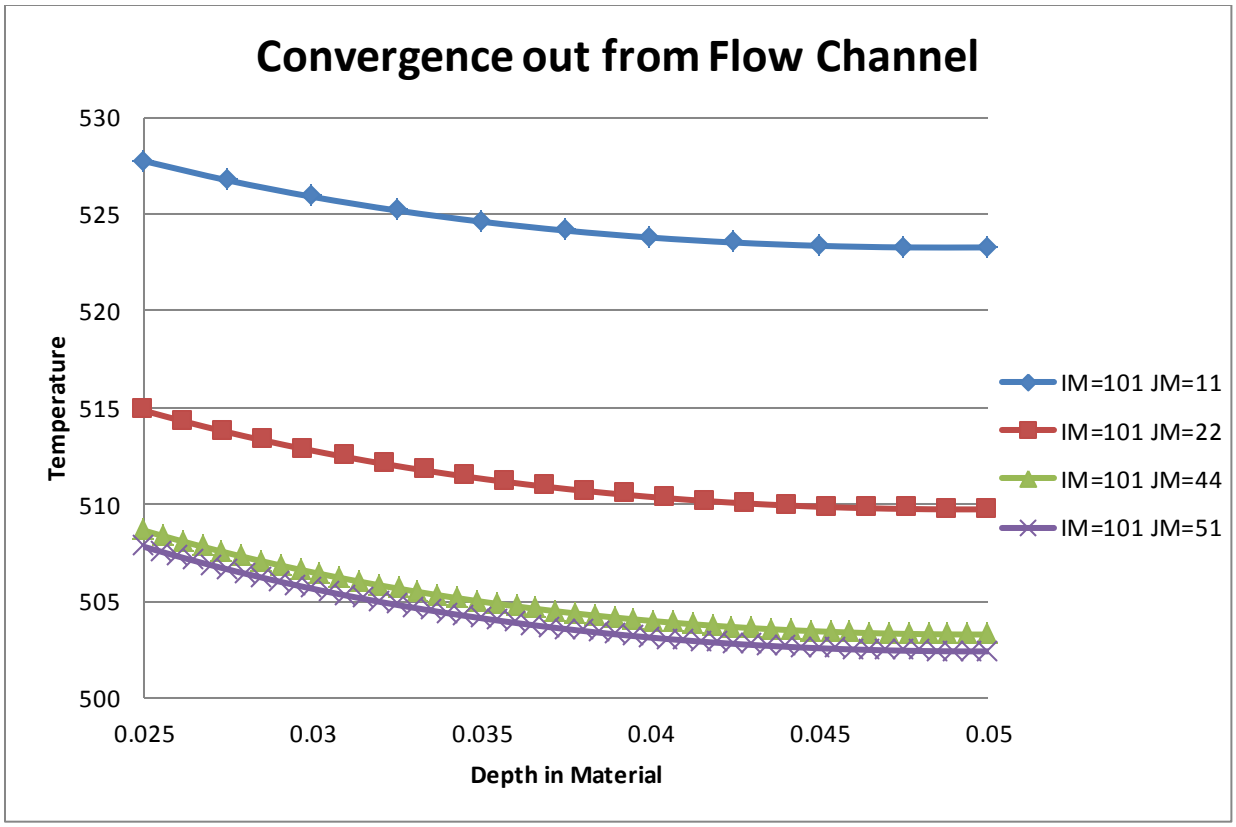


**Figure 4.1: Convergence in the radial direction for modeling programs used**

From the figure it is noted as more grid points are added into the model, the temperature distribution converges to a certain point. Using JM (radial grid points) equal to 51 allows for an accurate portrayal of the data from the model along with a decent running time for the program in use.

### *4.1.2 Axial Convergence*

Convergence along the z-direction of the flow path is an important factor as well. This allows for more points in the model that can take in the energy and heat from the HTF. With more points in this direction comes extra grid squares for the energy to be absorbed at each specific location along the height of the tank. This means that the energy from the HTF will be diminished at a faster rate as it moves throughout the height of the tank. Figure 4.2 is a plot of convergence in the z-direction of the model.

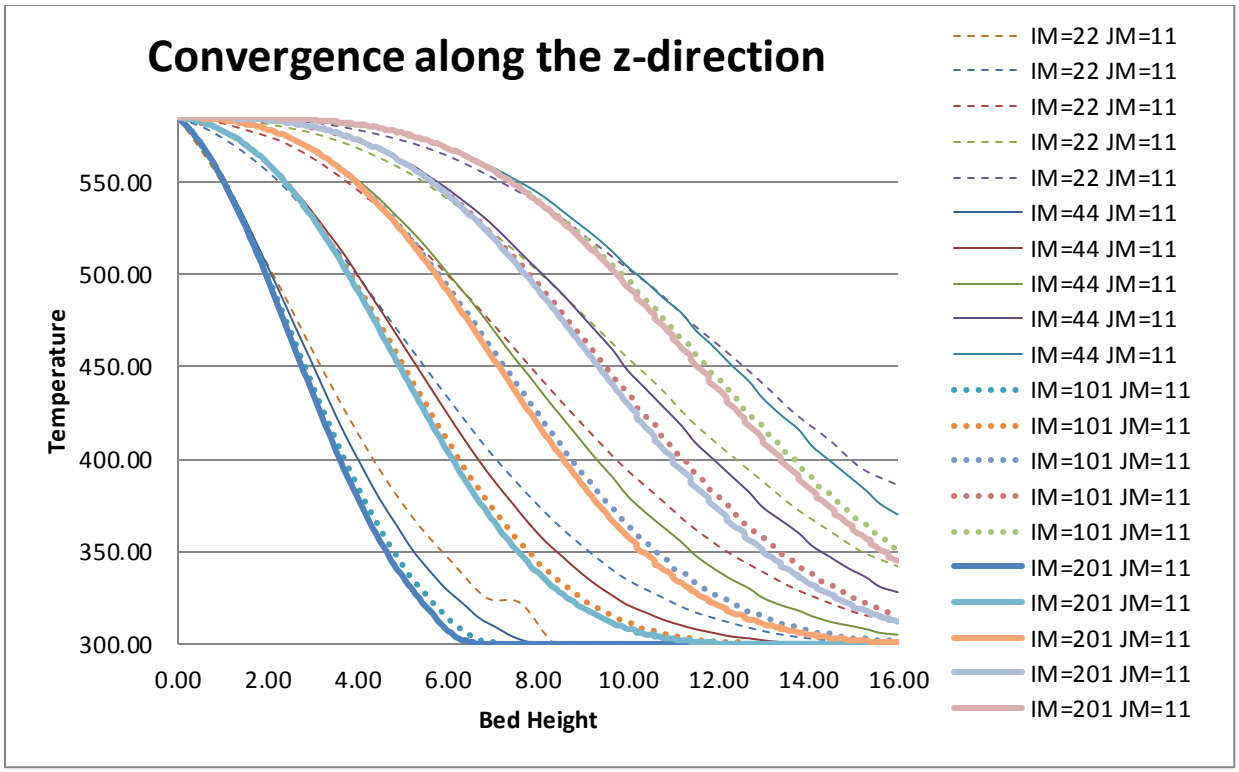


**Figure 4.2: Convergence along the z-direction for modeling program used**

From the figure it is noted as more grid points are added into the model, the temperature distribution converges to a certain point. Using IM (z-direction grid points) equal to 101 allows for an accurate portrayal of data from the model along with a decent running time for the program in use.

## 4.2 VARIABLE TRIALS

The first step that was done to run the models provided by Selvam (2011) was to test the input variables for their effect on the output of the model. It is important when beginning to model a scenario that a good understanding is achieved on the effects certain variables have on the outcome of the model.

The variables that can readily be changed in the model include the time, velocity, inner radius, and outer radius. The time relates to the time it takes to charge the system during the charging half-cycle in the plant or to discharge the system during the discharging half-cycle. The

correct velocity must be chosen for the salt flowing through the thermocline so that optimal heat transfer occurs between the liquid and the solid storage material for both the charging and discharging half-cycles. The inner radius/inner thickness is the size of the flow path that the salt will take through the thermocline tank. The outer radius/outer thickness correspond to the total amount of solid concrete storage media that is present to be able to store the thermal energy within the thermocline tank.

There are variables in the input files that can be changed but are held constant in order to keep similarities within the models for comparison. The variables include the length of the thermocline tank, the number of tubes used, and the temperature range. For modeling purposes, the thermocline tank was taken to be sixteen (16) meters in length. This was done for comparison to the models done by Pacheco et al. (2002). The number of tubes kept in the modeling procedure was set at one (1) tube. This was done so that the axisymmetric model and the 2-D plate model could be compared. The temperature range was set for 300° C to 585°C because those are the high and low operating temperatures for the HITEC solar salt used for this type of system (Coastal Chemical Company 2011) and are the values for salt temperatures used in the previous large scale testing apparatus used for research at the University of Arkansas (Skinner 2011).

### *4.2.1 Effects of Time*

To understand the effect that charging time had on the model, two iterations were run using the same variables with only the time variable being changed. Table 4.1 shows the input variables used in the two cases. For both of these cases, a larger modeling set-up was run using the axisymmetric model. There were a total of sixteen (16) tubes accounted for in order to retrieve larger numbers for power and energy stored for comparison purposes.

**Table 4.1: Time Variable Trial**

| | Velocity (m/s) | RI (m) | RO (m) | Time (min) |
|---|---|---|---|---|
| **Case 1** | 0.002 | 0.0254 | 0.0635 | *240* |
| **Case 2** | 0.002 | 0.0254 | 0.0635 | *360* |

Case 1 uses a time of 240 minutes (4 hrs) while case 2 uses a time of 360 minutes (6 hrs). This change in charging time is illustrated in a comparison presented in figure 4.3 of the fluid temperature distribution plot for thermocline zone movement.

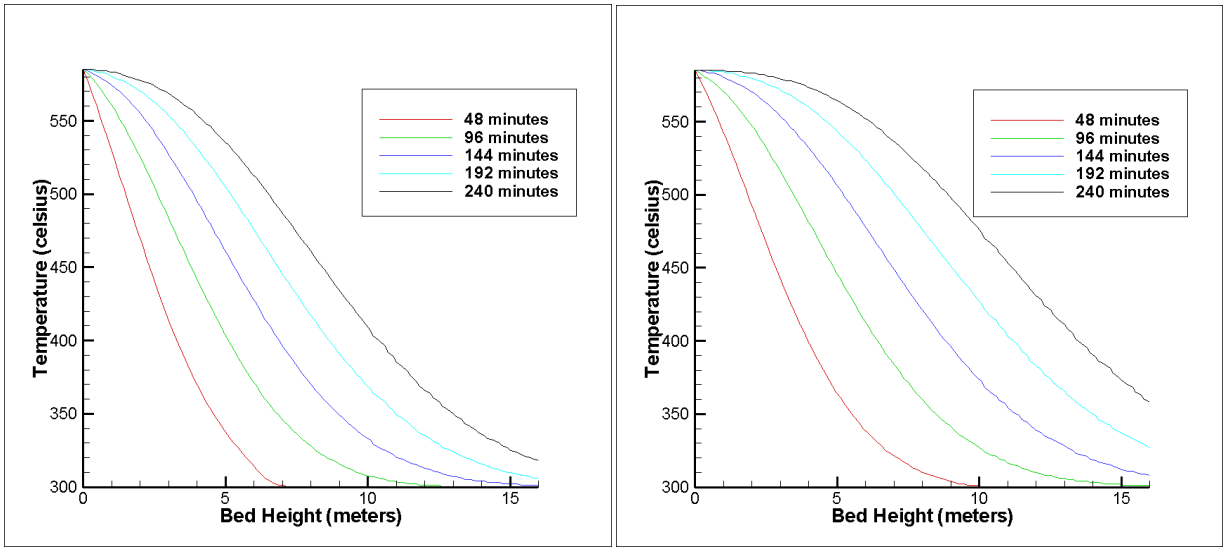


**Figure 4.3: Temperature comparison between Case 1 (left) and Case 2 (right) in regards to time change**

When changing the time variable, the fluid temperature distribution plot showed more of the concrete filler taking thermal energy from the molten salt, depicted by the rise in fluid temperature leaving the thermocline at the end of the charging half-cycle. This is to be expected because there is more time that the high temperature salt is in contact with the concrete filler. The problem is that the longer the salt flows through the thermocline tank, the wasted energy is increased. This is represented in figure 4.4 by the drop in useful power in the system between the four and six hour charging periods.

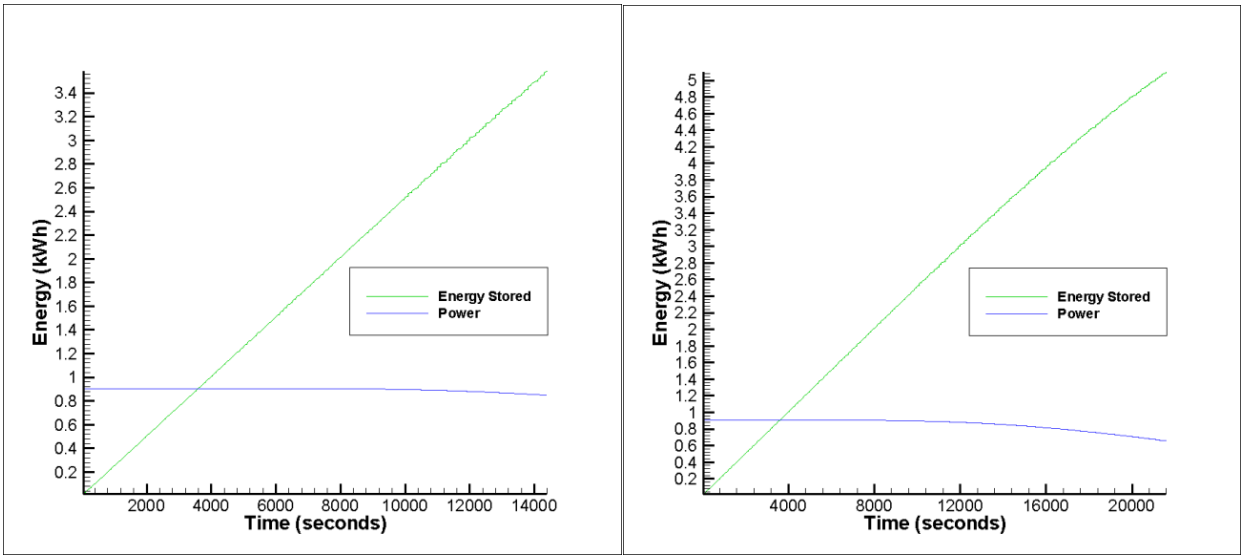


**Figure 4.4: Energy stored and power for Case 1 (left) and Case 2 (right) in regards to time change**

Since, according to the model, the plant could put out roughly 0.9 kWh of energy to this system, not using that much energy throughout the charging period would be a waste of energy. Not all of the energy that is available to the system is being pulled out of the molten salt. Therefore, the salt is then returning to the collector field above the cool operating temperature and is not able to receive a full new supply of energy to be transferred to the TES system. This means that the time should be managed to where the exit temperature of the fluid does not increase above the cold operating temperature.

Since the axisymmetric and 2-D plate model are similar in structure, the time variable was assumed to be equally effective in both models. Test cases run for the 2-D plate model proved this to be true.

### *4.2.2 Effects of Velocity*

To understand the effect that the velocity had on the model, two iterations were run using the same variables with only the velocity variable being changed. Table 4.2 shows the input parameters for the two cases. For both of these cases as well, a larger modeling set-up was run

using the axisymmetric model. There were a total of sixteen (16) tubes accounted for in the system in order to retrieve larger numbers for power and energy stored for comparison purposes.

**Table 4.2: Velocity Variable Trial**

| | Velocity (m/s) | RI (m) | RO (m) | Time (min) |
|---|---|---|---|---|
| **Case 3** | *0.002* | 0.01905 | 0.04445 | 240 |
| **Case 4** | *0.003* | 0.01905 | 0.04445 | 240 |

Case 3 uses a velocity of 0.002 m/s while case 4 uses a velocity of 0.003 m/s. The comparison of the temperature distribution plots is presented in figure 4.5 for the change in charging velocities.

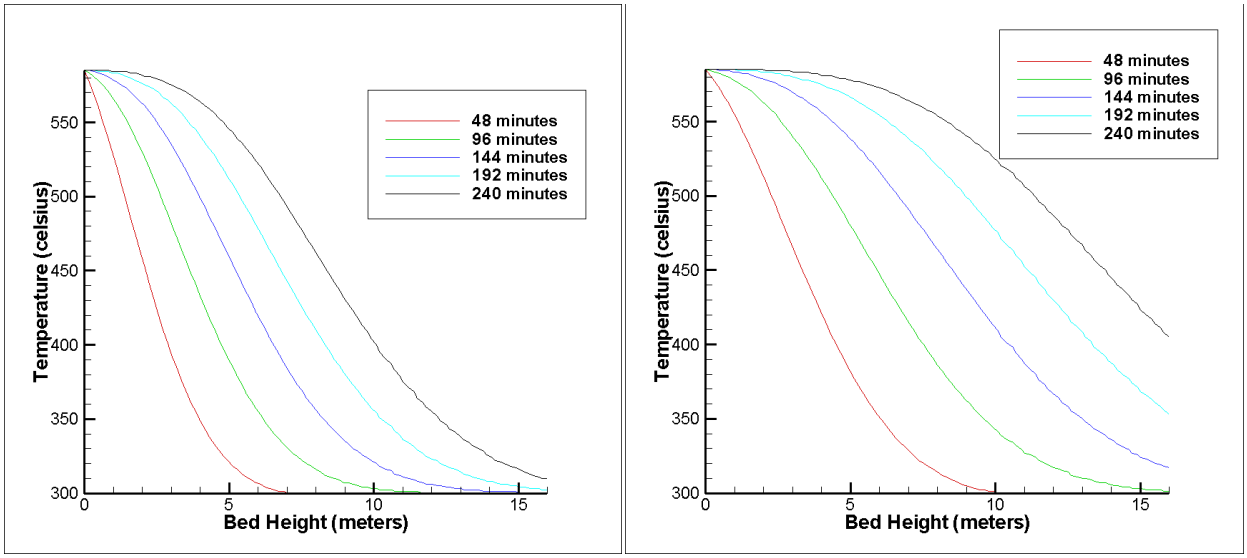


**Figure 4.5: Temperature comparison between Case 3 (left) and Case 4 (right) in regards to velocity**

Again, from the temperature distribution plot, the concrete appeared to be taking more thermal energy from the molten salt. This also happened to show that useful power was being wasted in the system, shown in figure 4.6, which would lower the overall efficiency of the system. This is represented by the drop in power being used by the system to charge the concrete filler material.

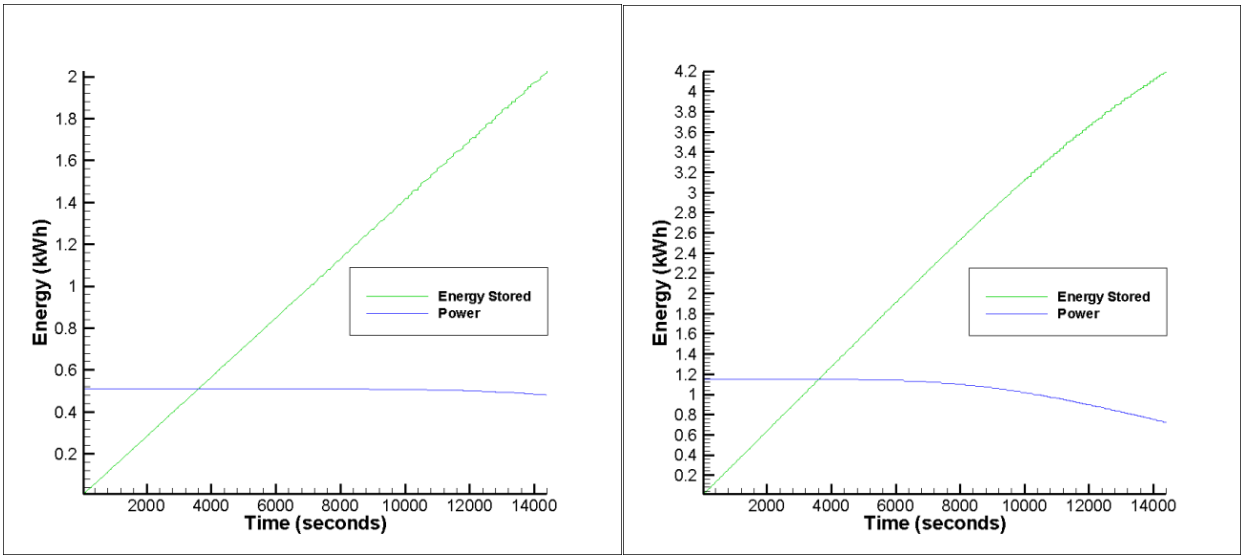


**Figure 4.6: Energy stored and power for Case 3 (left) and Case 4 (right) in regards to velocity**

Since an increase in velocity is presented, the power that is used to run the system is increased from case 3 (0.5 kW) to case 4 (1.15 kW). It is noted though that at the end of the charging period in case 4, there is a significant drop off in the power being used by the system. Again, this means that the salt is not transferring all of its energy to the concrete and therefore cannot gain a maximum amount of new energy in the collector field. This means that the velocity should be selected carefully for specific trial cases to where the exit temperature of the fluid at the end of charging does not exceed the cold operating temperature.

Since the axisymmetric model and the 2-D plate model are similar in structure, it was assumed that both models would be affected by the velocity change similarly. Trial cases run for the 2-D plate model proved this to be true.

### *4.2.3 Effect of Outer Radius*

To understand the effect that the outer radius has on the model, two cases were run while varying the outer radii. Table 4.3 shows the input parameters for the two cases. Again, for both of these cases, a larger modeling set-up was run using the axisymmetric model. There were a

total of sixteen (16) tubes accounted for in order to retrieve larger numbers for power and energy stored for comparison purposes.

**Table 4.3: Outer Radius Variable Trial**

| | Velocity (m/s) | RI (m) | RO (m) | Time (min) |
|---|---|---|---|---|
| **Case 5** | 0.002 | 0.0254 | *0.0635* | 240 |
| **Case 6** | 0.002 | 0.0254 | *0.0762* | 240 |

Case 5 uses an outer radius of 0.0635 m while case 6 uses an outer radius of 0.0762 m. The temperature distribution plots for the movement of the thermocline zone in these two cases are shown in figure 4.7.

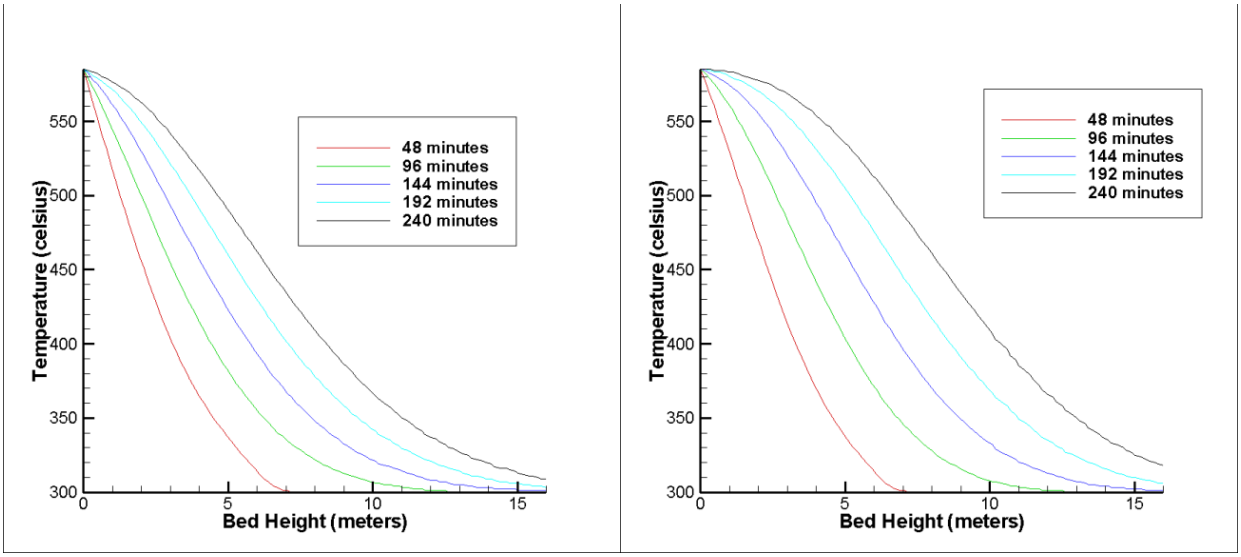


**Figure 4.7: Temperature comparison between Case 5 (left) and Case 6 (right) in regards to RO**

In these temperature distribution plots, it was noted that the increase in the outer radius allowed for a more developed thermocline zone with more thermal energy being put into the concrete storage material. This can be seen as case 6 shows more filler bed height holding more increased temperature volumes than in case 5. It is noted, though, that the increase in outer radius, which signifies an increase in storage material volume, does not make an addition to the

energy being stored by the system. This is shown in figure 4.8 as the energy stored remains roughly the same. It is noted that there is actually a slight increase in energy stored for case 5 (3.61 KWh) over case 6 (3.59 KWh).

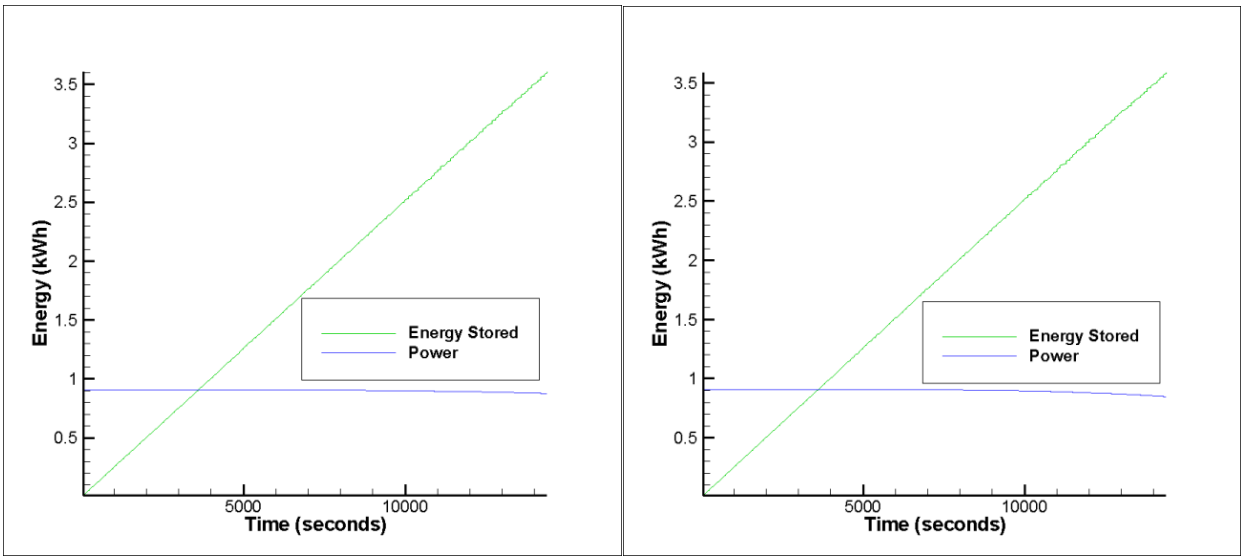


**Figure 4.8: Energy stored and power for Case 5 (left) and Case 6 (right) in regards to RO**

This is an interesting observation due to the fact that the increase in storage volume does not necessarily mean an increase in energy that can be stored in the system. When designing the system, a certain volume has to be taken up by the storage material. Each cell of concrete will take up a certain amount of space. Increasing the size of the cell means that the thermocline TES system will physically take up more space which increases the cost. The outer radius value must be optimized so that the system can remain as small as possible to reduce costs. This means increase the outer radius until further increasing does not change the amount of energy being stored.

### *4.2.4 Effect of Outer Thickness*

The next point of interest was using the 2-D plate model to check the effect of increasing the outer thickness. It is important to check also the effects of this thickness on the 2-D plate model because the geometry is different compared to the axisymmetric model. This means that

the thickness should have a different effect. Table 4.4 shows the input parameters for the two cases. In these two cases, only one unit width of the plate is taken for comparison because the program accurately portrays one meter. Multiplication can be done to determine the energy stored by the entire system.

**Table 4.4: Outer Thickness Variable Trial**

| | **Velocity (m/s)** | **TI (m)** | **TO (m)** | **Time (min)** |
|---|---|---|---|---|
| **Case 7** | 0.002 | 0.0127 | *0.0508* | 240 |
| **Case 8** | 0.002 | 0.0127 | *0.0635* | 240 |

The fluid temperature distribution is shown in figure 4.9, the concrete temperature distribution is shown in figure 4.10, and the stored energy and power is shown in figure 4.11. The concrete temperature distribution was added to the program in order to check the findings in section 4.2.3. The concrete needs to be checked for how much of the volume actually is heated to its full potential.

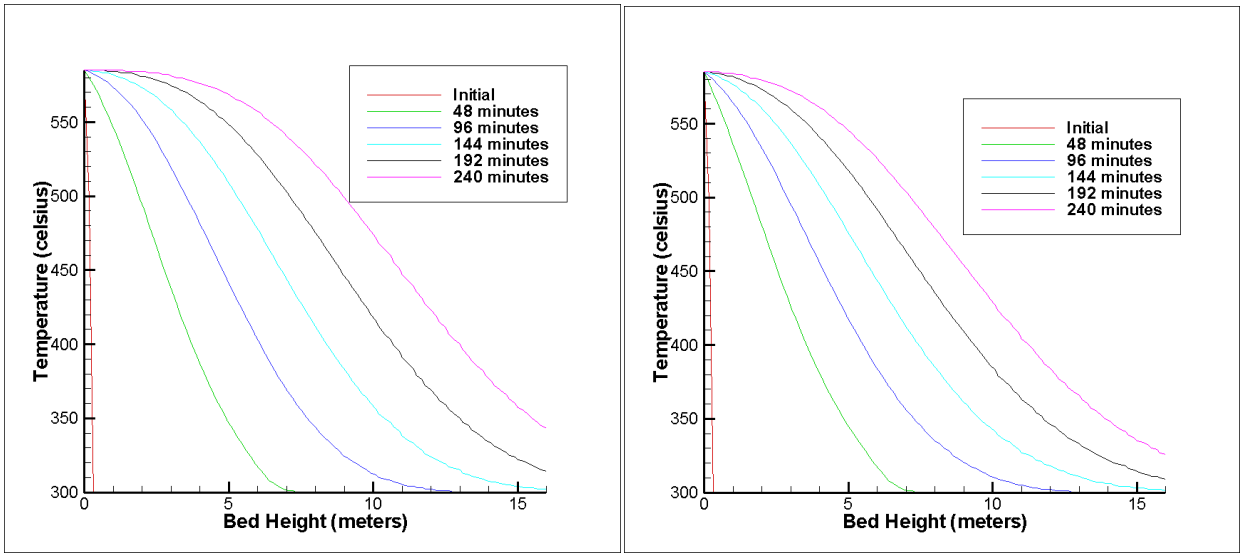


**Figure 4.9: Fluid temperature distribution for Case 7 (left) and Case 8 (right) in regards to TO**

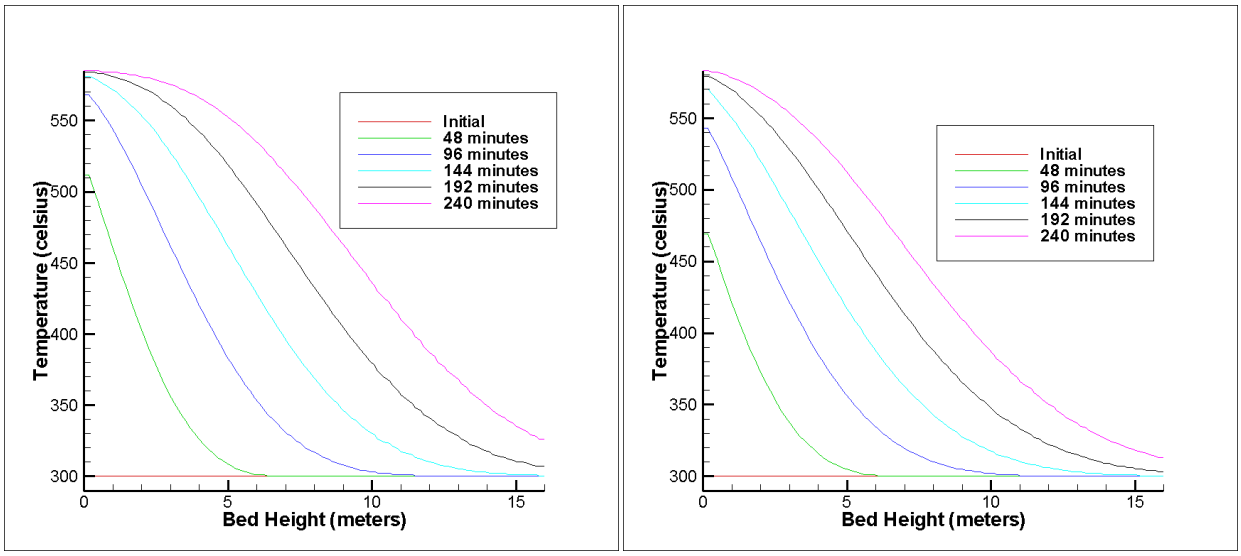


**Figure 4.10: Concrete temperature distribution for Case 7 (right) and Case 8 (left) in regards to TO**

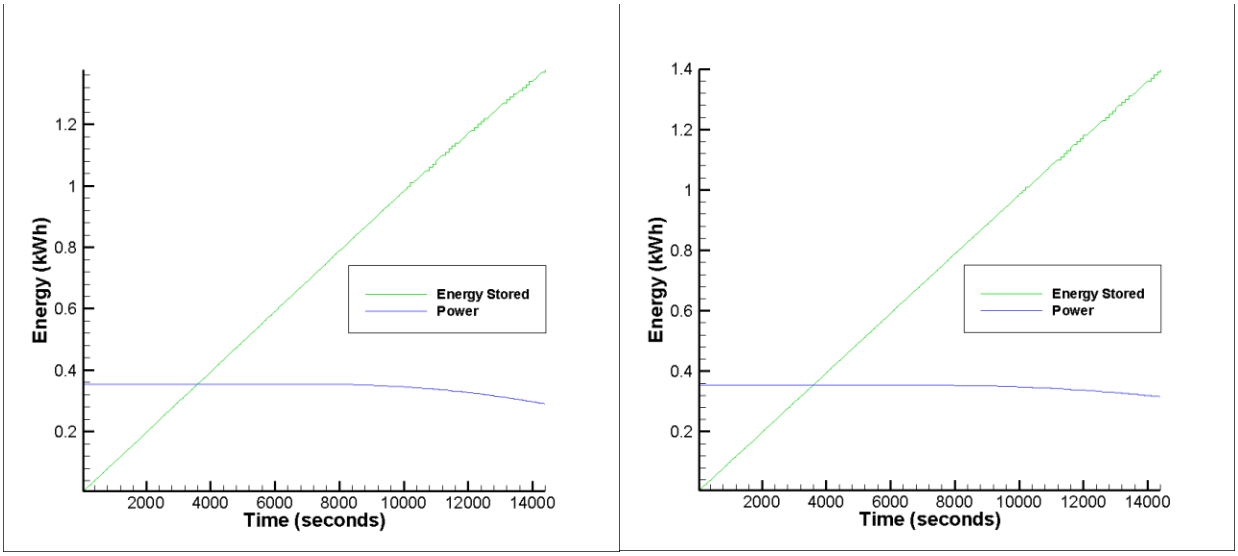


**Figure 4.11: Energy stored and power for the Case 7 (right) and Case 8 (left) in regards to TO.**

It is interesting to note that even though the thermocline zone in the tank for the increased outer thickness of case 8 seems to decrease in size with less of the material having a high outer surface temperature, the amount of energy stored increases and there is less wasted power. This means that the outer thickness can be increased up until energy storage is not increasing. The

important factor for this variable is the thermocline zone. Degradation of the thermocline zone during charging can cause a decrease in efficiency of the system.

### 4.3 CONCLUSIONS

The information gained from the variable trials was used in the actual modeling done for optimizing the geometric designs used in both the axisymmetric model and the 2-D plate model. Important information that was discovered included:

- The velocity must remain at a very low point of 0.003 m/s or less in order to keep the required thermocline shape.
- The time for charging and discharging must remain below six (6) hours because charging time is limited in a CSP plant and an increased charging time causes a degradation of the thermocline zone as well as a loss in useful power.
- The outer radius of the axisymmetric model must be increased to a point where any further increase leaves the energy being stored at a constant value.
- The outer thickness of the 2-D plate model must be increased to a point where the full amount of energy that can be stored in the system is stored in the system. The thermocline shape and zone movement must still be present.

# CHAPTER 5: MODELING RESULTS AND DISCUSSION

The preliminary modeling for the variable trials and the convergence of the FDM grid described in chapter 4 of this thesis paved the way for full testing of the modeling programs developed for this project which are described in chapter 3 of this thesis. Both modeling programs were exhausted with trials in order to fine tune the optimal combination of fluid velocities, charging and discharging times, inner radius/thickness, and outer radius/thickness. The results for both the axisymmetric model and the 2-D plate model follow in this chapter.

## 5.1 AXISYMMETRIC MODELING RESULTS

The axisymmetric modeling program represented the use of cylindrical concrete cells that stood vertical in a thermocline tank and had a cylindrical channel running vertically throughout the height of the cell for the fluid to flow through. This program was the first program to be run in the completion of this research. Because of this, a larger number of specific cases were run to fine tune the original thermocline zone shape, as well as fine tuning the effect of the changeable variables in the program.

### *5.1.1 Modeling Procedure*

The first step in determining the optimized setup for the axisymmetric program was conducting charging half-cycles, which are the first part of the daily TES cycle for the plant. The program "tcline3.exe" by Selvam (2011) was used for this step. The inner radius, outer radius, velocity, and time were all varied in order to achieve a thermocline zone that was able to move throughout the thermocline tank. At first, an inner radius and outer radius were set and were not changed. Then the velocity variable and time variable were changed in order to change the thermocline zone shape. Once the exit temperature at the end of the charging period began to

rise, the model was considered optimized for the inner and outer radius considered. Next, the outer radius was increased in small increments and the velocity and time variable were changed to optimize the increased outer radius. Finally, iterations were run for different inner radii while changing the velocity and time variables. Table 5.1 illustrates the range of values and the set values for the variables in the input file that can be changed.

**Table 5.1: Axisymmetric Changeable Variables for Charging Input**

| Variable | Range |
|---|---|
| **Inner Radius** | 0.0127 m - 0.03175 m |
| **Outer Radius** | 0.04445 m – 0.0762 m |
| **Time** | 4 hr – 6 hr |
| **Velocity** | 0.0015 m/s – 0.01 m/s |
| **Number of Tubes** | 1 tube |
| **Length of the Thermocline** | 16 m |
| **Temperature Range** | 300° C - 585° C |

The next step in running the program, after the charging half-cycle was optimized, was the optimization of the discharging half-cycle using "tcline42.exe" created by Selvam (2011). This was a simpler task with fewer steps because only two variables could be changed when adjusting this program: velocity and time. This is because after the charging half-cycle is run, the inner radius and outer radius are held constant for the discharging half-cycle. The velocity and time were varied to where the exit temperature at the top of the tank did not become lower than 500° C after the half-cycle was completed. A slower velocity was used in this program due to difficulty retrieving the energy that had been stored in the system. The range for the velocity during discharging was from 0.001 m/s to 0.015 m/s. Five (5) and six (6) hour discharge times were used because they produced the best results for energy retrieved. All other variables that could be changed in the model were held constant, as in table 5.1.

Once both programs were optimized for a specific case, the discharge efficiency was calculated to determine the efficiency of the system. This was done by comparing the energy stored in the system to the energy retrieved from the system.

### *5.1.2 Axisymmetric Modeling Results and Discussion*

Table 5.2 is a list of the 32 recorded trial cases run for the axisymmetric program. More trials were run but were not included in the table due to the fact that they consisted of extreme data that did not abide by the modeling assumptions listed in section 3.6 of this thesis. Charging (denoted by a "c" subscript) and discharging (denoted by a "d" subscript) data are listed in the table as well as discharge efficiencies. Energy stored (ES) and energy retrieved (ER) are also listed. Cases that have "Did Not Meet Thermocline Shape Standards" in the place of the discharging data represent cases that did not qualify as thermocline systems because the exit temperatures in the charging half-cycle were either too high, causing a loss of thermal stratification, or the thermocline zone did not move far enough through the tank, causing a low energy storage amount. These cases were then adjusted to achieve an adequate thermocline region and were recorded, or were aborted when a thermocline region was not able to be adequately achieved.

**Table 5.2: Axisymmetric Modeling Results**

| *Case* | *RI (m)* | *RO (m)* | *$v_c$ (m/s)* | *$t_c$ (hrs)* | *ES (kWh)* | *$v_d$ (m/s)* | *$t_d$ (hrs)* | *ER (kWh)* | *Eff.(%)* |
|---|---|---|---|---|---|---|---|---|---|
| **1** | 0.025 | 0.05 | 0.003 | 6 | *Did Not Meet Thermocline Shape Standards* | | | | |
| **2** | 0.025 | 0.05 | 0.003 | 4 | | | | | |
| **3** | 0.025 | 0.05 | 0.002 | 6 | | | | | |
| ***4a*** | 0.025 | 0.05 | 0.002 | 4 | 0.215 | 0.001 | 5 | 0.0647 | 30.09 |
| ***4b*** | 0.025 | 0.05 | 0.0015 | 5 | 0.153 | 0.001 | 5 | 0.0645 | 42.16 |
| ***4c*** | 0.025 | 0.05 | 0.0015 | 5 | 0.153 | 0.0015 | 5 | 0.0959 | 62.68 |
| ***4d*** | 0.025 | 0.05 | 0.0015 | 5 | 0.153 | 0.001 | 6 | 0.0754 | 49.28 |
| **5** | 0.0254 | 0.0508 | 0.003 | 4 | *Did Not Meet Thermocline Shape Standards* | | | | |
| **6** | 0.03175 | 0.0508 | 0.003 | 4 | | | | | |
| **7** | 0.03175 | 0.0762 | 0.003 | 4 | | | | | |
| **8** | 0.03175 | 0.0762 | 0.003 | 6 | | | | | |
| **9** | 0.03175 | 0.0762 | 0.01 | 6 | | | | | |
| **10** | 0.03175 | 0.0762 | 0.01 | 4 | | | | | |
| **11** | 0.0254 | 0.0762 | 0.01 | 6 | | | | | |
| **12** | 0.0254 | 0.0762 | 0.002 | 4 | | | | | |
| **13** | 0.0254 | 0.0762 | 0.002 | 6 | | | | | |
| **14** | 0.0254 | 0.0635 | 0.002 | 4 | | | | | |
| ***15a*** | 0.0254 | 0.0635 | 0.002 | 6 | 0.325 | 0.001 | 5 | 0.0669 | 20.58 |
| ***15b*** | 0.0254 | 0.0635 | 0.002 | 6 | 0.325 | 0.0015 | 5 | 0.141 | 43.38 |
| **16** | 0.0127 | 0.0508 | 0.002 | 4 | *Did Not Meet Thermocline Shape Standards* | | | | |
| **17** | 0.0127 | 0.0508 | 0.002 | 6 | | | | | |
| **18** | 0.0127 | 0.0508 | 0.003 | 4 | | | | | |
| **19** | 0.0127 | 0.0508 | 0.003 | 6 | | | | | |
| ***20a*** | 0.01905 | 0.04445 | 0.002 | 4 | 0.127 | 0.001 | 5 | 0.0367 | 28.90 |
| ***20b*** | 0.01905 | 0.04445 | 0.002 | 4 | 0.127 | 0.00125 | 5 | 0.0543 | 42.76 |
| **21** | 0.01905 | 0.04445 | 0.003 | 4 | *Did Not Meet Thermocline Shape Standards* | | | | |
| **22** | 0.0254 | 0.0635 | 0.002 | 4 | 0.225 | 0.001 | 5 | 0.0598 | 26.58 |
| ***23a*** | 0.0254 | 0.0635 | 0.003 | 4 | 0.474 | 0.001 | 5 | 0.0645 | 13.61 |
| ***23b*** | 0.0254 | 0.0635 | 0.003 | 4 | 0.474 | 0.0015 | 5 | 0.135 | 28.48 |
| **24** | 0.0254 | 0.0762 | 0.002 | 4 | *Did Not Meet Thermocline Shape Standards* | | | | |
| **25** | 0.0254 | 0.0762 | 0.003 | 4 | | | | | |
| ***26*** | 0.01905 | 0.0508 | 0.003 | 4 | 0.276 | 0.0015 | 5 | 0.0776 | 28.12 |

Case = Iteration being run

RI = Inner radius

RO = Outer radius

$v_c$ = Velocity during charging

$t_c$ = Time of charging

ES = Energy Stored

$v_d$ = Velocity during discharging

$t_d$ = Time of discharging

ER = Energy Retrieved

Eff. = Discharge efficiency

Notice that multiple cases in table 5.2 are separated into case "#a" and "#b" and one with "#c" and "#d." This represents cases that were able to be adjusted in the discharge half-cycle in order to increase the amount of energy retrieved by the system without sacrificing the thermal stratification in the tank.

To adjust the discharge half-cycle, the time and the velocity could be changed. Review of the data from previous lettered case numbers directed the change of the variables. The majority of the time, the velocity was the value changed. This was done as a result of the tests in case 4b and 4c. As shown in these cases, the increase in discharge efficiency was greatly increased by a slight change in velocity for the system. When looking at the same discharge variables from the previous comparison with only a slight change in the time between case 4b and 4d instead of velocity, the time proves to only increase the efficiency a fraction of the change caused by the velocity.

The efficiencies reported in the table are discharge efficiencies. This means that it is calculating the percentage of the energy that was stored in the system that was able to be retrieved during the discharge half-cycle. Yang and Garimella (2010b) presented discharge efficiencies in their modeling work on thermocline systems. Their packed bed thermocline

system model was adjusted using particle sizes for the packed bed and the height of the tank to come up with discharge efficiencies for set power and energy storage. They had a range of values from 57.6 - 88%. The values presented in table 5.2 reach a maximum discharge efficiency of 62.68% in case 4c.

### *5.1.3: Low Efficiency Case Results*

Low efficiency cases were best illustrated by the discharge temperature distribution output file. If the time steps held a tight configuration during the discharging period, it was noted that the discharge efficiency would be reduced. This was proven by the energy retrieved and power output file. Figure 5.2 shows the comparison between case 15a and 15b, illustrating the difference between a low discharge efficiency (20.58%) and a higher discharge efficiency (43.38%) on the fluid temperature distribution plot. The efficiency was increased by a slight increase in the velocity of the discharge half-cycle from 0.001 m/s to 0.0015 m/s. The same time period of five (5) hours was used.

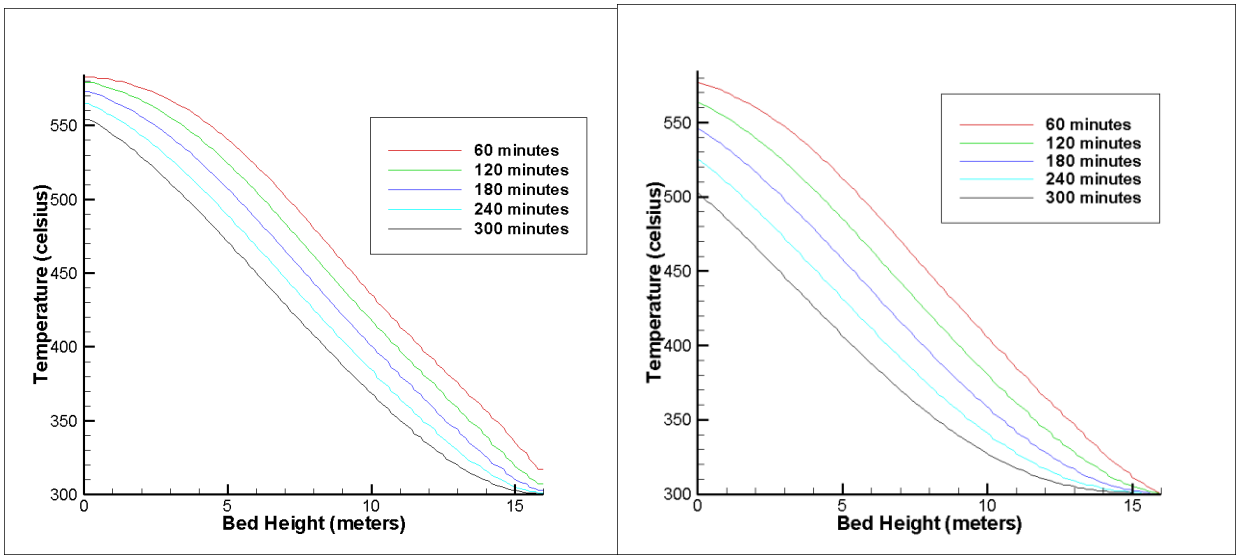


**Figure 5.1: Comparison of discharge output for Case 15a (left) and Case 15b (right)**

The energy stored and power for both cases is shown in figure 5.2. Notice that for case 15a, the energy retrieved reaches 0.0669 kWh while the energy retrieved from case 15b reaches a

higher value of 0.141 kWh. This shows that more of the original energy is retrieved from the system, therefore increasing discharge efficiency.

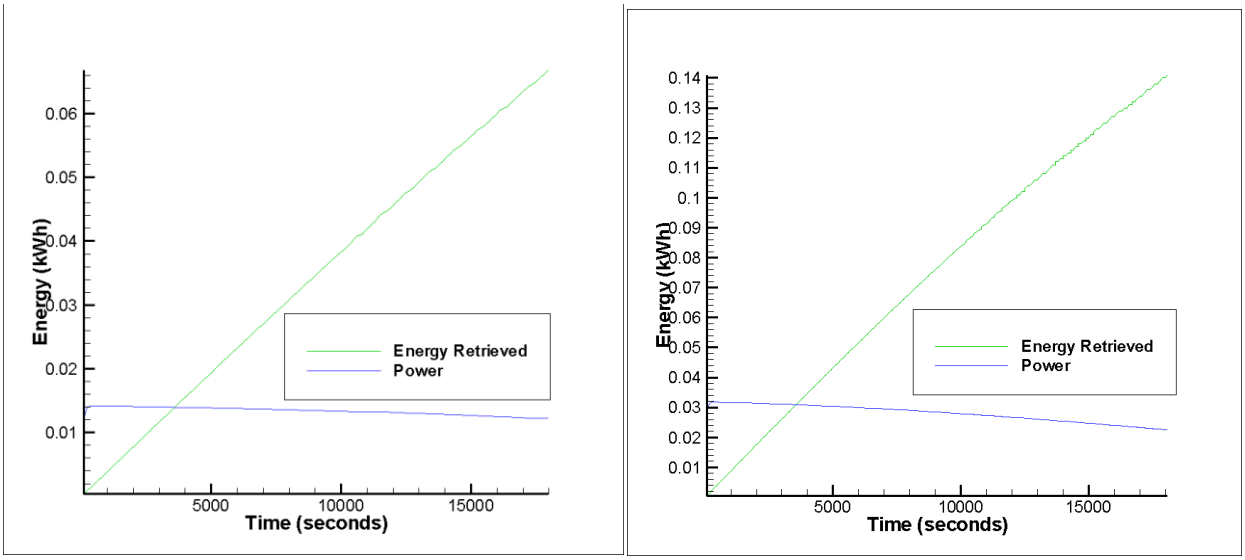


**Figure 5.2: Energy retrieved and power for Case 15a (left) and Case 15b (right)**

### *5.1.4 Optimized Model*

The most efficient thermocline system developed for the axisymmetric model was case 4c in table 5.2. This case had a discharge efficiency of 62.68%. From this data, optimization of the 2-D plate model can be compared. The geometry behind this concrete cell is a 0.025 m inner radius for the fluid flow channel and a 0.05 m outer radius for the total radius of the cell. Table 5.3 summarizes the geometric properties of case 4c.

**Table 5.3: Case 4c physical properties**

| Inner Radius | Inner Area | Outer Radius | Outer Area | Concrete Area | Porosity |
|---|---|---|---|---|---|
| 0.025 m | 0.00196 $m^2$ | 0.050 m | 0.00785 $m^2$ | 0.00589 $m^2$ | 0.25 |

This size of the concrete cell was chosen as a basis for the beginning of the modeling because the porosity of each cell was closely related to the porosities used in other previous research, as reported in section 2.4.2. One of the most important aspects of a thermocline is that

it reduces costs compared to two-tank systems. This is done by using a low cost filler material that displaces the high cost HTF. A porosity of 0.22-0.25 has been used for packed bed system (Brosseau et al. 2005, Flueckiger et al. 2011, Pacheco et al. 2002, Yang and Garimella June 2011)

To understand how the cell reacts to charging and discharging, the thermocline zone shapes need to be compared. Case 4c had the most distinct thermocline shape within the tank out of any of the models run. This shape is important when designing a thermocline system because thermal stratification is the key to a successful and efficient system. Figure 5.3 shows the charging and discharging shape for case 4c. The exit temperature at the end of the charging period was allowed to get up to 385°C for any given case shown in table 5.2. The exit temperature at discharging was allowed to get to within plus or minus ten (10) from 500°C for any given case shown in table 5.2. This allows for the thermocline zone shape to be upheld, as well as allowing for adequate superheating of steam for electrical generation upon discharging.

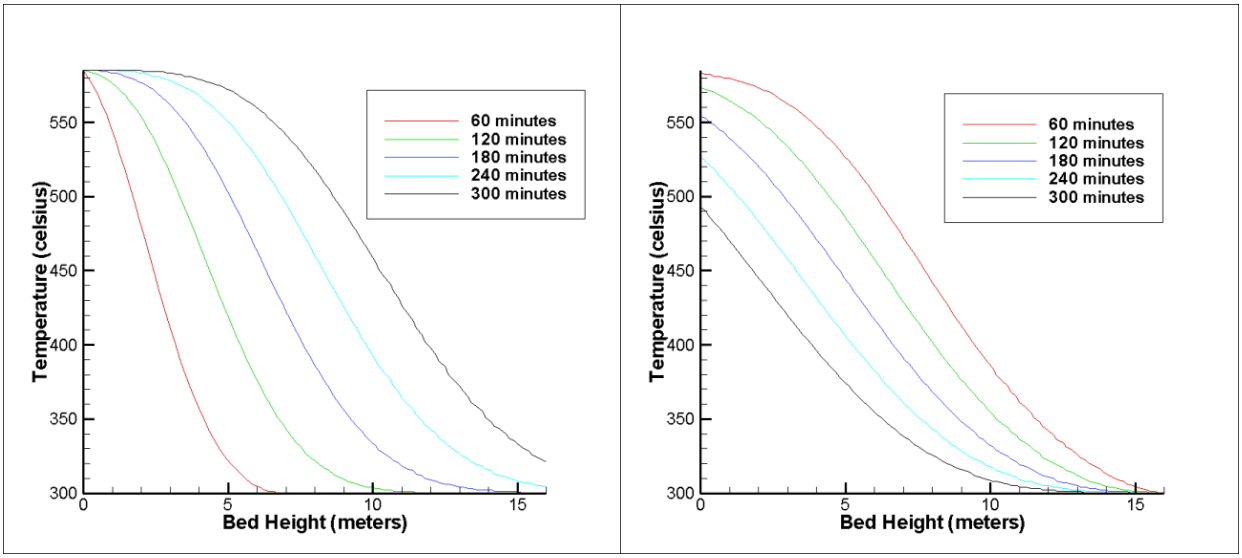


**Figure 5.3: Charging (left) and discharging (right) for Case 4c fluid temperature distribution**

The charging temperature distribution plot of the fluid shows that the thermocline zone moves from the top of the tank towards the bottom of the tank. It does not, however, make it to the bottom of the tank as a very tight thermocline zone. This is shown in the plot by the final line, which is the thermocline zone at 300 minutes, taking 7.5 m to span the thermal range. The problem with this is that not all of the concrete that could possibly store the thermal energy is being used. This is assumed to be because the low thermal conductivity of the concrete does not allow for the energy to be absorbed into the concrete at a high enough rate.

The discharging temperature distribution plot was not as defined as the charging profile in terms of thermocline shapes. It did however show signs of the thermocline zone shape, seen by the time step temperature distributions keeping a faint "S" shape, but not as drastic as in the charging profile. This is most likely due to the fact that only roughly a third (1/3) of the volume of the tank was heated all the way to 585°C and only one half (1/2) of the volume of the tank was heated to above 550°C. This suggests that the energy that was stored in the tank at full operating temperatures was easily pulled out of the system and the temperatures began to decrease for the available energy yet to be retrieved.

Another important factor in analysis of a thermocline system is the amount of storage material actually being used for full temperature storage. Figure 5.4 shows the thermocline temperature distribution for the outer edge (RO) of the concrete storage material for both the charging and discharging half-cycles.

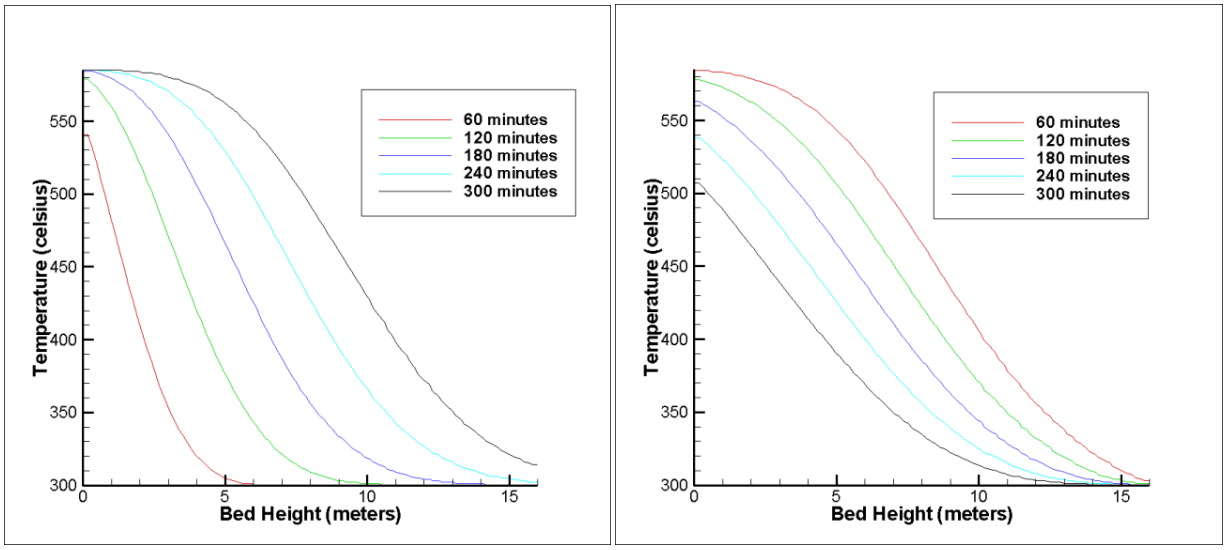


**Figure 5.4: Charging (left) and discharging (right) for Case 4c concrete temperature distribution**

The charging and discharging half-cycles for the concrete show that the energy is being put into the concrete and taken out of the concrete with a thermal stratification similar to the fluid. Notice that the outside of the concrete does not reach as high of a temperature throughout as the fluid during charging and does not reach as low of a temperature as the fluid during discharging. This is proof that the low thermal conductivity of the concrete causes a slow transfer of thermal energy throughout the storage material from the fluid. Again, this thermocline temperature distribution profile is the most defined out of any of the cases that were evaluated.

The amount of energy being stored and retrieved in the cycle of charging and discharging are the most important pieces of data in regards to the discharge efficiency of a system. Figure 5.5 shows the amount of energy stored and retrieved from case 4c.

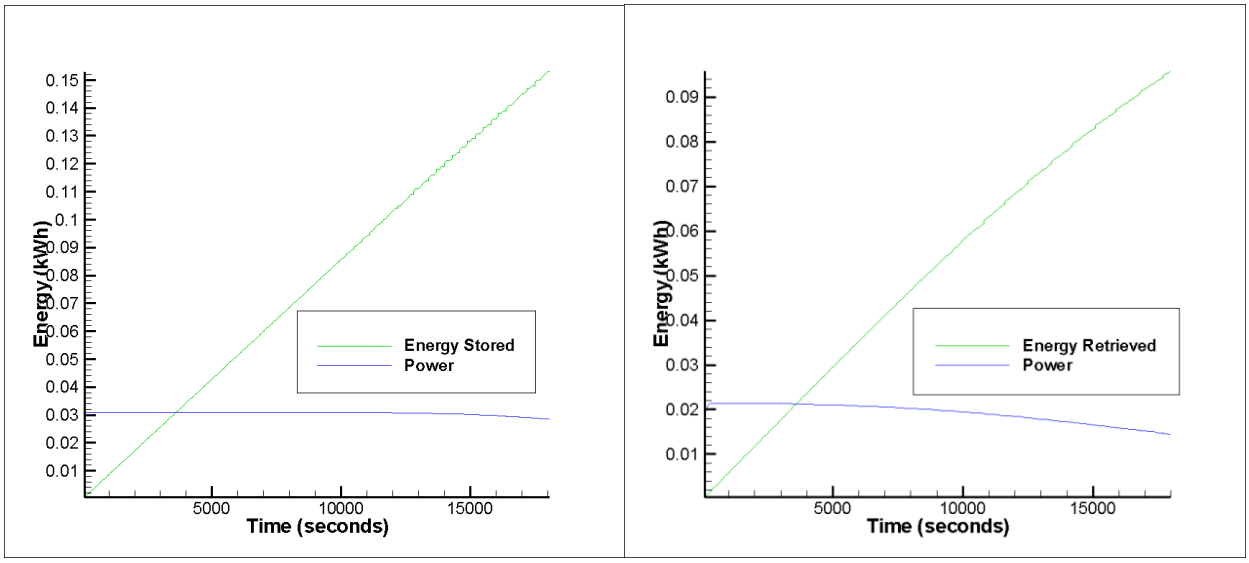


**Figure 5.5: Energy stored (left) and energy retrieved (right) for Case 4c**

Case 4c allowed for 0.153 kWh of energy to be stored in the system. It also allowed for 0.0959 kWh of energy to be retrieved from the system. This calculated to a discharge efficiency of 62.68%. This is a high discharge efficiency when compared to the other cases that were evaluated. The reason the discharge efficiency is only 62.68% is due to the fact that the concrete filler was only able to store the full amount of energy in one third (1/3) of the material. Because of this, the thermocline shape starts to degrade quickly upon discharging; meaning that the discharging period had to be ended.

### *5.1.5 Conclusions*

The discharge efficiency is a delicate value in regards to the optimization process. Case 4c is the best fit for the axisymmetric model because of the combination of variables that are present in both the charging program and the discharging program. The following observations are the reasons that this model is optimized:

- Increasing the velocity of the charging file for the given inner and outer radius causes the fluid exit temperature to become too high at the end of the normal

charging period. This causes degradation of the thermal stratification in the tank. To fix this, the charging time must be decreased causing less energy to be stored and consequently having less energy that can be retrieved.

- Decreasing the velocity of the charging file for the given inner and outer radius causes the fluid exit temperature to remain roughly the same and increases the energy stored. The problem with this is that less of the concrete is heated to its full capacity because the energy available becomes exhausted near the top of the tank. Due to this, the amount of energy that can be retrieved during discharging is decreased, therefore lowering discharge efficiency.
- Increasing the outer radius causes less of the concrete to be heated to its full capacity. This is because there is more concrete volume that is able to be heated by the same amount of fluid. The energy in the fluid becomes exhausted at a more evenly distributed, widespread pattern in the tank. Since the concrete is not heated to its full capacity, the discharge efficiency is lowered because of a fast degrading thermocline zone during the discharge half-cycle.
- Decreasing the outer radius causes the concrete to heat up quicker which requires shortening of the charging cycle. Because of this, less energy is stored and therefore less can be retrieved.
- Increasing the inner radius has the same effect as decreasing the outer radius.
- Decreasing the inner radius has the same effect as increasing the outer radius.
- If the dimensions used are doubled, therefore keeping the 0.25 porosity for the cell, the efficiency begins to drop off of the 62.68% that was found for the original dimensions. The new efficiency for a cell that is twice the size of case 4c

is 56.69%. The thermocline zone shape also begins to degrade. To change dimensions, another round of optimization must be done on the velocity and time for both charging and discharging.

## 5.2 2-DIMENSIONAL PLATE MODELING RESULTS

The 2-D plate program models the filler material for the thermocline that is being designed as a number of vertical concrete plates inside of the thermocline tank. Each plate runs the width of the tank at the given point and has a narrow space separating it from the next plate. This space is where the HTF will run in order to charge and discharge the plate. The program models the plates as a half thickness of both the flow channel and the plate. This program was the second program run in conducting this research.

### *5.2.1 Modeling Procedure*

The first step in running this program was the use of the charging program "TCLP2.exe" created by Selvam (2011). Each attempt began with an inner and outer thickness that was set. Different iterations were run using changes in velocity and time to achieve the best thermocline zone shape with the maximum amount of storage material being used to its full potential for each attempt. Once a set inner and outer thickness was optimized, either the inner thickness or outer thickness was changed and the process would begin again to optimize a new set of thicknesses.

After the charging program was completed for a number of different variable combinations, the discharging program was used to finish the optimization process. The program used for this was "TCLP4.exe" created by Selvam (2011). Since the thicknesses were already established, the velocity and time variables were adjusted for the optimization process. A base set of variables was used when starting the discharge half-cycle. These variables were decided upon as a result of the information gathered from the axisymmetric modeling program.

The base velocity was 0.001 m/s and the base time was 5 hours for the discharge half-cycle. After a trial with the base variables, the time or velocity would be changed as the fine tuning was finished. An optimized design was the result of this process.

### *5.2.2 2-Dimensional Plate Modeling Results and Discussion*

Table 5.4 is a compilation of the 20 recorded cases run for the 2-D plate program. There were more iterations run but not recorded due to extreme data that did not meet the requirements of the assumptions presented in section 3.6. The table presents the charging (denoted by a "c" subscript) and discharging data (denoted by a "d" subscript) as well as the discharge efficiency for the plate geometry as a thermocline filler material. Energy stored (ES) and energy retrieved (ER) are also presented in the table. The phrase "Does Not Meet Thermocline Shape Standards" is present in the place of discharge data for multiple cases. This was entered for data that was close to the thermocline shape but had exit temperatures that barely exceeded the 385°C limitation at the end of the charging period set for the use of this program. Like the axisymmetric model, the 2-D plate model has multiple cases labeled as "#a" and "#b." This designation represents cases that were able to be adjusted from the base discharging variables to optimize a more efficient model.

**Table 5.4: 2-D Plate Modeling Results**

| *Iteration* | *TI (m)* | *TO (m)* | *$v_c$ (m/s)* | *$t_c$ (hrs)* | *ES (kWh)* | *$v_d$ (m/s)* | *$t_d$ (hrs)* | *ER (kWh)* | *Eff. (%)* |
|---|---|---|---|---|---|---|---|---|---|
| ***1a*** | 0.0127 | 0.0508 | 0.002 | 4 | 1.39 | 0.001 | 5 | 0.411 | 29.57 |
| ***1b*** | 0.0127 | 0.0508 | 0.002 | 4 | 1.39 | 0.00125 | 5 | 0.615 | 44.24 |
| ***2a*** | 0.0127 | 0.0508 | 0.0015 | 5 | 0.989 | 0.001 | 5 | 0.411 | 41.56 |
| ***2b*** | 0.0127 | 0.0508 | 0.0015 | 5 | 0.989 | 0.001 | 6 | 0.475 | 48.03 |
| ***3a*** | 0.0127 | 0.0508 | 0.0015 | 6 | 1.16 | 0.001 | 5 | 0.427 | 36.81 |
| ***3b*** | 0.0127 | 0.0508 | 0.0015 | 6 | 1.16 | 0.0125 | 5 | 0.646 | 55.69 |
| ***4*** | 0.0127 | 0.0508 | 0.003 | 4 | Does Not Meet Thermocline Shape Standards | | | | |
| ***5*** | 0.0127 | 0.0635 | 0.002 | 4 | 1.4 | 0.001 | 5 | 0.392 | 28.00 |
| ***6a*** | 0.0127 | 0.0635 | 0.002 | 5 | 1.7 | 0.001 | 5 | 0.415 | 24.41 |
| ***6b*** | 0.0127 | 0.0635 | 0.002 | 5 | 1.7 | 0.0015 | 5 | 0.873 | 51.35 |
| ***7*** | 0.0127 | 0.0635 | 0.003 | 4 | Does Not Meet Thermocline Shape Standards | | | | |
| ***8*** | 0.01905 | 0.0508 | 0.002 | 4 | | | | | |
| ***9*** | 0.01905 | 0.05715 | 0.002 | 4 | | | | | |
| ***10*** | 0.01905 | 0.05715 | 0.0015 | 4 | 1.18 | 0.001 | 4 | 0.495 | 41.95 |
| ***11a*** | 0.01905 | 0.05715 | 0.0015 | 5 | 1.43 | 0.001 | 5 | 0.629 | 43.99 |
| ***11b*** | 0.01905 | 0.05715 | 0.0015 | 5 | 1.43 | 0.00125 | 5 | 0.938 | 65.59 |
| ***12*** | 0.01905 | 0.0635 | 0.002 | 4 | Does Not Meet Thermocline Shape Standards | | | | |
| ***13*** | 0.01905 | 0.06955 | 0.002 | 4 | | | | | |
| ***14a*** | 0.01905 | 0.0762 | 0.002 | 4 | 2.03 | 0.001 | 5 | 0.592 | 29.16 |
| ***14b*** | 0.01905 | 0.0762 | 0.002 | 4 | 2.03 | 0.001 | 6 | 0.686 | 33.79 |

Case = Iteration being run

TI = Inner thickness

TO = Outer thickness

$v_c$ = Velocity during charging

$t_c$ = Time of charging

ES = Energy Stored

$v_d$ = Velocity during discharging

$t_d$ = Time of discharging

ER = Energy Retrieved

Eff. = Discharge efficiency

### *5.2.3 Low Efficiency Case Results*

Low efficiency cases showed similar trends to those in the axisymmetric model. The comparison of cases 6a (24.41%) and 6b (51.35%) is testimony to this observation. Figure 5.6 is the comparison of the discharging output file visualization for the fluid temperature distributions for cases 6a and 6b. Notice that the thermocline zone moves a very short distance and covers a smaller temperature range in case 6a than it does in 6b. The tighter formation of the thermocline zone over the time of discharging shows that the variable for velocity used in case 6a was too low and resulted in less of the stored energy being able to be retrieved. Increasing the velocity for case 6b allowed for the amount of energy retrieved to be increased.

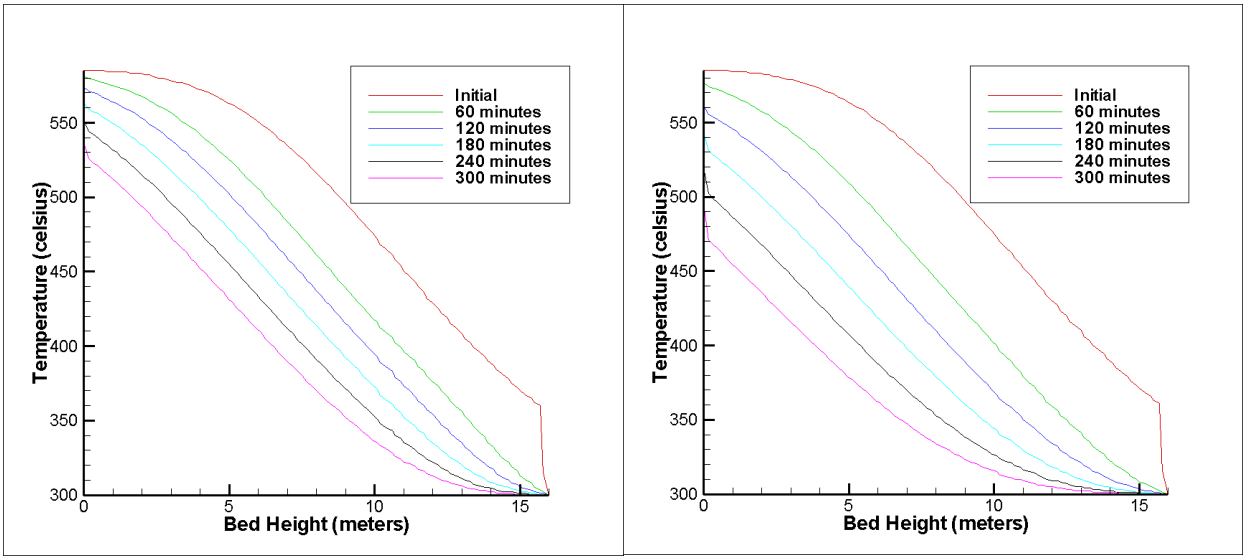


**Figure 5.6: Fluid temperature distribution for case 6a (left) and 6b (right)**

Figure 5.7 illustrates the concrete temperature distribution at the outer thickness for both case 6a and case 6b. This visualization of the output files shows that more of the concrete is being drained of the energy that was stored during the charging half-cycle. The temperature represented by the 300 minute line reveals that more of the concrete is giving away its stored energy in case 6b than in case 6a.

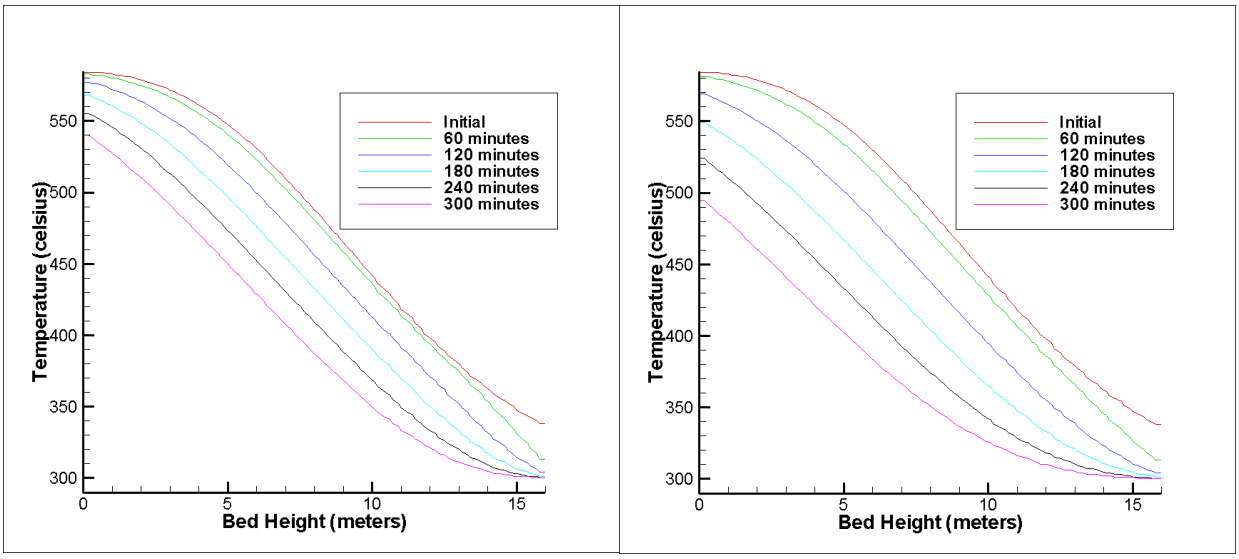


**Figure 5.7: Concrete temperature distribution for case 6a (left) and 6b (right)**

The energy retrieved output file proves the statements made for both the fluid temperature distribution plots and the concrete temperature distribution plots. Figure 5.8 is an illustration of plots for case 6a and case 6b. It is noted that the energy retrieved in case 6a is 0.415 kWh while the energy retrieved in case 6b is 0.873 kWh. Both cases had the same 1.7 kWh of energy stored in the system, as seen in table 5.3. More energy was able to be retrieved from the energy stored in case 6b than in case 6a which increases the discharge efficiency of the system.

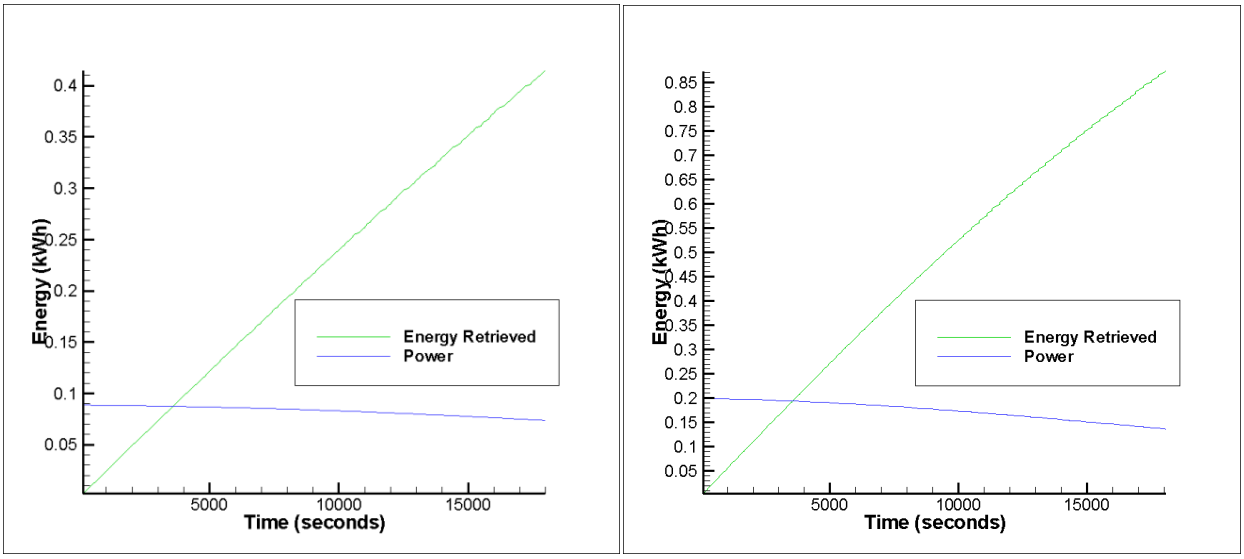


**Figure 5.8: Energy retrieved for case 6a (left) and 6b (right)**

### *5.2.4 Optimized Model*

The most efficient thermocline system developed for the 2-D plate model was case 11b in table 5.4. This case had a discharge efficiency of 65.59%. This data will be compared to the axisymmetric model optimization. The geometry of this case was an inner thickness for the flow channel of 0.01905 m and an outer thickness to half of the plate of 0.05715 m. Table 5.5 summarizes the geometric properties of case 11b.

**Table 5.5: Case 11b physical properties**

| Inner Thickness | Inner Area | Outer Thickness | Outer Area | Concrete Area | Porosity |
|---|---|---|---|---|---|
| 0.01905 m | 0.01905 $m^2$ | 0.05715 m | 0.05715 $m^2$ | 0.0381 $m^2$ | 0.33 |

The porosity reported for this case is 0.33. This is higher than the porosities of 0.22-0.25 used by researchers that modeled a packed bed system, referenced in section 2.4.2. From the modeling done in this research, it was discovered that the increased porosity of case 11b produced higher discharge efficiencies than the cases that had porosities around 0.25. Because of this, case 11b was chosen as the optimized case for the 2-D plate modeling program.

To understand how the geometry of the concrete plate reacts to charging and discharging, the thermocline shapes must be compared for the fluid temperature distributions. Figure 5.9 shows the charging and discharging thermocline zone shapes for case 11b.

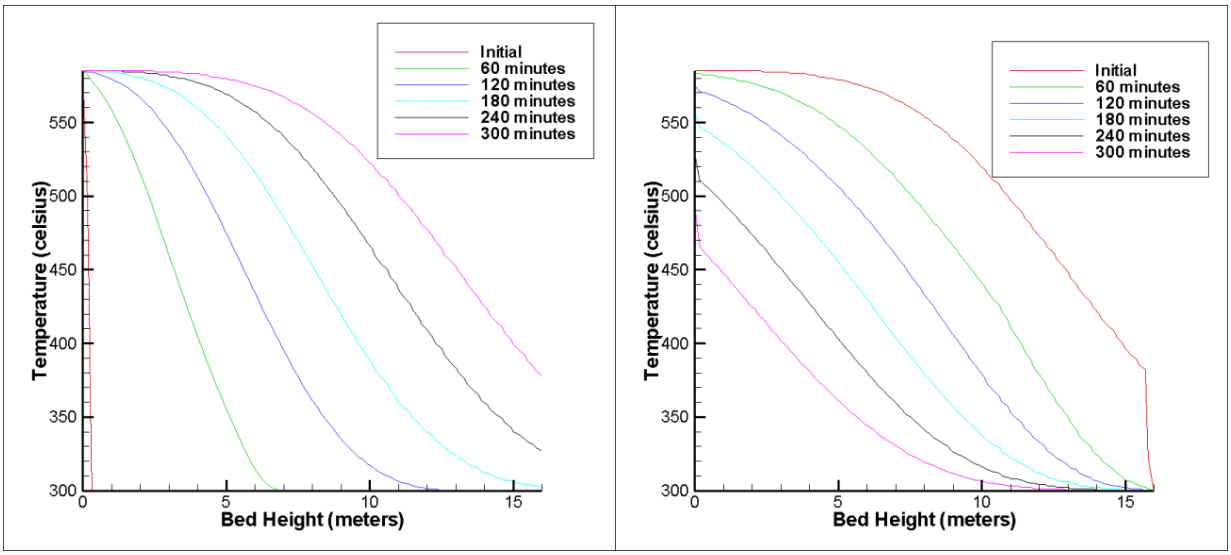


**Figure 5.9: Charging (left) and discharging (right) for Case 11b fluid temperature distribution**

The charging temperature distribution plot of the fluid shows the thermocline zone moving throughout the tank from the top towards the bottom. The thermocline zone is still rather large, taking up roughly three quarters (3/4) of the tank while it moves. It is noted that the maximum temperature of the fluid (585°C) is extended to one third (1/3) of the tank with a temperature of above 500°C taking up two thirds (2/3) of the tank at the end of charging. The exit temperature at the end of charging is 380°C. This is favorable for the transfer of energy to the concrete for storage.

The discharge half-cycle thermocline zone is not as defined as the charging half-cycle or the discharging half-cycle for the optimized axisymmetric model. The zone loses its "S" shape as discharging continues. The final exit temperature of the fluid is 490°C at the end of discharging. This was the lower limit of allowable discharging temperatures. The discharging

exit temperature drops rapidly as discharging continues. This is likely due to the amount of concrete that is storing the maximum amount of energy. As the available temperature of the material decreases, the fluid temperature decreases. This is proven by the comparison of the concrete outer thickness temperature distribution for case 11b shown in figure 5.10.

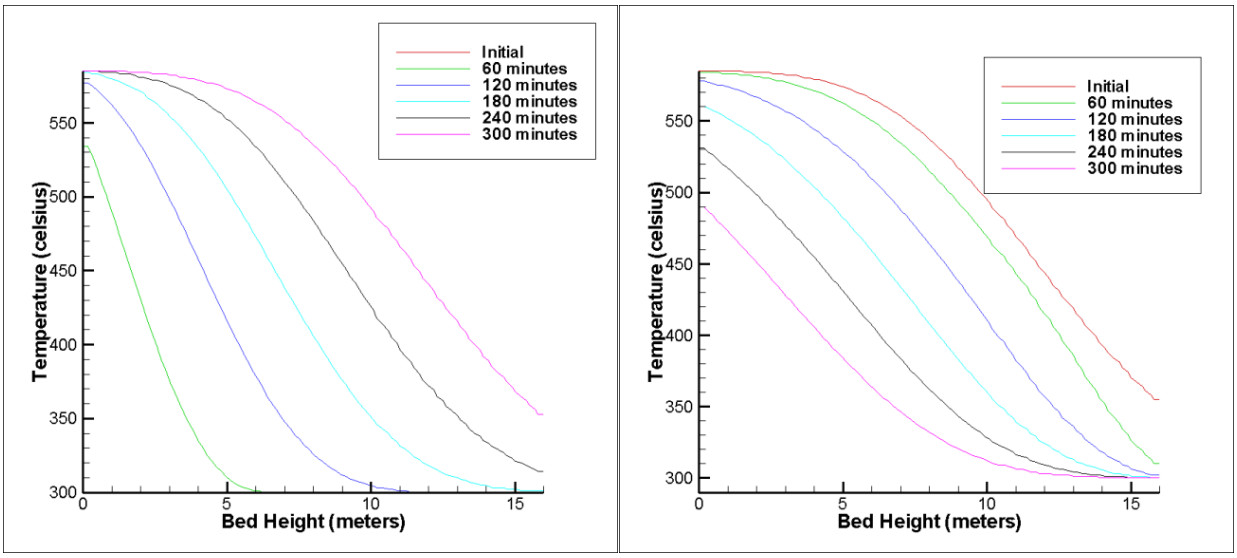


**Figure 5.10: Charging (left) and discharging (right) for Case 11b concrete temperature distribution**

Like the axisymmetric model, the charging and discharging half-cycles for the concrete show that the material is following a similar temperature distribution plot as the fluid. The concrete does not reach as high of temperatures during charging or as low of temperatures during discharging as the fluid. This is proof again that the poor thermal properties of the concrete delay the thermal stratification that is present in the fluid. Fluid exit temperatures decreased rapidly because only one quarter (1/4) of the concrete reached maximum temperatures. It is noted that one half (1/2) of the concrete in the tank reaches a temperature of 500°C or greater during charging. This allows for a solid basis for retrieving energy during the discharge half-cycle.

The amount of energy being stored and retrieved from the concrete is the most important piece of information. This is what determines the discharge efficiency of the system. Figure 5.11 shows the amount of energy being stored and retrieved when running case 11b.

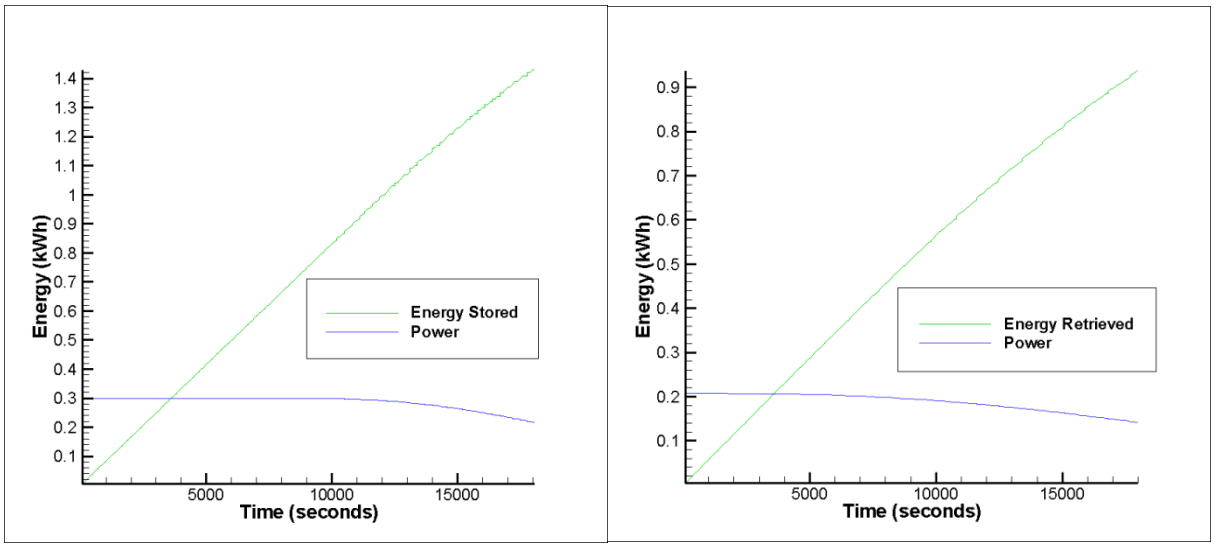


**Figure 5.11: Energy stored (left) and energy retrieved (right) for Case 11b**

Case 11b allowed for 1.43 kWh of energy to be stored in the system during the charging half-cycle. During the discharging half-cycle, 0.938 kWh of energy was able to be retrieved. From this, the discharge efficiency of 65.59% was able to be computed. The discharge efficiency is capped at this amount due to the thermocline zone illustrated in the fluid temperature distribution for discharging. Since the zone is degraded to a minimum allowable exit temperature, the discharging half-cycle has to be ended.

### *5.2.5 Conclusions*

For the 2-D plate model, the optimization process produces a relatively high discharge efficiency for case 11b. This made for the most optimized geometry for the concrete plates. The following observations are the reason that this model is optimized:

- Increasing the velocity of the charging file for the given thicknesses has the same effect as for the axisymmetric model in section 5.1.3.

- Decreasing the velocity of the charging file for the given thicknesses has the same effect as for the axisymmetric model in section 5.1.3.
- Increasing the outer thickness with the given inner thickness held constant allows for more thermal energy to be stored during charging but the temperatures in the concrete do not reach a maximum value for a large portion of the material. This decreases the energy retrieved because the exit temperature of the fluid drops rapidly, as it cannot be heated fully by the concrete. This lowers the discharge efficiency.
- Decreasing the outer thickness causes the concrete to heat up quicker. Because of this, the time for charging would have to be shortened to preserve the thermocline zone, therefore decreasing the amount of energy that can be stored. This leads to decreases in discharging time, energy retrieved, and discharge efficiency.
- Increasing the inner thickness while holding the outer thickness the same has the same effect as decreasing the outer thickness.
- Decreasing the inner thickness while holding the outer thickness the same has the same effect as increasing the outer thickness.
- Doubling the size of the flow channel and concrete plate causes the same drop in discharge efficiency and thermal stratification as found for the axisymmetric model. Any change in the variables calls for a re-optimization of the geometry.

## 5.3 COMPARISON OF RESULTS

To be able to determine the best choice between the two geometric designs that were used, a comparison must be made. Aspects of each design that must be looked at include the discharge efficiency, the energy retrieval capabilities based on tank area, and the thermocline zone shapes.

### *5.3.1 Discharge Efficiencies*

The two designs that were optimized in this research are shown in table 5.6. The first set of information is for the axisymmetric model and is from table 5.2, case 4c. The second set of information is from the 2-D plate model and is from table 5.4, case 11b.

**Table 5.6: Case summary for axisymmetric and 2-D plate modeling programs**

| Case | RI/TI (m) | RO/TO (m) | $v_c$ (m/s) | $t_c$ (hrs) | ES (kWh) | $v_d$ (m/s) | $t_d$ (hrs) | ER (kWh) | Eff.(%) |
|---|---|---|---|---|---|---|---|---|---|
| ***Case 4c - Axisymmetric Model*** | | | | | | | | | |
| ***4c*** | 0.025 | 0.05 | 0.0015 | 5 | 0.153 | 0.0015 | 5 | 0.0959 | 62.68 |
| ***Case 11b - 2-D Plate model*** | | | | | | | | | |
| ***11b*** | 0.01905 | 0.05715 | 0.0015 | 5 | 1.43 | 0.00125 | 5 | 0.938 | 65.59 |

As seen in the table, the discharge efficiencies for the two optimized cases were very close. The 2-D plate model, case 11b, had the higher discharge efficiency of 65.59%. The axisymmetric model, case 4c, had the lower discharge efficiency of 62.68%. Both of these cases have a decent discharge efficiency that could be used in a thermocline TES system.

### *5.3.2 Energy Retrieval*

The axisymmetric model and the 2-D plate model consist of two completely different geometries as a filler material. Comparing the energy that each model is able to retrieve for each cell or unit width would be very inaccurate. To compare the amount of energy that would be able to be retrieved for each system, a 1 m x 1 m cross section of the tank was taken into account. Figure 5.12 illustrates the two geometries and their differences in a cross section of the same size.

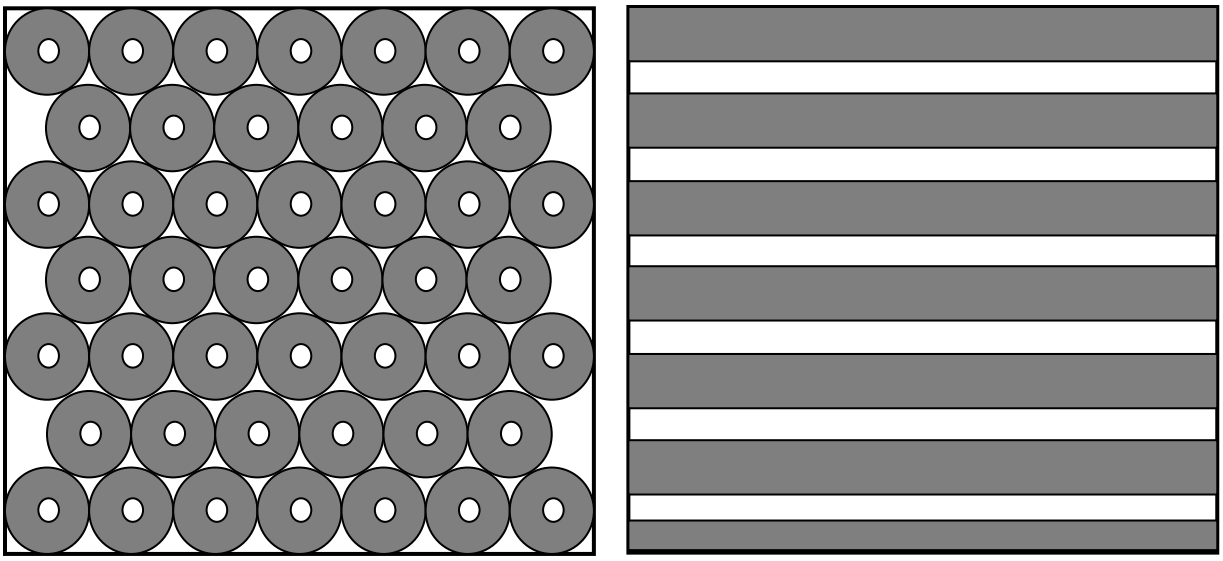

**Figure 5.12: One square meter cross section for axisymmetric model (left) and 2-D plate model (right)**

Each of the concrete cells in both parts of figure 5.12 illustrates the size of the cell that would be responsible for the value of the energy retrieved in table 5.5. To calculate the amount of energy that one (1) square meter of concrete and HTF can produce, the energy retrieved value must be divided by the total area of the cell used for each of the cases. Table 5.6 is a representation of the energy retrieved per square meter of thermocline tank. The total area is taken from tables 5.3 and 5.5. This value is calculated for each of the optimized concrete geometries.

**Table 5.7: Energy retrieved per square meter of tank cross section**

| *Case* | *Total Area ($m^2$)* | *ER (kWh)* | *ER per Meter Square (kWh)* |
|---|---|---|---|
| ***Case 4c - Axisymmetric Model*** | | | |
| ***4c*** | 0.00785 | 0.0959 | 12.22 |
| ***Case 11b - 2-D Plate model*** | | | |
| ***11b*** | 0.05715 | 0.938 | 16.41 |

Converting the energy retrieved per concrete cell to energy retrieved per meter square of tank helps to compare the two geometries that are present. The optimized 2-D plate model was

able to retrieve 16.41 kWh/m$^2$ after the discharging half-cycle was completed. The optimized axisymmetric model was only able to retrieve 12.22 kWh/m$^2$ after the discharging half-cycle was completed. Although a small difference, when looking at the size of the thermocline tank needed for a large scale system, the difference of 4.19 kWh/m$^2$ ultimately means a larger tank will be needed for the axisymmetric geometry.

### *5.3.3 Thermocline Zone Shapes*

In order for a thermocline TES system to be considered a thermocline, the thermocline zone must be present in the tank throughout charging and discharging. The thermocline zone shapes are important when comparing the two models. The charging half-cycle fluid temperature distribution comparison for the axisymmetric (case 4c) and 2-D plate (case 11b) models is presented in figure 5.13.

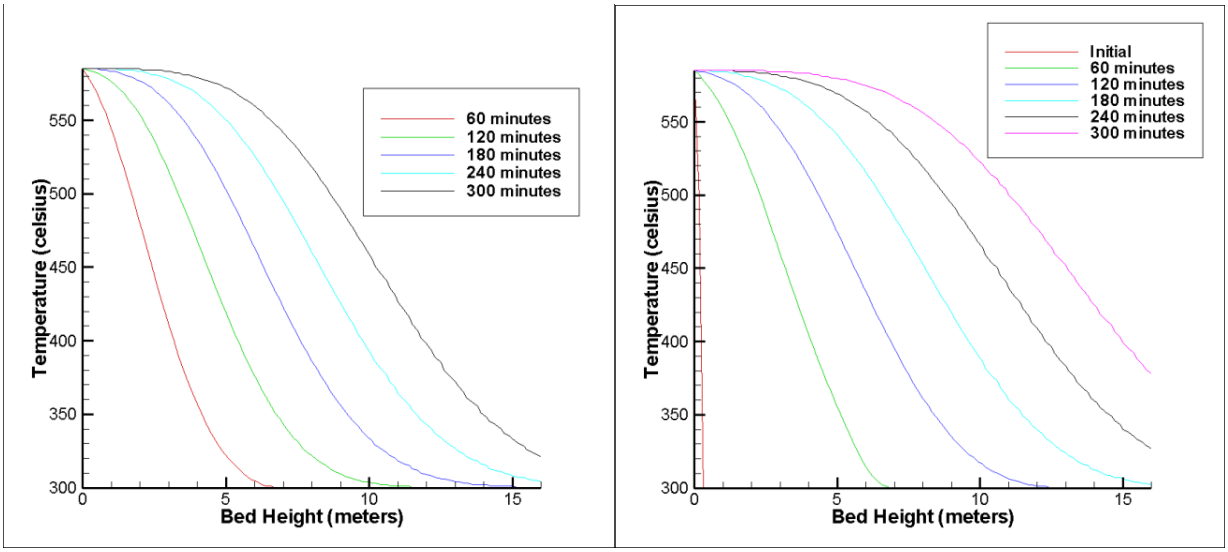


**Figure 5.13: Charging thermocline zone shape for Case 4c (left) and Case 11b (right)**

Both of the thermocline zones are defined for the charging program. The exit temperature is slightly higher for case 11b after the charging half-cycle but is in the 385°C temperature limitation for the programs. It is also noted that more of the tank is in the upper limits of the temperature range in case 11b than in case 4c. This allows for the increase in

discharge efficiency because the higher temperature range of the storage material facilitates the rate at which the thermocline zone degrades during the discharge half-cycle.

The concrete temperature distribution plots for the two programs are important to look at as well when comparing these two optimized models. Figure 5.14 presents the thermocline zone movement on the outside of the concrete cells, at the furthest point from the HTF. Notice, like the fluid temperature distribution plots, case 11b has more of the concrete in the upper limits of the temperature range than case 4c. Again, this points towards better discharge efficiency.

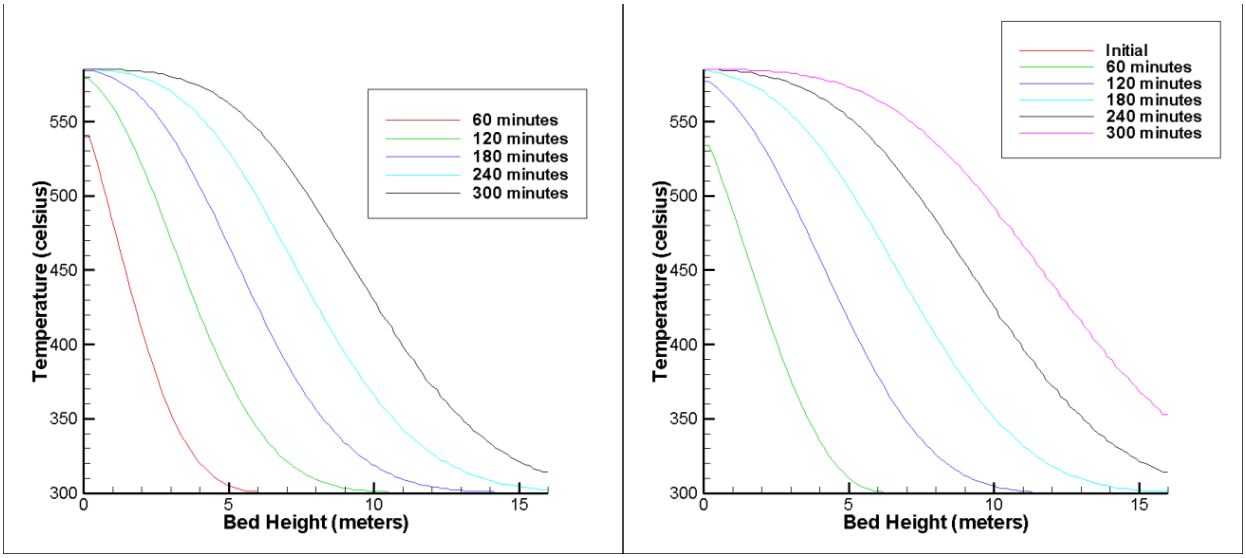


**Figure 5.14: Concrete temperature distribution plots for case 4c (left) and case 11b (right)**

The discharging thermocline zone movement is important to look at as well. From the modeling results, the discharging half-cycles produce a less defined thermocline zone shape. The comparison between case 4c and 11b is presented in figure 5.15.

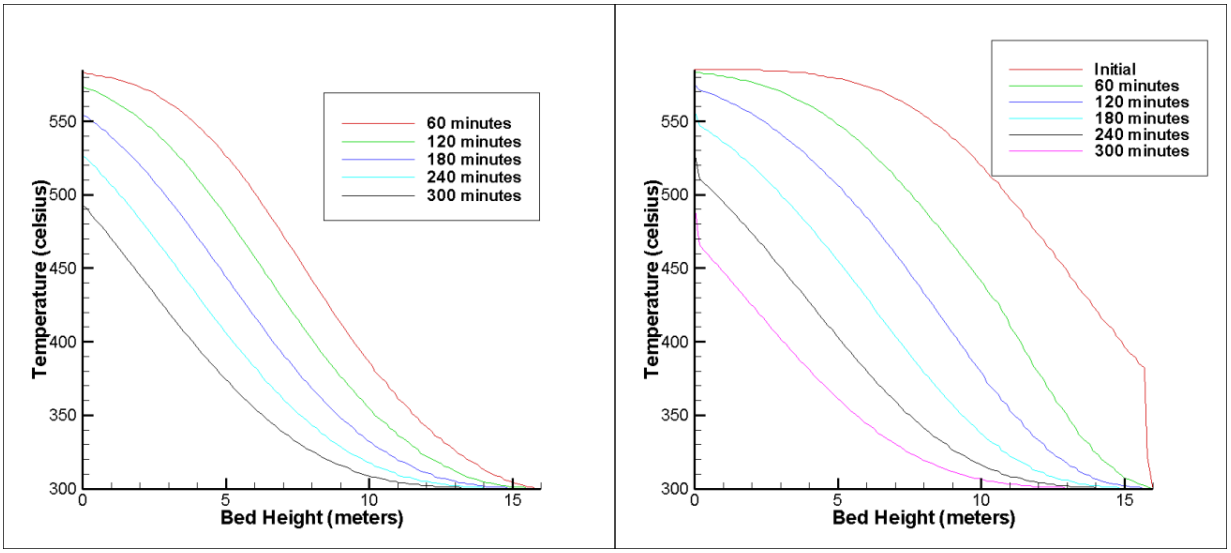


**Figure 5.15: Discharge fluid temperature distribution plots for Case 4c (left) and Case 11b (right)**

Notice that in this comparison, the exit temperature for case 4c on the left side of the plot is a much smoother transition than that of case 11b. As time continues during discharging, heading towards the end of the discharging half-cycle, the exit temperature for case 11b begins to jump up to a higher temperature. The exit temperature for both models in the discharging half-cycle is 490°C which is the lower limitation for the discharging program.

The concrete temperature distribution plot for the discharging half-cycle is the final plot to compare. This illustrates how much of the concrete is being reduced back down to lower temperatures as discharging continues. Figure 5.16 compares the temperature distribution in the concrete at the furthest point from the fluid. Notice that more of the concrete in case 11b is reduced to lower temperatures in the top of the tank at the end of the discharging half-cycle.

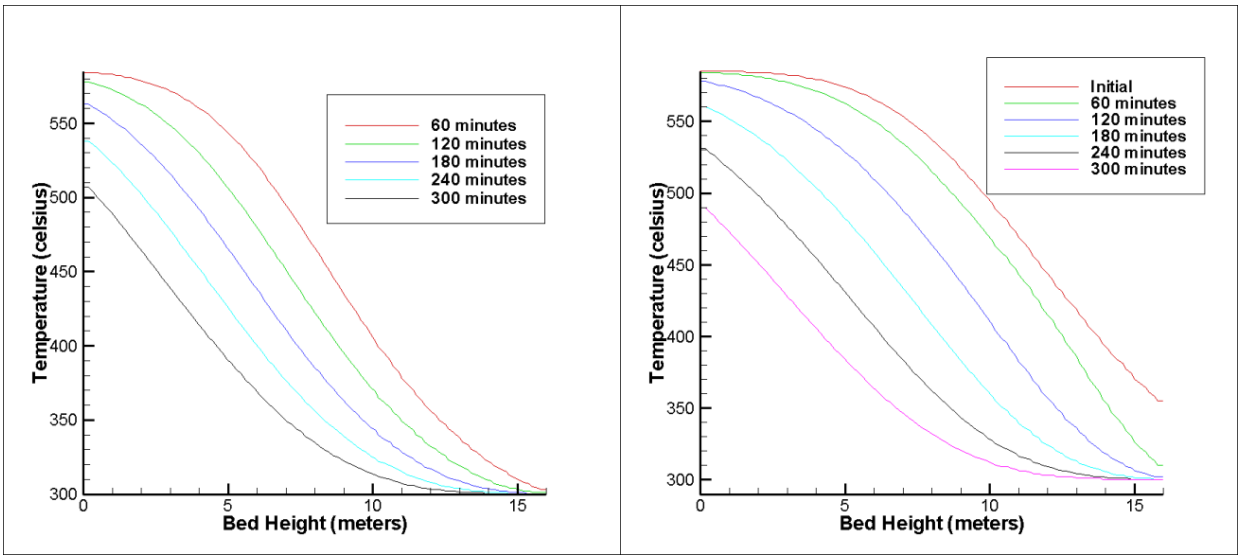


**Figure 5.16: Discharge concrete temperature distribution plots for Case 4c (left) and Case 11b (right)**

### *5.3.4 Conclusions*

After the comparison between case 4c from the axisymmetric modeling program and case 11b of the 2-D plate modeling program, one of the geometric designs had to be picked as the best choice for construction of a large scale system. With a higher discharge efficiency of 65.59% and energy stored per meter squared of tank cross-section of 16.41 kWh, the 2-D plate model case 11b is the best choice in design optimization. The thermocline zone shape in both the charging half-cycle and discharging half-cycle is an adequate representation of a thermocline TES system also. It remains in the limitations of the temperature ranges of no more than 385°C exit temperatures for charging and no less than 490°C exit temperature for discharging.

# CHAPTER 6: LABORATORY TESTING OF HIGH TEMPERATURE CONCRETE MIX DESIGNS

Testing has been done in order to check the potential of using a concrete mixture as a filler material in the thermocline tank. A concrete mix usually is composed of a coarse aggregate, fine aggregate, cement, and water. This basic concrete mix design was adjusted using different coarse aggregates and different cementitious materials in order to make a mix design that was able to withstand the extreme conditions that are part of the usage cycle for the filler material in the thermocline TES system.

## 6.1 AGGREGATE TESTING

Pacheco et al (2002) suggested that it is important to choose the right filler material for compatibility with molten salt. The molten salt environment is extremely corrosive and causes degradation in many different mineral species. They ran tests on common minerals and decided that quartzite rock with silica sand would be a viable option as a filler material in a molten salt thermocline tank. Brosseau et al (2005) continued this proof with isothermal salt tests and cycling tests with salt flow.

Since the coarse aggregate is a cost saving addition to a concrete mix, it was decided that tests must be done on the aggregate to check for compatibility with the molten salt environment. Two readily available, easy to access, and cheap aggregates in Northwest Arkansas are AR limestone and sandstone. Limestone was chosen due to it being available at the University of Arkansas Engineering Research Center and sandstone was chosen because it is the younger stage of quartzite rock. These two aggregate types were tested to check molten salt compatibility.

### *6.1.1 Test Regimen*

Each aggregate sample was carefully washed and then allowed to dry completely by being placed in a test oven at 80°C for 2 hours. The samples were then weighed out to 567 g (1.25 lbs). The frozen salt was then placed in the oven for 2 hours at 300°C so that it could melt into its liquid state. After the 2 hours, the aggregate was placed in the salt and the combined sample, as seen in figure 6.1, was brought up to 550°C. The samples were left in the oven for 500 hours and then the temperature was dropped back down to 300°C. At this point, the aggregate and salt were poured through a mesh basket to catch the aggregate and drain the salt. The aggregate basket was suspended over an empty bucket at 350°C to let as much salt as possible drain away from the aggregate. The aggregate was then weighed again and observations were made to determine their compatibility with the molten salt.

**Figure 6.1: Sandstone aggregate in molten salt bucket before heating**

### *6.1.2 Aggregate Test Results*

Both of the aggregate samples faired very well with the exposure to the molten salt. The AR limestone, shown in figure 6.2, had a weight gain of 22 grams (0.05 lbs). The color of the

aggregate changed from a gray and white to a more tan and white. The aggregate also still held its sharp edges with no visible degradation. This is in contrast to the NM limestone tested by Pacheco et al (2002) which fell apart and became "like mud" during their tests.

**Figure 6.2: Limestone before (left) and after (right) 500 hours at 550°C**

The AR sandstone was similar to the limestone in the results of the tests. The total weight after the test for the sandstone showed an increase of 50 grams (.11 lbs). The sandstone is shown in figure 6.3. The color change in the sandstone went from a light and dark gray to a brown color. The aggregate also held its sharp edges with no visible degradation of the sample.

**Figure 6.3: Sandstone before (left) and after (right) 500 hours at 550°C**

The tests done were done with the equipment and resources available at the research facility. The weight gain is most likely attributed to the excess molten salt that penetrated inside of the aggregates or was left as a film on the outside of the aggregate. Other tests could be performed in another lab in order to figure out the actual strength of the aggregates before and after the test, as well as a chemical analysis of the salt to check to see if the aggregates had any negative effect on the salt. The salt after both tests appeared to be the same as before the test in both its liquid and solid states. After testing the aggregates for 500 hours at 550°C, both the AR limestone and the AR sandstone were deemed viable for use in concrete mixtures for the thermocline filler material.

## 6.2 CONCRETE MIX DESIGNS

The concrete mix designs were designed by Emerson John, a concrete materials PhD candidate at the University of Arkansas who is working on the DOE project that is the basis of this thesis. The concrete mixes that were tested had different combinations of aggregates and cementitious materials, as well as the addition of polypropylene fibers for spalling resistance, in order to figure out which combination is best for use in a thermocline TES system.

The mixes done prior to the suggestion of a thermocline TES system were made mostly of a cementitious material known as calcium aluminate cement. Calcium aluminate cement has proven to help a mixture hold its strength when heated up to temperatures in excess of 600°C in a test oven. Normal concrete, when subjected to high temperatures tends to chemically break down and lose its durability. The addition of calcium aluminate cement helps to hold off this process until higher temperatures. This type of cement is very expensive compared to ordinary portland cement, the cement found in normal concrete mixtures. The fine aggregate used in the mixtures was silica sand which is commonly found in Arkansas.

To reduce the cost of the concrete mixtures, different approaches were taken. The first approach was to add a cheap coarse aggregate. Since the limestone and sandstone proved to be compatible with the molten salt, these were added to the mix designs. The cement paste is the most expensive part of a concrete mix so the addition of aggregate cheapens the mix design by filling volume originally taken by the paste. Since the calcium aluminate cement is very expensive, the cementitious material fly ash was used as a replacement. Some of the mixtures included the replacement of 50%-70% of the calcium aluminate cement with fly ash. Ordinary portland cement was also added to a few of the mixtures to reduce the cost.

## 6.3 CONCRETE CUBE TESTS

The concrete mix designs described above were tested to see their compatibility with the molten salt. Twelve different mix designs were tested by immersing the specimens in the molten salt. The test specimens were two (2) inch cubes that were made during concrete batching with the exception of one that was made from a concrete cylinder due to failure in making cubes during the batching process. The specimens were allowed to cure for a minimum of 28 days before testing.

### *6.3.1 Test Regimen*

Once the specimens had been cured, they were weighed and measured and then placed in a stainless steel pan, as shown in figure 6.4. Fresh salt was then heated up to 300°C so that it could melt. Once the salt was melted, it was poured slowly into the stainless steel pan containing the concrete cubes. The pan was then placed in the oven at 300°C and raised to 585°C. The cubes were held at 585°C for 500 hours. After the time elapsed, the specimens and salt were brought down to a temperature of 300°C. The specimens were then taken out of the salt and placed into another stainless steel pan, raised off the bottom of the pan, to drain the excess salt

off of them. This was done in the oven at 350°C. The specimens were then taken from the pan, weighed, and measured for final results.


**Figure 6.4: Specimens before heating to 585°C**

### *6.3.2 Concrete Cube Test Results*

The concrete cubes needed to be measured and tested for compressive strengths to be able to conclude their viability as a possible mix design to be used in a structured concrete thermocline TES system. Figure 6.5 shows the specimens in the pan after the test was complete. The result of the weights and measurements are shown in table 6.1 for both before and after the testing was completed. The specimens were then broken in a concrete compression test machine in order to see the difference in strengths between the cubes before and after the time immersed in the salt. These results are presented in table 6.2.

**Figure 6.5: Specimens after heating to 585°C for 500 hours**

**Table 6.1: Concrete Cube Test Results**

| Mix Design | Wt. before (lbs) | Wt. after (lbs) | Percent Wt. of original (%) | Width before (in) | Width after (in) |
|---|---|---|---|---|---|
| **1** | 0.6850 | 0.7625 | ***111.3*** | 2.036 | 2.036 |
| **2** | 0.7000 | 0.7730 | ***110.4*** | 2.015 | 2.019 |
| **3** | 0.7080 | 0.7810 | ***110.3*** | 2.011 | 2.018 |
| **4** | 0.6795 | 0.7600 | ***111.8*** | 2.029 | 2.036 |
| **5*** | 0.3725* | 0.4255* | ***114.2*** | 3.848* | 3.886* |
| **6** | 0.6540 | 0.7450 | ***113.9*** | 2.012 | 2.022 |
| **7** | 0.6955 | 0.7855 | ***112.9*** | 2.015 | 2.027 |
| **8** | 0.6840 | 0.7800 | ***114.0*** | 2.043 | 2.036 |
| **9** | 0.6660 | 0.7410 | ***111.3*** | 2.008 | 2.007 |
| **10** | 0.7010 | 0.7825 | ***111.6*** | 2.008 | 2.017 |
| **11** | 0.6955 | 0.7815 | ***112.4*** | 2.003 | 2.006 |
| **12** | 0.6360 | 0.7340 | ***115.4*** | 2.008 | 2.016 |

*= Test specimen was not a cube due to cubes not being made while batching

**Table 6.2: Concrete Cube Compression Test Results**

| Mix Design | Compressive Strength Before (psi) | Compressive Strength After (psi) | Percent Strength of Original (%) |
|---|---|---|---|
| **1** | 8347 | 12648 | ***151.5*** |
| **2** | 6377 | 16950 | ***265.8*** |
| **3** | 8663 | 12000 | ***138.5*** |
| **4** | 8719 | 14359 | ***164.7*** |
| **5*** | N/A | N/A | ***N/A*** |
| **6** | 6614 | 13213 | ***199.8*** |
| **7** | 5898 | 11615 | ***196.9*** |
| **8** | 5867 | 14675 | ***248.9*** |
| **9** | 10441 | 19843 | ***190.0*** |
| **10** | 9297 | 23262 | ***250.2*** |
| **11** | 11145 | 12944 | ***116.1*** |
| **12** | 8328 | 17465 | ***209.7*** |

*= Test specimen was not a cube due to cubes not being made while batching

The concrete specimens fared very well in the test after being immersed in molten salt. All of the specimens gained weight and had either no increase or a slight increase in size. The weight gain was attributed to the addition of molten salt into the pores of the concrete. Increases in size could be contributed to a salt film on the outside of the cubes or could be attributed to assumed experimental error. As a whole, the concrete cubes seemed to turn a little lighter in color than before being immersed in the salt. Only two of the specimens showed any sign of degradation but it was only slight crumbling that appeared on the edges of the cubes.

The compression test showed very interesting results. As shown in table 6.2, every specimen that could be measured showed an increase in compressive strength of 116% to 266%. The reason for the strength increase was unknown but could possibly be attributed to the molten salt filling the pores of the test specimens and hardening after it froze again. The salt would take

the space of air voids and the melted polypropylene fibers. Tests done by John (2011) showed that these same mix designs, when exposed only to heating and cooling cycles in air, had compressive strength degradation. The bonds in the cement mix could possibly have been broken in the oven heating test but the test by immersion in molten salt showed that the salt could have helped bond the concrete together. Also, the compression test showed that the interiors of the cubes changed colors after being immersed in the salt as shown in figure 6.6. The colors of each of the interiors was a shade of red or orange, as shown in figure 6.7 with a comparison to the respective cube from before the test.

**Figure 6.6: Concrete cube before (left) and after (right) 500 hours at 585°C**

**Figure 6.7: Concrete cubes before (left) and after (right) 500 hours at 585°C**

## 6.4 CONCLUSIONS

After testing of the concrete mix designs that were developed for this project, the mixes proved to be adequate for immersion and use within a molten solar salt environment. With these results, the mix designs that were developed can be cleared for use in a structured concrete thermocline TES system that has been developed via the modeling done in this research. For the size of the tank involved, the concrete will be able to withstand the environmental conditions it will be subjected to, as well as its own weight. Further testing of these mixtures could be done as well in order to verify any questions that may arise for strength issues and degradation issues.

For testing purposes, both geometries modeled in chapter 5 of this thesis should be evaluated for constructability. With the nature of concrete, one geometry could prove to be more difficult to build than the other.

# CHAPTER 7: CONCLUSIONS AND FUTURE WORK

## 7.1 CONCLUSIONS

The goal of this research was to optimize a structured concrete thermocline TES system geometry. The two geometries that were modeled and compared were concrete blocks with holes running vertically throughout the height and concrete plates standing vertical within a tank with a flow path between plates for the molten salt to flow through. Novel concrete mixtures were also tested in the molten salt in a laboratory in order to suggest an acceptable mix for testing of a large scale system.

The modeling programs developed by Selvam (2011) were used in this work to optimize both types of geometries for this system. It turns out that the 2-dimensional plate modeling program that models concrete plates standing vertically within the thermocline tank produced the most efficient system with a discharge efficiency of 65.69%.

The AR sandstone and limestone tested in this thesis proved to withstand the extreme conditions of exposure to a molten salt environment. The concrete mixtures created by John (2011) incorporated the AR sandstone and limestone. These mixtures also proved to withstand the extreme conditions of the molten salt environment, making them viable options for the structured concrete plates as a thermocline filler material.

The key results for this thesis work are presented below:

*Task 1:* A literature review was conducted on thermal energy storage technologies. A focus was made on sensible heat systems and specifically thermocline TES systems, but included information about other types of sensible heat storage.

*Task 2:* The axisymmetric FDM modeling program was used to optimize a concrete filler material designed as concrete cylinders with holes running vertically throughout the height of the tank. The nitrate solar salt heat transfer fluid had a range of 300° C to 585° C. A total of 32 iterations were recorded with values ranging from 0.01905 m - 0.03175 m for RI, 0.04445 m - 0.0762 m for RO, 0.0015 m/s - 0.01 m/s for velocity at charging, 4 h - 6 h for time of charging, 0.001 m/s to 0.0015 m/s for velocity at discharging, and 5 h - 6 h for time of discharging. The efficiencies recorded were 13.61% - 62.68%. The optimized size for one cell had an inner radius for the salt flow path of 0.025 m and an outer radius to the furthest point of the concrete away from the center of the molten salt flow path of 0.05 m. The suggested velocity for charging and discharging is 0.0015 m/s for 5 h. The discharge efficiency was 62.68%.

*Task 3:* The 2-D plate modeling program was used to optimize a concrete filler material designed as concrete plates standing vertically within the thermocline tank. A total of 20 iterations were recorded with values ranging from 0.0127 m – 0.01905 m for TI, 0.0508 m -0.06955 m for TO, 0.0015 m/s - 0.002 m/s for charging velocity, 4 h - 6 h for charging time, 0.001 m/s - 0.0015 m/s for discharging velocity, and 5 h - 6 h for discharging time. The efficiencies recorded ranged from 24.41% - 65.59%. The optimized size was a half thickness of the flow path of 0.01905 m and a thickness from the center of the flow path to the center of the plate of 0.05715 m. The velocity for charging was 0.0015 m/s for 5 h and the velocity for discharging was 0.00125 m/s for 5 h. The discharge efficiency was 65.59%.

*Task 4:* A comparison was made between both optimized models. The 2-D plate model from task 3 was determined to be the best geometric configuration due to a higher discharge

efficiency and a higher energy retrieved per meter square of tank cross section over the axisymmetric optimized model. The design also had an adequate thermocline shape.

*Task 5:* Arkansas sandstone and limestone were evaluated in a molten salt bath for 500 hours at 585°C. Both aggregates withstood the molten salt environment and were considered to be adequate for use in a molten salt resisting concrete mixture.

*Task 6:* Concrete mixtures made by John (2011) were tested in the molten salt bath for 500 hours at 585°C. The concrete cubes gained 116-266% of their original compressive strengths after being submerged in the salt. No significant degradation was found for the cubes. The tested mix designs are adequate for testing in a laboratory scale structured thermocline TES system.

*Task 7:* Both geometries designed using the models should be tested in a laboratory scale. One may be easier to build than the other so constructability should be tested. Any of the concrete mix designs created for this project can withstand the molten salt conditions and therefore can be used when doing laboratory testing.

## 7.2 FUTURE WORK

From this research, more work can be done to further prove that the structured concrete thermocline system is a viable option for TES systems in CSP plants. One thing that could be done is modeling the geometries provided in this research at different temperature ranges. The range provided in this work is 300°C - 585°C. Another temperature range may provide higher discharge efficiencies. Also, other geometries need to be tested to challenge the geometries presented in this research with higher discharge efficiencies.

Other future work is in regards to the material aspect. The concrete mix designs used in this research need further testing. In order to cover all aspects of the design, tests need to be run

on thermal cycling, chemical evaluations of the concrete's bonds, and densities of the concrete before and after salt testing. Also, the salt needs to have a chemical evaluation to be sure that it is not affected by the introduction of the concrete filler material. Other options for materials should also be evaluated.

The final item that needs to be addressed is a cost evaluation of this potential new filler material for thermocline systems. With the information given in this thesis, a system can be sized and a cost evaluation done for the construction of a structured concrete thermocline TES system.

**REFERENCES**


Brosseau, D., Hilava, P., Kelly, M. (2004). Testing Thermocline Filler Materials and Molten-Salt Heat Transfer Fluids for Thermal Energy Storage Systems Used in Parabolic Trough Power Plants. Sandia National Laboratories, Albuquerque, NM, SAND2004-3207.

Brosseau, D., Kelton, J., Ray, D., Edgar, M., Chisman, K., Emms, B. (2005). Testing of Thermocline Filler Materials and Molten-Salt Heat Transfer Fluids for Thermal Energy Storage Systems in Parabolic Trough Power Plants. *Journal of Solar Energy Engineering*, vol. 127, 109-116.

Burolla, V., Bartel, J. (1979). The High Temperature Compatibility of Nitrate Salts, Granite Rock and Pelletized Iron Ore. Sandia National Laboratories Report, Albuquerque, NM, SAND79-8634.

Castro, M. (2010). 3-D FEM Model to Study and Improve the Heat Transfer in Concrete for Solar Thermal Energy Storage. Master's Thesis, University of Arkansas, Department of Mechanical Engineering.

Çengel, Y and Ghajar, A. (2011). *Heat and Mass Transfer: Fundamentals and Applications (4th ed.)*. New York: McGraw-Hill.

Coastal Chemical Company L.L.C. (2011). *Hitec Solar Salt*. 2011, http://www.coastalchem.com/PDFs/HITECSALT/Hitec%20Solar%20Salt.pdf

DOE (2011). *Thermal Storage Research and Development*. Solar Energy Technologies Program, U.S. Department of Energy, http://www1.eere.energy.gov/solar/thermal_storage_rnd.html

EIA (2011). *Energy Perspectives*. U.S. Energy Information Administration, Washington, DC, *http:*//www.eia.gov/totalenergy/data/annual/pdf/perspectives_2009.pdf

EPRI (2010). *Solar Thermocline Storage Systems: Preliminary Design Study*. EPRI, Palo Alto, CA: 2010. 1019581.

Faas, S., Thorne, L., Fuchs, E., Gilbertsen, N. (1986). 10 MWe Solar Thermal Central Receiver Pilot Plant: Thermal Subsystem Evaluation-Final Report. Sandia National Laboratories, Albuquerque, NM, SAND86-8212.

Flueckiger, S., Yang, Z., Garimell, S. (2011). An integrated thermal and mechanical investigation of molten-salt thermocline energy storage. *Applied Energy* xx, xxx-xxx. In Press.

Gil, A., Medrano, M., Martorell, I., Lazaro, A., Dolado, P., Zalba, B., Cabeza, L (2010). State of the art on high temperature thermal energy storage for power generation. Part 1-Concepts, materials, modellization. *Renewable and Sustainable Energy Reviews* 14, 31-55.

Haller, M., Yazdanshenas, E., Andersen, E., Bales, C., Streicher, W., and Furbo, S. (2010). A Method to Determine Stratification Efficiency of Thermal Energy Storage Processes Independently from Storage Heat Loses. *Solar Energy* 84, 997-1007.

Hammerschlag, R., Pratt, R., Schaber, C., Widergreen, S. (2006). *Handbook of Energy Efficiency and Renewable Energy*. Chapter 18. Taylor and Francis Group, LLC.

Herrmann, U., Kearny, D. W. (2002). Survey of Thermal Energy Storage for Parabolic Trough Power Plants. *Journal of Solar Energy Engineering*, vol. 124, 145-152.

Hess, C., Miller, C. (1982). An Experimental and Numerical Study on the Effect of the Wall in a Thermocline-Type Cylindrical Enclosure-I. Solar Energy 28, 145-152.

John, E. (2011) Oven Testing of and Acquiring Thermal Conductivities of High Strength Concrete. *Private Communication.*

John, E., Hale, W., and Selvam, R. (2010). Effect of High Temperatures and Heating Rates on High Strength Concrete for Use as Thermal Energy Storage. *ASME Conf.Proc.*, 2010(43956), 709-713

Kolb, G. (2006). Performance Analysis of Thermocline Energy Storage Proposed for the 1MW Saguaro Solar Trough Plant. *Proceedings of the ISEC2006*, July 8-13, 2006, Denver, CO.

Mawire, A., McPherson, M., van den Heetkamp, R., Mlatho, S. (2009). Simulated Performance of Storage Materials for Pebble Bed Thermal Energy Storage (TES) Systems. *Applied Energy* 86, 1246-12552.

Pacheco, J., Showalter, S., Kolb, W. (2002). Development of a Molten-Salt Thermocline Thermal Storage System for Parabolic Trough Plants. *Proceedings of ASME 2009 International Mechanical Engineering Congress and Exposition*, November 13-19, 2002, Lake Buena Vista, Florida.

Schmidt, F. and Willmott, A. (1981). *Thermal Energy Storage and Regeneration.* New York: McGraw-Hill.

Selvam, R. P. (2011). Thermal Finite Difference Model. *Private Communication.*

Skinner, J. (2011). Testing of Ultra-High Performance Concrete as a Thermal Energy Storage Medium at High Temperatures. Master's Thesis, University of Arkansas, Department of Civil Engineering.

Turchi, C (2011). Heat Transfer Fluid Properties. *Private Communication.*

Van Lew, J., Li, P., Chan, C., Karaki, W., Stephens, J. (2009). Transient Heat Delivery and Storage Process in a Thermocline Heat Storage System. *Proceedings of ASME 2009 IMEC,* November 13-19, 2009, Lake Buena Vista, FL.

Yang, Z., Garimella, S. (2010a). Molten-salt Thermal Energy Storage in Thermoclines Under Different Environmental Boundary Conditions. *Applied Energy* 87, 3322-3329.

Yang, Z., Garimella, S. (2010b). Thermal Analysis of Solar Thermal Energy Storage in a Molten-Salt Thermocline. *Solar Energy* 84, 974-985.